PB84-168921

Effects of Temperature and Pressure on Particle Collection Mechanisms Experimental Program

Air Pollution Technology, Inc., San Diego, CA

Prepared for

Industrial Environmental Research Lab.
Research Triangle Park, NC

Mar 84

U.S. Department of Commerce
National Technical Information Service
NTIS

PB84-168921

EPA-600/7-84-030
March 1984

EFFECTS OF TEMPERATURE AND PRESSURE ON PARTICLE COLLECTION MECHANISMS: EXPERIMENTAL PROGRAM

by

Richard Parker, Roop Jain, Toai Le, and Seymour Calvert

Air Pollution Technology, Inc.
5191 Santa Fe Street
San Diego, CA 92109

Contract No. 68-02-2137

EPA Project Officer: Dennis C. Drehmel
Industrial Environmental Research Laboratory
Research Triangle Park, NC 27711

Prepared for
U. S. Environmental Protection Agency
Office of Research and Development
Washington, D.C. 20460

INDUSTRIAL ENVIRONMENTAL RESEARCH LABORATORY
OFFICE OF RESEARCH AND DEVELOPMENT
U.S. ENVIRONMENTAL PROTECTION AGENCY
RESEARCH TRIANGLE PARK, NC 27711

REPRODUCED BY
NATIONAL TECHNICAL
INFORMATION SERVICE
U.S. DEPARTMENT OF COMMERCE
SPRINGFIELD, VA. 22161

TECHNICAL REPORT DATA

(Please read Instructions on the reverse before completing)

1. REPORT NO. EPA-600/7-84-030	2.	3. RECIPIENT'S ACCESSION NO. PB84 168921
4. TITLE AND SUBTITLE Effects of Temperature and Pressure on Particle Collection Mechanisms: Experimental Program		5. REPORT DATE March 1984
		6. PERFORMING ORGANIZATION CODE
7. AUTHOR(S) Richard Parker, Roop Jain, Toai Le, and Seymour Calvert		8. PERFORMING ORGANIZATION REPORT NO.
9. PERFORMING ORGANIZATION NAME AND ADDRESS Air Pollution Technology, Inc. 4901 Morena Boulevard, Suite 402 San Diego, California 92117		10. PROGRAM ELEMENT NO.
		11. CONTRACT/GRANT NO. 68-02-2137
12. SPONSORING AGENCY NAME AND ADDRESS EPA, Office of Research and Development Industrial Environmental Research Laboratory Research Triangle Park, NC 27711		13. TYPE OF REPORT AND PERIOD COVERED Final; 12/75 - 7/80
		14. SPONSORING AGENCY CODE EPA/600/13

15. SUPPLEMENTARY NOTES IERL-RTP project officer is Dennis C. Drehmel, Mail Drop 4, 919/541-7505. EPA-600/7-77-002 is a related report, covering a theoretical study.

16. ABSTRACT The report gives results of a theoretical and experimental investigation of the effects of high temperatures and high pressures (HTPs) on fundamental particle collection mechanisms. It gives experimental results of inertial impaction, cyclone separation, Brownian diffusion, and electrical migration tests at HTPs. The inertial impaction tests showed that existing impaction models are adequate for HTP predictions. Practical problems (e.g., materials, seals, and particle adhesion) pose more difficulties than any fundamental variations from impaction theory. The cyclone tests showed that cyclone efficiency decreases at high temperature and increases at high pressure for a constant inlet velocity. Available theoretical models could not predict the observed effects of HTP on collection efficiency. An empirical correlation for predicting the cyclone cut diameter was derived. Existing pressure-drop models predict the effects of HTP fairly well. The Brownian diffusion tests showed no detectable effects of HTP. This result is consistent with predictions for the particle size used in the tests ($d_p > 0.5$ micrometer). No useful high temperature data were obtained with the electrical migration apparatus.

17. KEY WORDS AND DOCUMENT ANALYSIS

a. DESCRIPTORS		b. IDENTIFIERS/OPEN ENDED TERMS	c. COSATI Field/Group	
Pollution	Electrical Properties	Pollution Control	13B	
Particles		Stationary Sources	14G	20C
High Temperature Tests		Particle Collection	14B	
Pressure	Brownian Movement	High Pressure Tests		
Impactors		Inertial Impaction	13I	07D
Cyclone Separators		Electrical Migration		

18. DISTRIBUTION STATEMENT Release to Public	19. SECURITY CLASS *(This Report)* Unclassified	21. NO. OF PAGES 169
	20. SECURITY CLASS *(This page)* Unclassified	22. PRICE

EPA Form 2220-1 (9-73)

NOTICE

This document has been reviewed in accordance with U.S. Environmental Protection Agency policy and approved for publication. Mention of trade names or commercial products does not constitute endorsement or recommendation for use.

ABSTRACT

A theoretical and experimental investigation of the effects of high temperatures and high pressures on fundamental particle collection mechanisms has been conducted. This report presents the experimental results of the inertial impaction, cyclone separation, Brownian diffusion and electrical migration tests at high temperatures and pressures.

The inertial impaction experiments revealed that existing impaction models are adequate for high temperature and pressure (HTP) predictions. Practical problems such as materials, seals, and particle adhesion pose more difficult problems than any fundamental variations from impaction theory.

Cyclone experiments showed that the cyclone efficiency decreased at high temperature and increased at high pressure for a constant inlet velocity. Available theoretical models could not predict the observed effects of high temperature and high pressure on collection efficiency. An empirical correlation for predicting the cyclone cut diameter was derived. Existing pressure-drop models predict the effects of temperature and pressure fairly well.

Brownian diffusion experiments showed no detectable effects of temperature and pressure. This result is consistent with predictions for the particle size used in the experiment ($d_p >$ 0.5 μm). No useful high temperature data were obtained with the electrical migration apparatus.

TABLE OF CONTENTS

Abstract.. Page
List of Figures.................................... iii
List of Tables..................................... vi
Nomenclature....................................... ix
.... xi

SUMMARY, CONCLUSIONS AND RECOMMENDATIONS..............
INTRODUCTION....................................... 1
EXPERIMENTAL APPARATUS AND METHODS................. 6
Detailed Process Design............................ 10
Analytical Procedures and Data Analysis.......... 10
INERTIAL IMPACTION................................. 36
Theory... 46
Apparatus..
Results.. 46
Conclusions.. 55
.... 59
CYCLONE SEPARATION................................. 65
Background... 66
Theory...
Apparatus and Test Methods......................... 66
Results.. 67
Discussion and Conclusions......................... 76
.... 80
BROWNIAN DIFFUSION................................. 103
Theory... 108
Apparatus and Experimental Procedure...............
Results.. 108
Discussion and Conclusions......................... 115
.... 118
ELECTRICAL MIGRATION............................... 123
Theory... 126
Apparatus..
Experimental Procedure............................. 126
Results and Discussion............................. 127
.... 131
REFERENCES... 139
.... 144

TABLE OF CONTENTS (cont.)

Page
APPENDIX A.. 149
Inertial Impaction Data.......................... 150
APPENDIX B.. 152
Cyclone Separation Data.......................... 153

LIST OF FIGURES

Page

1. Schematic of Experimental System.................. 11
2. High temperature and pressure components.......... 16
3. Rupture life of Hastelloy X and Haynes 188 at high temperatures.. 19
4. Theoretical design for primary heater............. 23
5. Theoretical design for secondary heater........... 24
6. Results of heat transfer experiment............... 25
7. Test apparatus.................................... 26
8. Control panel..................................... 28
9. Blender dust generator............................ 30
10. Fluidized bed dust generator...................... 32
11. HTP sampling apparatus............................ 33
12. Fly ash size distribution......................... 43
13. Example penetration data for hot test............ 45
14. Drag coefficient as a function of particle Reynolds number................................. 48
15. Stopping distance for particle Reynolds numbers beyond the Stokes region......................... 50
16. HTP sampling apparatus for impaction studies...... 56
17. Inertial impaction test section................... 57
18. Calibration curve for impactor test section....... 60
19. Experimental efficiency curves.................. 62
20. Comparison between predicted and experimental cut diameters....................................... 63
21. Schematic diagram of experimental setup for HTP tests.. 77

LIST OF FIGURES (continued)

Page

22. Dimensions for Plexiglas™ cyclone (C1) and HTP cyclone (C3).. 78

23. Dimensions for circular inlet cyclone (C2)........ 79

24. Experimental data for Plexiglas™ cyclone (C1)..... 83

25. Experimental data for circular inlet cyclone (C2) at low temperature.............................. 84

26. Experimental data for circular inlet cyclone (C2) at high temperature............................. 85

27. Effect of temperature on cyclone efficiency....... 88

28. Effect of pressure on cyclone efficiency.......... 89

29. Combined effects of high temperature and pressure. 90

30. Comparison with model of Leith and Licht (1972)... 91

31. Comparison with model of Sproull (1970)........... 93

32. Comparison with model of Dietz (1981)............. 94

33. Comparison with models at low temperature and pressure.. 95

34. Comparison with models at high pressure........... 96

35. Comparison with models at high temperature........ 97

36. Comparison with models at high temperature and pressure.. 98

37. Reynolds number correlation....................... 101

38. Cut diameter with pressure drop correlation....... 102

39. Data correlation with cut diameters............... 104

40. Comparison with data of Smith, et al. (1979)...... 105

41. Data correlation with 90% cut diameters........... 106

42. Diffusion battery and precutter setup............. 109

43. Schematic diagram of Brownian diffusion experiment.. 117

LIST OF FIGURES (continued)

Page

44. The effects of temperature and pressure on the ratio of "C'/μ_G"........................ 128

45. Electrical migration experimental setup........... 129

46. Corona charger.................................... 130

47. Electrical migration test section................. 132

48. Particle trajectory in electrical migration test section.. 134

49. Current ratio at 29°C and 160°C, (I_2/I_1).......... 140

50. Current ratio at 29°C and 160°C (I_3/I_1)........... 141

LIST OF TABLES

Page

1. HTP Particle Collection Devices and Fundamental Mechanisms.................................... 8
2. Mechanical Strength of High Temperature Metals..... 14
3. Maximum Service Temperatures....................... 17
4. Usable Life of High Temperature Tubing............. 20
5. Gasket Materials.................................... 21
6. Filter Material Test Results........................ 35
7. Sample Test Run #28-32.............................. 38
8. Sample Test Run #28-34.............................. 40
9. Sample Test Run #28-35.............................. 41
10. Sample Test Run #28-36.............................. 42
11. Inertial Impaction Test Conditions and Results..... 61
12. Cyclone Performance Models.......................... 68
13. Test conditions for preliminary cyclone tests...... 82
14. Test conditions for HTP cyclone runs............... 86
15. Experimental and theoretical cut diameters......... 99
16. Experimental and theoretical pressure drop......... 100
17. Inertial, interception, and diffusion efficiencies for diffusion battery............................ 114
18. Predicted penetration for screen diffusion battery.. 116
19. Diffusion battery data for 1 atm, 100°C............ 119
20. Diffusion battery data for 1 atm, 300°C............ 120
21. Diffusion battery data for 1 atm, 500°C............ 121
22. Summary of Results for Diffusion battery experiments...................................... 122

LIST OF TABLES (continued)

Page

23. Extrapolated predictions for screen diffusion battery tests.................................. 124

24. Results from electrical migration charge measurements.................................... 142

NOMENCLATURE

A = surface area of collection electrode, cm²

A, B, C = empirical constants in slip correction factor, dimensionless

A_i = surface collection area of electrode "i", cm²

a_m = momentum accommodation coefficient, dimensionless

a_t = thermal accommodation coefficient, dimensionless

C' = Cunningham slip correction factor, dimensionless

$= 1 + N_{Kn} \, (1.257 + 0.4 \exp(-1.1/N_{Kn}))$

C_D = drag coefficient, dimensionless

D = cyclone diameter, cm

D = distance between central electrode and collection electrode, cm

D_e = cyclone exit diameter, cm

D_p = diffusion coefficient, cm²/s

d_c = wire diameter, cm

d_c = characteristic length, cm

d_{crit} = critical diameter larger than which 100% of the particles are collected, cm

d_H = hydraulic diameter of cyclone inlet, cm

d_{pa} = aerodynamic particle diameter, μmA ≡ μm $(g/cm^3)^{1/2}$

d_p = particle diameter, cm or μm

d_{p50} = particle diameter at which 50% of the particles are collected, μmA

d_{p90} = particle diameter at which 90% of the particles are collected, μmA

d_{pc} = 50% cut diameter, μm

d_{pg} = mass median diameter of test aerosol, cm

d_s = median surface diameter of particle, cm

E = electric field strength, v/cm

E_c = charging field strength, statvolt/cm

E_p = precipitating field strength, statvolts

e = 4.8×10^{-10} esu = electronic charge

F_r = resistance force, dynes

f = function of N_{Re} (equation 6), dimensionless

I_1 = current collected on electrode "1", A

I_2 = current collected on electrode "2", A

I_3 = current collected on electrode "3", A

K_p = inertial impaction parameter, dimensionless

k = Boltzmann's constant, erg/°K

L = length of wire in screen diffusion battery, cm

L_i = length of collection electrode "i", cm

l_m = mean free path length, μm

M_s = molecular weight of surface material, g/g-mol

N_{Kn} = Knudsen number, dimensionless

N_{Re} = Reynolds number, dimensionless

N_{Stk} = Stokes number, dimensionless

n = cyclone vortex component, dimensionless

n_1, n_2 = inlet and outlet particle concentrations, cm^{-3}

n_p = number of elementary charge units

n_s = saturation charge, elementary charge units

P = absolute gas pressure, kPa

Pt_d = penetration for diameter "d_p", fraction

Q_G = volumetric flow rate, cm^3/s

S = solidity factor dimensionless

T = gas temperature, °C or K

T_g = temperature of gas molecules incident on surface, K

T_r = temperature of gas molecules reflected from surface, K

T_s = surface temperature, K

u_c = cyclone inlet velocity, cm/s

u_e = electrical migration velocity, cm/s

u_r = relative velocity between particle and gas, cm/s

u_t = terminal velocity, cm/s

V = applied voltage, v

v_f = void fraction, dimensionless

x_s = particle stopping distance, cm

Z_p = electrical mobility of particle, $cm^2/s-V$

Greek

η_G = gravity settling efficiency, fraction

η_R = interception efficiency, fraction

η_D = collection efficiency by diffusion, fraction

μ_G = gas viscosity, g/cm-s

ρ_G = gas density, g/cm^3

ρ_p = particle density, g/cm^3

SECTION 1
SUMMARY, CONCLUSIONS AND RECOMMENDATIONS

When designing, troubleshooting, or evaluating the performance of particulate control equipment, it is important to have a firm understanding of the physical mechanisms by which the particles are removed from the gas stream. This is especially true when the control device is to be used at high temperature and pressure (HTP) conditions where current design models are unproven. In order to provide a rational basis for dealing with HTP particulate control equipment, a sound theoretical understanding of the HTP effects on particle collection mechanisms is essential.

Calvert and Parker (1977) made a thorough examination of the literature concerned with HTP effects on particle collection. Although HTP particle collection has been of interest for over 30 years no fundamental evaluation of the theory has been attempted. In general, conventional models for particle collection (valid at low temperatures and pressures) have been extrapolated to predict performance in HTP situations. Insufficient performance data are available to evaluate these models at HTP conditions, especially efficiency as a function of particle size.

This report presents the results of the experiments. Four collection mechanisms were studied at temperatures up to 800°C and pressures up to 25 atm. Of the four mechanisms (inertial impaction, cyclone separator, Brownian diffusion, and electrical migration), electrical migration did not yield useful results because of problems with the electrical insulators. The results are briefly summarized below and presented in detail in the body of this report.

EXPERIMENTAL APPARATUS AND METHODS

A high temperature and high pressure test facility was built which could provide a test aerosol at a maximum of 1,100°C and 15 atm. Pressures up to 25 atm could be handled at lower temperatures. The nominal flow rate was 28 liters/min (1 acfm) and ranged from about 7 liters/min to 60 liters/min for various runs. The gas could be either compressed nitrogen or compressed air. Redispersed coal fly ash was used as the test aerosol.

For each collection mechanism a different test section (inertial impactor, cyclone separator, diffusion battery, electrostatic precipitator) was installed in the system. Samples were obtained in three locations: inlet, test section, and outlet. The inlet sample was obtained using an isokinetic sampling probe and a total filter. The outlet sample was obtained by either filtering the entire flow or by pulling an isokinetic sample at the outlet. The test section samples were obtained by acetone wash. All particle size and concentration analyses were done quantitatively using a Coulter counter model TAII particle size analyzer.

INERTIAL IMPACTION

A single stage inertial impactor, which had a cut diameter of approximately 1 to 2 μm at a flow rate of 14 to 28 liters/min (0.5 to 1 acfm), was used as the test section for studying the particle collection by inertial impaction. Tests were conducted at temperatures up to 800°C and pressures up to 15 atm.

Theoretical and experimental cut diameters were compared as a function of temperature and pressure. There was a considerable amount of scatter in the data which was attributed to difficulties associated with finding a suitable high temperature substrate material. Thin ceramic paper was found to work best however it was far from ideal as an impaction substrate.

On average, the experimental cut diameters agreed with predictions and no unexpected temperature or pressure effects were observed. However for all test conditions the standard deviations of the differences between experimental and predicted cut diameters were greater than the differences themselves.

The major conclusion from this work is that existing models can be used to predict inertial collection at high temperature and pressure with the same precision and accuracy obtainable at normal conditions using ceramic fiber substrates. The performance of inertial sizing devices, such as cascade impactors, operating at high temperature and pressure will be limited more by practical design problems (substrates, seals, materials) than by any fundamental temperature and pressure effects.

Particle collection equipment which depend on the inertial impaction mechanism should perform as predicted based on present test results. Devices which fall into this category include granular filters, dry scrubbers, molten salt scrubbers and to a lesser extent fiber and membrane filters (before cake filtration becomes dominant). The performance-limiting problems are likely to be particle adhesion and reentrainment, granule attrition, corrosion and other secondary problems not directly related to the primary particle collection efficiency.

CYCLONE SEPARATOR

A high temperature and pressure cyclone was built and tested at temperatures up to 700°C and pressures up to 25 atm. Inlet velocities of 1.8, 2.6, and 5.2 m/s were used. The inlet Reynolds number covered the range from about 3,000 to 400,000 so that transition from laminar to turbulent flow occurred in the cyclone.

The results were presented as grade efficiency curves (efficiency as a function of particle diameter) and were compared with theoretical models from the literature. The results were very surprising. The collection efficiency decreased much more drastically than predicted for the high temperature tests. For the high pressure tests, the efficiency actually increased significantly while no change in efficiency at high pressure is expected based on the theory. Nine theoretical models were evaluated and although some predicted the efficiency fairly well for specific conditions, none could adequately predict the effects of temperature and pressure which were observed.

An empirical correlation of cyclone cut diameter against the inlet cyclone Reynolds number was derived. The effects of temperature and pressure for this cyclone could be adequately accounted for by variations in the Reynolds number. No theoretical explanation for this result is available.

The correlation was modified to include the square root of Stoke's number and present data were then compared with high temperature and high pressure data from the literature. The comparisons were good considering the variations in cyclone geometry and size which were not accounted for.

The major result of this work has been the use of the empirical correlation between cyclone cut diameter and Reynolds number for predicting the effects of temperature and pressure. The cyclone flow characteristics and the effect of pressure on them need to be studied in more detail if a rational design basis for high temperature and pressure cyclones is to be developed. Furthermore, present results are only for one cyclone geometry and are limited to relatively low velocities and small cyclones. More data at higher Reynolds numbers for larger cyclones and various cyclone geometries should be obtained to determine how they affect the empirical correlation.

BROWNIAN DIFFUSION

A screen diffusion battery was used to investigate the effects of temperature and pressure on the particle collection mechanism of Brownian diffusion. Theory predicted that for the particles (≥ 0.5 μm dia.) used in the experiments, there would be no significant temperature or pressure effects. Present results are qualitatively consistent with this prediction. The experimental apparatus was not sufficiently accurate to detect the small effects anticipated, however no noticeable difference between runs at 100°C and 800°C was found. It is likely that Brownian diffusion will play a secondary role in high temperature and pressure particulate control in a similar manner to its role in conventional control devices.

ELECTRICAL MIGRATION

An electrostatic precipitator was built for high temperature and pressure experiments on the mechanism of electrical migration. The apparatus was operated at low temperature but could not be made to operate at high temperature because of breakdown of electrical insulators and loss of particle charge at high temperatures. No useful data were obtained.

RECOMMENDATIONS

Further work on cyclone separation could include testing of larger cyclones at higher Reynolds number and with variable geometries. This work could then be used to develop a design model for high temperature and pressure cyclones and to develop criteria for optimizing cyclone design for high temperature and pressure applications.

More fundamental work on the mechanism of electrical migration would require a more elaborate experimental facility than was possible under this contract. It may not be possible to separate the phenomena of particle charging and particle precipitation at high temperature.

SECTION 2
INTRODUCTION

The commercial development of advanced energy processes, such as pressurized fluidized bed coal combustion, and low-BTU coal gasification, is hindered by the problem of removing fine particles from hot, pressurized gases. In many cases the gas is to be expanded from high temperature and pressure through a gas turbine. Any temperature or pressure losses during the dust collection stage will reduce the overall thermodynamic efficiency of the process. Therefore it is desirable to clean the gas at system pressure and at a temperature no lower than the desired turbine inlet temperature.

Another problem encountered in high temperature and pressure (HTP) gas streams is the problem of sampling and measuring the size of dust particles as they exist in the gas stream. This information is needed to establish gas cleanup requirements based on gas turbine tolerances for fine particles. It also is essential information for the design of HTP fine particle control devices.

When designing, troubleshooting, or evaluating the performance of fine particle control or measurement equipment, it is important to have a firm understanding of the physical mechanisms by which the particles are removed from the gas stream. This is especially true when the equipment is to be used at high temperature and pressure conditions where current design models are unproven. In order to provide a rational basis for dealing with HTP particle collection equipment, a sound understanding of the HTP effects on particle collection mechanisms is essential.

The purpose of this project was to conduct a theoretical and experimental evaluation of the effects of high temperature and pressure on fundamental particle collection mechanisms. The theoretical review was reported by Calvert and Parker (1977). This report presents the results of the experimental program and the final theoretical evaluation.

BACKGROUND

Although particle collection at HTP conditions has been recognized as a serious technical problem for over thirty years, no satisfactory solutions have been demonstrated. During the past five years a large number of new concepts have been proposed and many of these have shown good potential for efficient particle collection. However all of these devices are still in the developmental stage.

Table 1 lists the major devices and fundamental collection mechanisms associated with each device. The developer is also indicated. The technical status of these devices has been reported in various symposium papers and reports including EPA/DOE Symposium HTP Particulate Control (1977), DOE Contractor's Meeting (1981), and Parker and Calvert (1979).

By far the most important collection mechanism is inertial impaction since almost all devices rely on this mechanism. Cyclone separation, electrical migration, interception and Brownian diffusion also are important to a lesser extent. Acoustic agglomeration and magnetic attraction are only important for special devices designed to utilize these mechanisms.

In addition to the control devices listed in Table 1, there are a number of particle sizing instruments which have been used to characterize the size of dust particles in HTP gas streams. The two sizing instruments often used for these tests are cascade impactors and cyclone separators. The calibration and size selectivity of these devices at high temperature and pressure are uncertain. For this reason filter samples are usually collected and analyzed later by Coulter counter or microscopy. Since this

TABLE 1. HTP PARTICLE COLLECTION DEVICES AND FUNDAMENTAL MECHANISMS

Device (Developer)	Mechanisms*
CYCLONES	
Conventional reverse flow	CS, IN
Rotary flow cyclone (Aerodyne)	CS, IN
Cyclocentrifuge (Mechanical Technology, Inc.)	CS, IN
Electrocyclone (General Electric)	CS, IN, EM
Centrifuge wedge separator (Linhardt & Assc)	CS, IN
Acoustic agglomeration and cyclone (SUNY Buffalo)	AG, CS, IN, IP
Glass slag particle capture (General Elec.)	IN, CS
FILTERS	
Ceramic bag filter (Acurex)	IN, IP, BD
Ceramic Cross Flow Filter (Westinghouse)	IN, IP, BD
Fixed granular bed filter (Westinghouse/DUCON)	IN, EM, BD, IP
Moving granular bed filter (Combustion Power)	IN, EM, BD
Magnetic stabilized-bed filter (EXXON)	IN, MG, BD
Electro-Fluidized-bed filter (MIT)	IN, EM, BD
SCRUBBERS	
Molten salt scrubber (Battelle Northwest)	IN
PxP dry scrubber (Air Pollution Technology)	IN, EM
Dry plate scrubber (Air Pollution Technology)	IN, EM
ELECTROSTATIC PRECIPITATORS	
HTP ESP (Research Cottrell)	EM

---

*Mechanisms Abbreviations

IN = inertial impaction
IP = interception
EM = electrical migration
CS = cyclone separation
BD = Brownian diffusion
AG = Acoustic agglomeration
MG = Magnetic attraction

approach does not size segregate the particles in-situ, at HTP conditions, there is some question as to whether or not the size measurements are representative of the dust as it existed in the gas stream. For example, large agglomerated particles may be collected and subsequently broken apart and analyzed as fine single particles in the Coulter analysis. Conversely, fine single particles may agglomerate in the filter and be viewed as larger agglomerated particles under the microscope.

It is important, both for particle control and for particle sizing, to evaluate the theoretical models and determine whether or not they are suitable for HTP applications.

PROJECT OBJECTIVES

The overall project objective is to evaluate the theoretical models for high temperature and pressure particle collection mechanisms. A detailed theoretical review was reported by Calvert and Parker (1977). In general it was predicted that high temperature and pressure should adversely affect the performance of particle collection equipment. Previous studies were reviewed which verified this finding qualitatively, however no experimental data were found which were sufficient for a quantitative evaluation of the theories and models.

This experimental program looked at four basic collection mechanisms: inertial impaction, cyclone separation, Brownian diffusion, and electrical migration. Following the experimental work, the theories were reviewed and re-evaluated. This report presents the results of the experimental program.

SECTION 3

EXPERIMENTAL APPARATUS AND TEST METHODS

The purpose of the experimental apparatus is to provide a controlled environment for evaluating the effects of high temperature and high pressure on specific particle collection mechanisms. The operating ranges for the main test parameters are listed below.

Temperature = 20 to 1,100°C
Pressure = 1 to 15 atm
Particle diameter = 0.5 to 10 μm
Gas Flow Rate = 250 to 1,000 cm^3/s

In addition to these parameters, particle mass concentration, particle size distribution, and pressure drop were measured at the inlet and outlet of the test section. These data were then used to determine the experimental particle removal efficiency for comparison with theoretical predictions. Different test sections were used corresponding to the four collection mechanisms studied.

DETAILED PROCESS DESIGN

A schematic diagram of the experimental apparatus and gas flow is shown in Figure 1. High pressure gas is supplied from nitrogen cylinders. A portion of the gas is used in the high pressure dust generator and the rest is used for dilution. The dust generator is heated to about 150°C. The gas and dust are heated in a two-stage electrical heating system consisting of high temperature heating tapes and tube furnaces. The high temperature gas and dust then pass through the test section, quencher, flow metering system, and finally vent to the atmosphere.

Isokinetic dust samples are pulled at the inlet and outlet

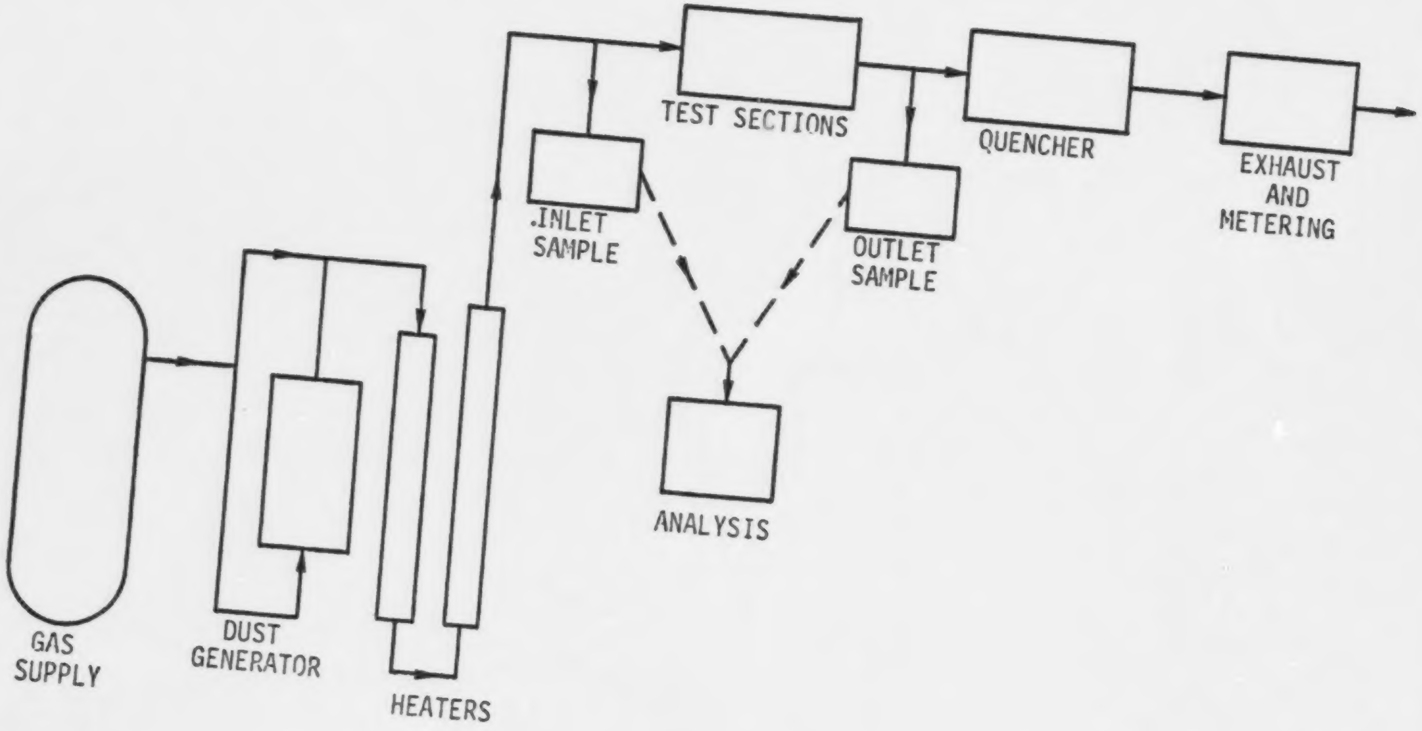
GAS SUPPLY
DUST GENERATOR
HEATERS
INLET SAMPLE
TEST SECTIONS
OUTLET SAMPLE
ANALYSIS
QUENCHER
EXHAUST AND METERING

Figure 1. Schematic of experimental system.

of the test section. The samples are collected on filters and analyzed in the laboratory to determine the total mass collected and the size distribution at the inlet and outlet. All high temperature and pressure components were kept behind a high pressure barricade. Tests were run from a control panel located outside the barricade.

The design approach for each major system component is discussed below.

Gas Supply

The purpose of the gas supply system was to provide a flow of up to about 1,000 cm^3/s (2 acfm) at pressures up to 15 atm. Nitrogen gas was selected in order to minimize high temperature oxidation problems which could contaminate the samples and to minimize the threat of combustion and possible explosion of the apparatus.

High pressure nitrogen gas was supplied from a manifold of twenty-four gas cylinders arranged in parallel. The total volume available was approximately 200 Nm^3. The supply pressure was regulated at a maximum of 35 atm (500 psig). From there it was further regulated to the desired system pressure for each test. Relief valves were used to assure that the system did not get pressurized above the maximum design pressure (17 atm).

The gas supply was used to supply four gas streams: the main flow stream, dust generator flow, inlet sample dilution, and outlet sample dilution. Each stream had its own pressure regulator, flow control valve, and rotameter.

Piping and Materials

Materials selection for the high temperature and pressure piping presented a major problem. The pipe should be heated externally to keep the internals clean for washing and sample recovery. For this reason, ceramic or refractory lining could not be used since it is abrasive and would contaminate the samples. External heaters needed to be approximately 100°C hotter than the maximum gas temperature so a machinable metal with a high allowable stress at temperatures up to 1,200°C was needed. Since the external surfaces would be exposed to air, it was also desirable that the metal be resistant to oxidation at this temperature.

Table 2 presents mechanical strength data for the metals which were considered. Haynes 25, Haynes 188, and Hastelloy "X" were the only metals considered to be acceptable. Hastelloy "X" was selected for its slightly superior oxidation resistance, availability, and machinability. Haynes 188 has superior tensile strength at high temperatures however it is not readily available in the sizes and quantities required.

Table 2 also presents data for some refractory metals. These metals show extraordinary strength at high temperature, however they oxidize so rapidly that they were not practical for the present application.

The high temperature piping layout is shown in Figure 2. The experimental system is too small (less than 6-inch diameter pipe) to come under the standard ASME Boiler and Pressure Vessel Code. Therefore, California state law specified that good engineering judgement and a factor of safety of four are used in the design.

There were two important material design considerations. The first was the short time tensile strength of the material. The tubing must be designed with a wall thickness sufficient to maintain the pipe stresses below the allowable stress for the material at the service temperature. Using the required factor of safety of four, the allowable stress may be estimated as one quarter of the ultimate tensile strength of the material at service temperature. The service temperatures for our experiments are summarized in Table 3.

Table 2. MECHANICAL STRENGTH OF HIGH TEMPERATURE METALS

MATERIAL	ULTIMATE TENSILE STRENGTH MPa (psi) 980°C (1,800°F)	ULTIMATE TENSILE STRENGTH MPa (psi) 1,090°C (2,000°F)	ULTIMATE TENSILE STRENGTH MPa (psi) 1,200°C (2,200°F)	ALLOWABLE STRESS MPa (psi) 980°C (1,800°F)	ALLOWABLE STRESS MPa (psi) 1,090°C (2,000°F)	ALLOWABLE STRESS MPa (psi) 1,200°C (2,200°F)	COMMENTS
High Temperature Metals and Alloys							
316 Stainless[1]	59.2 (8,600)	27.5 (4,000)	--	14.8 (2,150)	6.9 (1,000)	--	
Inconel 600[2]	75.8 (11,000)	--	--	18.9 (2,750)	--	--	No data above 980°C (1,800°F).
Inconel 601[2]	82.7 (12,000)	48.2 (7,000)	--	20.7 (3,000)	12.1 (1,750)	--	Oxidation resistance comparable to Hast. X or Haynes 188. No data above 1,150°C (2,100°C).
Inconel 625[2]	117.1 (17,000)	62 (9,000)	--	29.3 (4,250)	15.5 (2,250)	--	Resistance to oxidation & nitriding not as good as Inconel 601. No data above 1,095°C (2,000°F).
Inconel X-750[2]	55.1 (8,000)	--	--	13.8 (2,000)	--	--	Heat treated, runs out of strength rapidly after 760°C (1,400°F). No data above 980°C (1,800°F).
Incoloy 802[2]	110 (16,000)	75.8 (11,000)	--	27.6 (4,000)	18.9 (2,750)	--	Oxidation resistance not as good as Inconel 601. No data above 1,095°C (2,000°F).
Haynes 25[3]	230.8 (33,500)	135 (19,600)	76.5 (11,100)	57.7 (8,375)	33.8 (4,900)	19.1 (2,775)	Resistance to oxidation & nitriding to 1,040°C (1,900°F).

Table 2. MECHANICAL STRENGTH OF HIGH TEMPERATURE METALS (Continued)

MATERIAL	ULTIMATE TENSILE STRENGTH MPa (psi)			ALLOWABLE STRESS MPa (psi)			COMMENTS
	980°C (1,800°F)	1,090°C (2,000°F)	1,200°C (2,200°F)	980°C (1,800°F)	1,090°C (2,000°F)	1,200°C (2,200°F)	
Hastelloy X[3]	155 (22,500)	89.6 (13,000)	37.2 (5,400)	38.8 (5,625)	22.4 (3,250)	9.3 (1,350)	Resistance to oxidation to 1,200°C (2,200°F).
Haynes 188[3]	253.5 (36,800)	133 (19,300)	76.5 (11,100)	63.4 (9,200)	33.2 (4,825)	19.1 (2,775)	Resistance to oxidation to 1,150°C (2,100°F).
Refractory Metals							
Molybdenum[4]	207 (30,000)	138 (20,000)	96.5 (14,000)	51.7 (7,500)	34.5 (5,000)	24.1 (3,500)	Accelerated oxidation above 395°C (743°F).
Columbium[5]	117 (17,000)	--	--	29.3 (4,250)	--	--	Accelerated oxidation above 425°C (797°F). No data above 980°C (1,800°F).
Tantalum[5]	186 (27,000)	--	--	46.5 (6,750)	--	--	Accelerated oxidation above 425°C (797°F). No data above 980°C (1,800°F).
Tungsten[4]	655 (95,000)	586 (85,000)	448 (64,000)	164 (23,750)	146 (21,250)	112 (16,250)	Accelerated oxidation above 190°C (375°F). Brittle at room temp.

---

[1] *Steels for Elevated Temperature Service*, U.S. Steel, 1970.

[2] *Technical Bulletins*, from Huntington Alloy Products Division, The International Nickel Company, Inc., Huntington, West Virginia.

[3] *Technical Bulletins*, from Stellite Division of the Cabot Corporation, Kokomo, Indiana.

[4] *Technical Bulletins*, from Schwarzkopf Development Corporation, Holliston, Massachusetts.

[5] *Machine Design*, Materials Reference Issue, March 4, 1976.

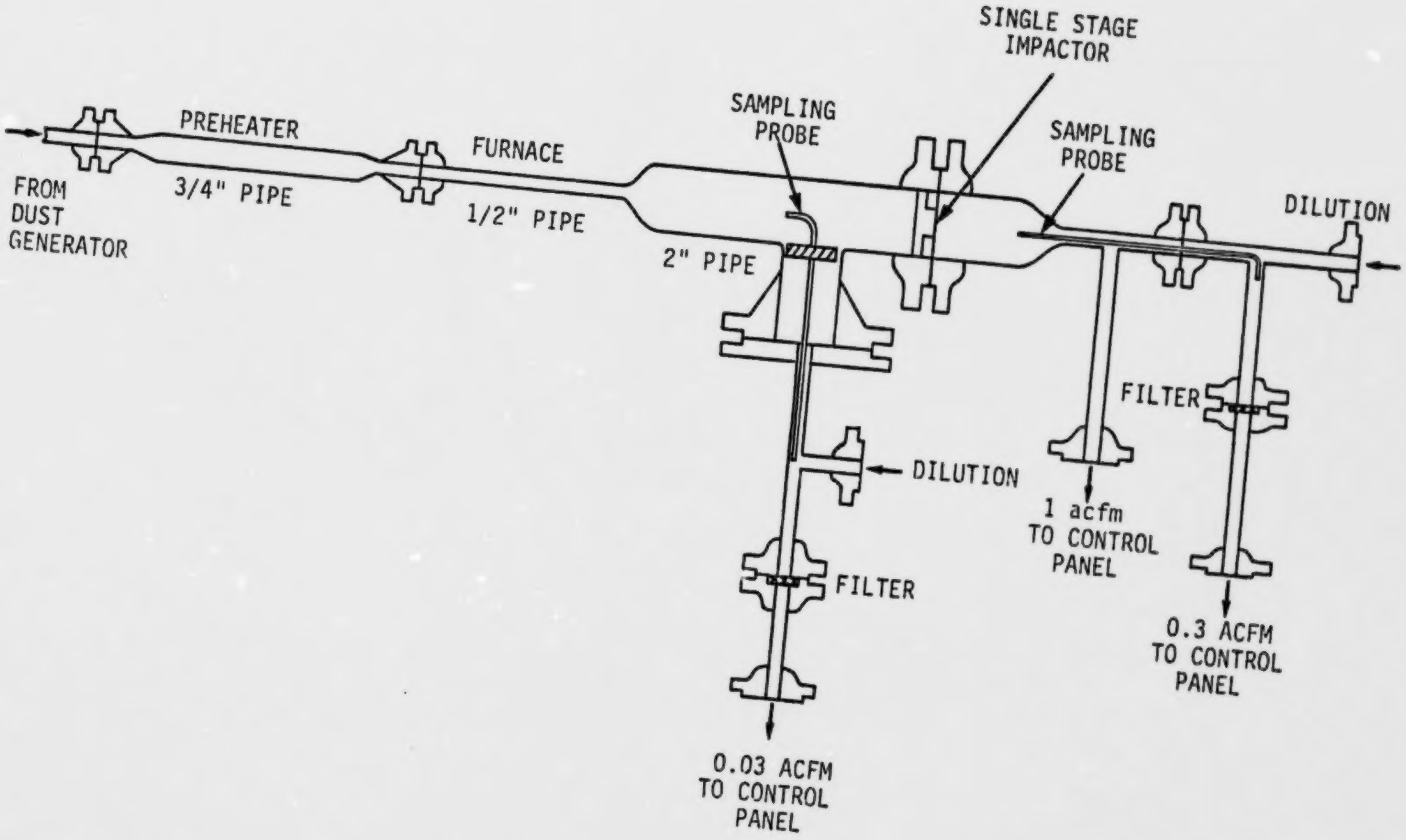
SINGLE STAGE IMPACTOR
SAMPLING PROBE
SAMPLING PROBE
PREHEATER
FURNACE
DILUTION
FROM DUST GENERATOR
3/4" PIPE
1/2" PIPE
2" PIPE
FILTER
DILUTION
1 acfm TO CONTROL PANEL
FILTER
0.3 ACFM TO CONTROL PANEL
0.03 ACFM TO CONTROL PANEL

Figure 2. High temperature and pressure components.

Table 3. MAXIMUM SERVICE TEMPERATURES

Component	Maximum Service Temperature
Dust generator and associated piping	200°C
Primary heater (pre-heater)	800°C
Secondary heater	1,150°C
Test sections and sampling chambers	1,100°C

Hastelloy "X" with a wall thickness large enough to give a safety factor of four at the required service temperatures was finally chosen for the secondary heater and test sections. Hastelloy "X" tubing for the secondary heater is not available in the wall thickness required. Therefore, it was fabricated by gun-drilling 2.2 cm (7/8 in.) diameter round stock to the proper diameter. Inconel 600 (Schedule 40) was selected for the primary heater. Type 304 stainless steel was used for the dust generator and associated piping.

Although the above design provides sufficient short term strength at the required temperatures, the second design consideration, and a more critical problem is the long term degradation in strength resulting from metal creep at high temperture.

Figure 3 presents curves of rupture life versus applied stress for Hastelloy "X" and Haynes 188, at various temperatures. The solid lines are from the manufacturer's technical bulletin. The dashed lines were extrapolated from tabulated data.

The rupture life is the time it takes to produce rupture of a test specimen with a constant applied stress at a specified temperature. As an example, an applied stress of 4.8 MPa (700 psi) as anticipated for the secondary heater tubing would cause rupture after about 650 hours. A safety factor of four would allow a usable life of one quarter the rupture life, or about 160 hours.

Usable lives for the high temperature tubing are given in Table 4. The estimated stress was obtained by considering the tube diameter and wall thickness, and a maximum internal pressure of 1.7 MPa (250 psia).

The above design considerations are based on the short term tensile strength, and the rupture life of the material. This does not consider any weakening of the metal caused by heating and cooling cycles, or by high pressure and low pressure cycles at high temperature. Also, the data used in this design are the

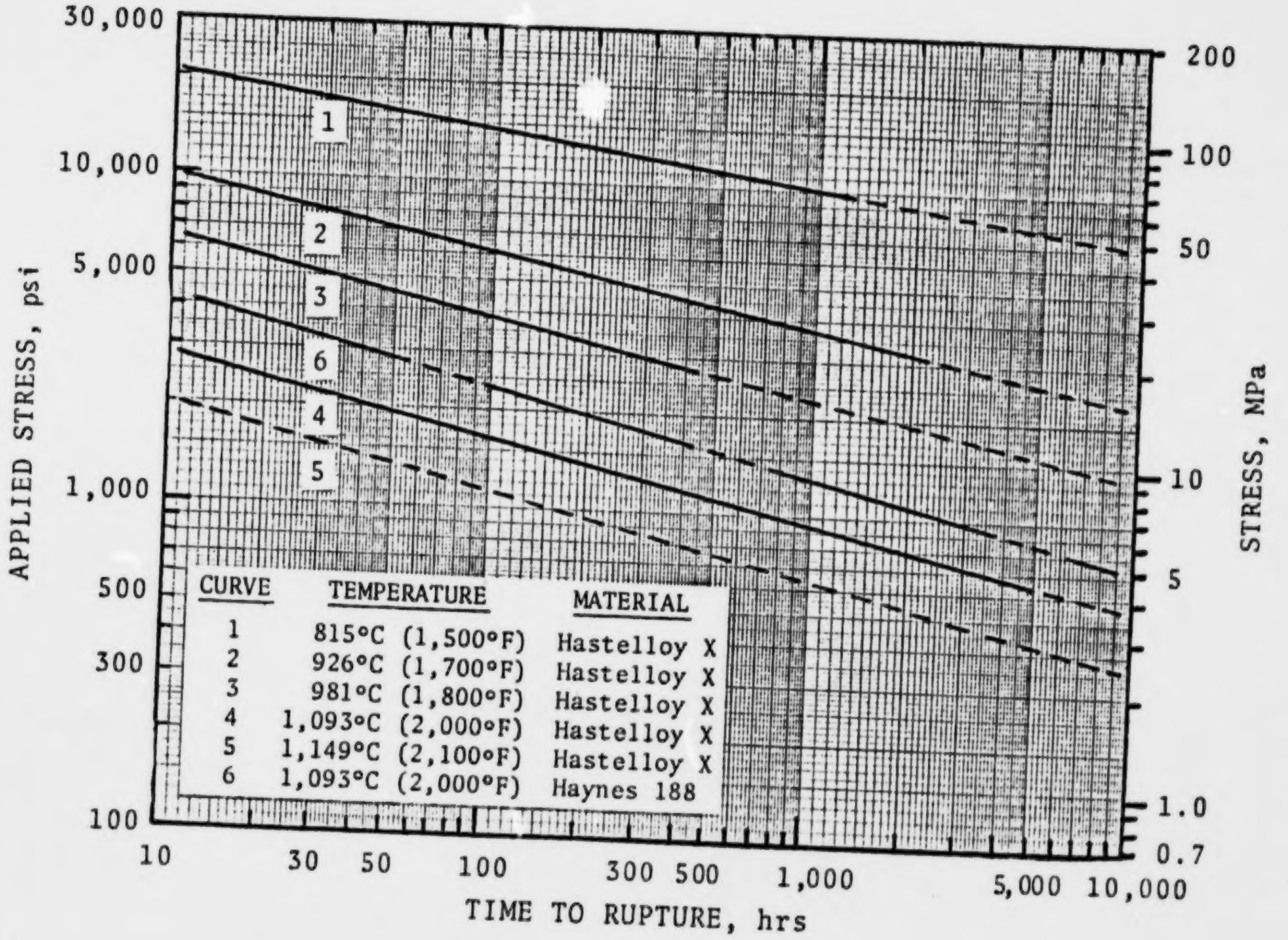

Figure 3. Rupture life of Hastelloy X and Haynes 188 at high temperatures.

TABLE 4. USABLE LIFE OF HIGH TEMPERATURE TUBING

Component	Material	Estimated Stress	Usable Life*
Primary Heater	Inconel 600	1,200 psi	>2,500 hrs
Secondary Heater	Hastelloy X	700 psi	160 hrs
Test Sections and Sampling Chambers	Hastelloy X	1,200 psi	80 hrs
	Haynes 188	1,200 psi	320 hrs

*Usable life is defined as ¼ the rupture life at design temperature.

best available, but are still based on a limited number of test results. For these reasons, it was necessary to take further precaution against possible metal failure at high temperature and pressure. Therefore, a protective barricade was designed to enclose the high temperature and pressure components. The barricade design is discussed later.

Flanges were machined out of Hastelloy "X", Inconel 600, or 304 stainless steel as required to be consistent with the piping. Various gasket materials were used depending on the temperature. The gasket materials are summarized below in Table 5.

TABLE 5. GASKET MATERIALS

Material	Maximum Service Temperature
Neoprene	120°C
Asbestos	260°C
Teflon	260°C
Copper Shim	500°C
316 Stainless Steel Shim	800°C
Inconel Shim	1100°C
Ceramic fiber paper (Alumina and silica)	1250°C

Heating System

The approach for heating the gas and particles was to use external heat to heat the pipe above the desired gas temperature. The gas was then heated by convection as it flowed through the hot pipe. This approach had the advantage that no electrical heating coils were in contact with the gas and dust particles. Furthermore it made washing and cleaning of the pipe relatively straight forward and effective.

Two sections of heaters were used. The first section was a

240 cm (8 ft) length of Inconel pipe with 2.1 cm inside diameter and 2.9 mm wall thickness (3/4 in. nominal pipe, Schedule 40). The pipe was wrapped with seven high temperature heating tapes (850°C maximum). The predicted gas temperature as a function of pipe length is shown in Figure 4, for maximum temperature and pressure.

The second heating section consisted of 150 cm (5 ft) of Hastelloy "X" pipe with 1.3 cm inside diameter and a wall thickness of 0.5cm. The pipe was surrounded by four tube furnaces which could go up to a maximum temperature of 1,200°C. The theoretical prediction for the secondary heater, based on an inlet temperature of 800°C, is shown in Figure 5.

Additional heating tapes and furnaces were used as needed to keep the test section and sample line pipe temperatures at the required gas temperature and to prevent heat loss from the gas to the pipe.

As a check on the theoretical predictions, a heat transfer experiment was conducted on a 240 cm long, 1.27 cm diameter pipe. Air was passed through the pipe at atmospheric pressure and a flow rate of 76 liters/min (2.7 acfm). Heat was supplied by high temperature heating tapes. The results are presented in Figure 6. Assuming 10% heat loss through the insulation, the agreement between the data and predictions is good.

Cooling and Metering

Cooling jackets were used to cool off the pipe and gas after leaving the test sections and sample filters (when operated at high temperature). The cooling jackets kept the pipe immersed in cold water. The gas was cooled by convection as it flowed through the cold pipe.

Flow rates were measured and controlled using calibrated, high pressure rotometers, regulators, and needle valves located as shown in Figure 7. The rotameters at the main gas outlet and

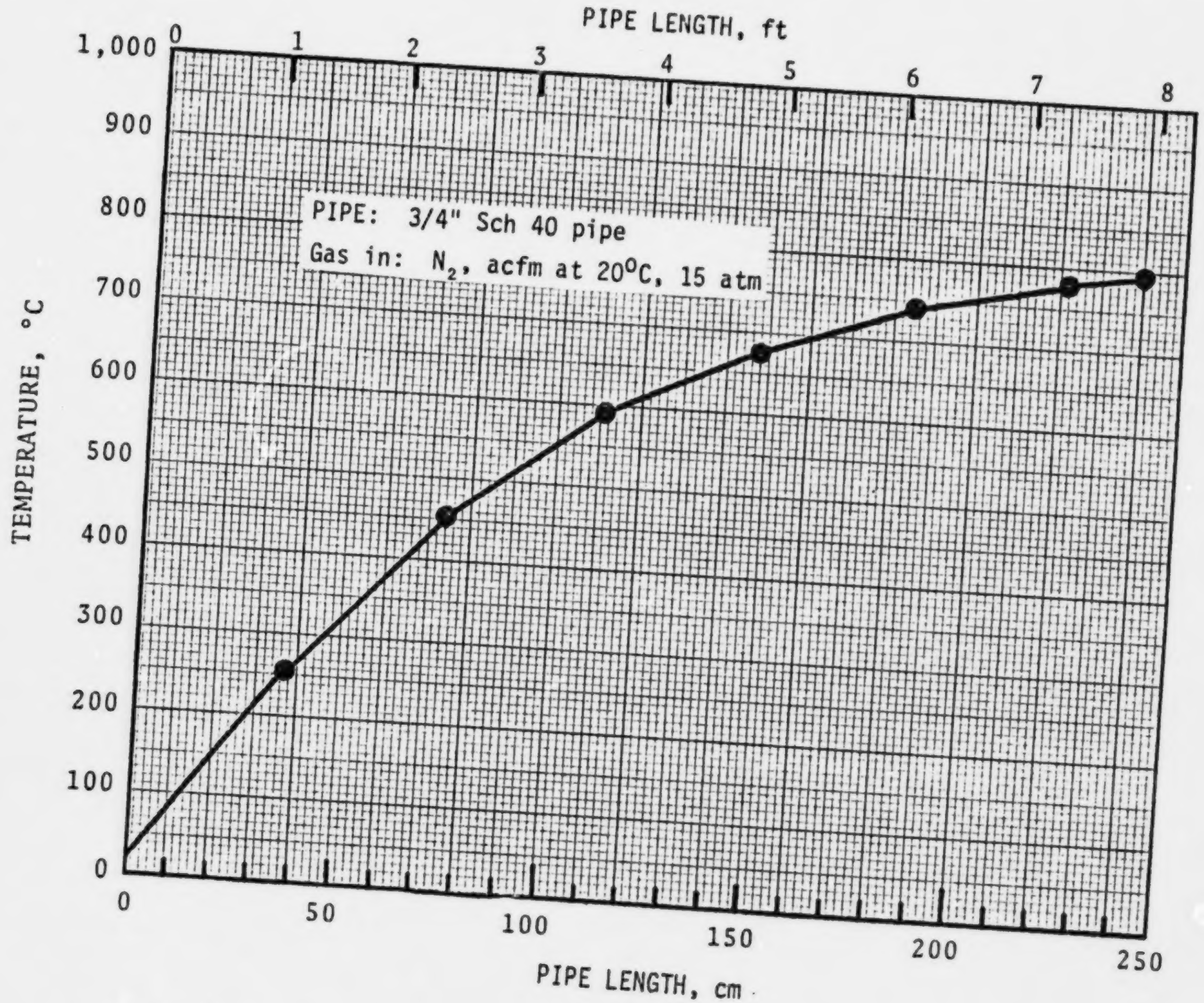

Figure 4. Theoretical design for primary heater.

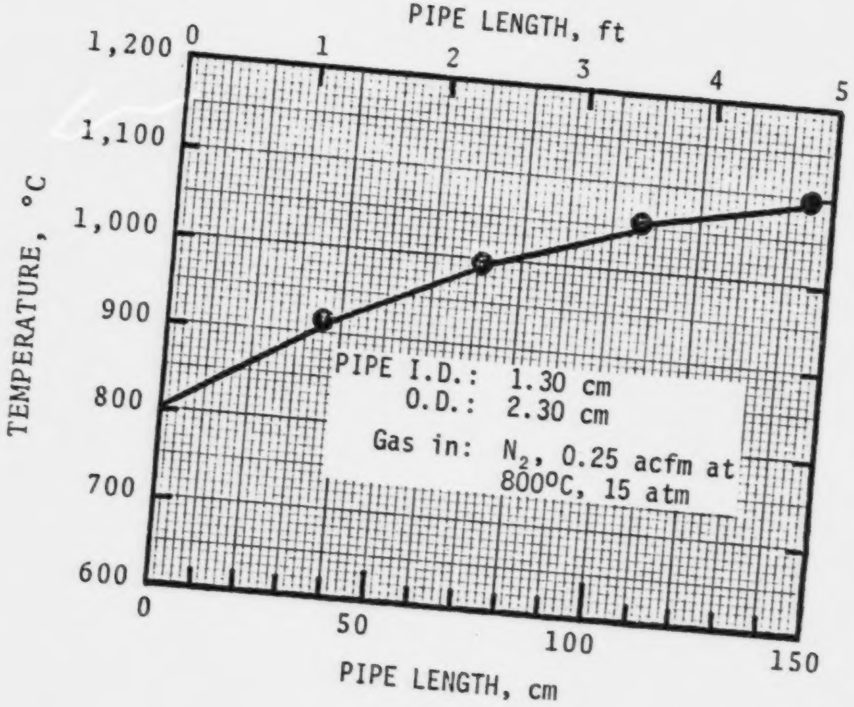

Figure 5. Theoretical design for secondary heater.

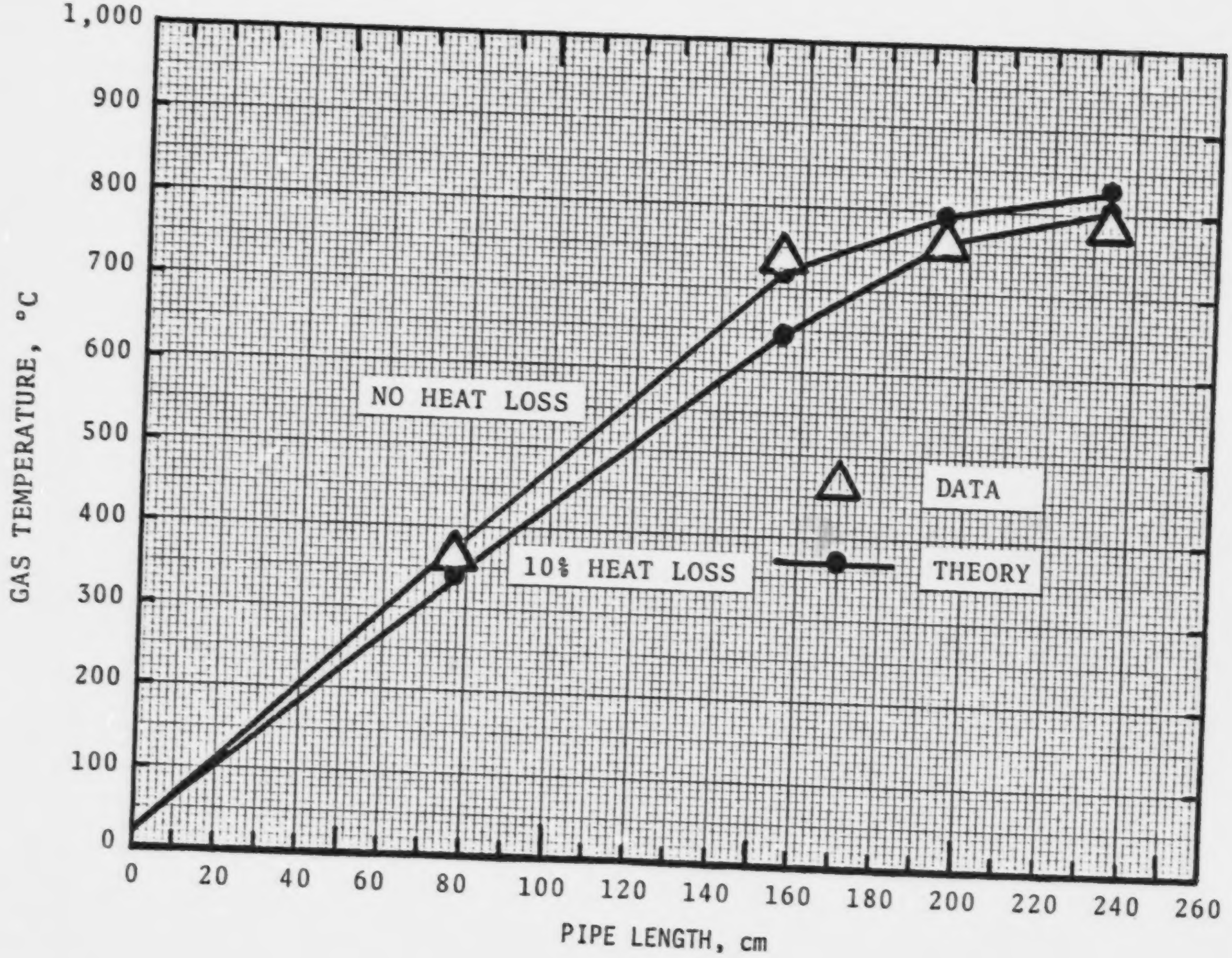

Figure 6. Results of heat transfer experiment.

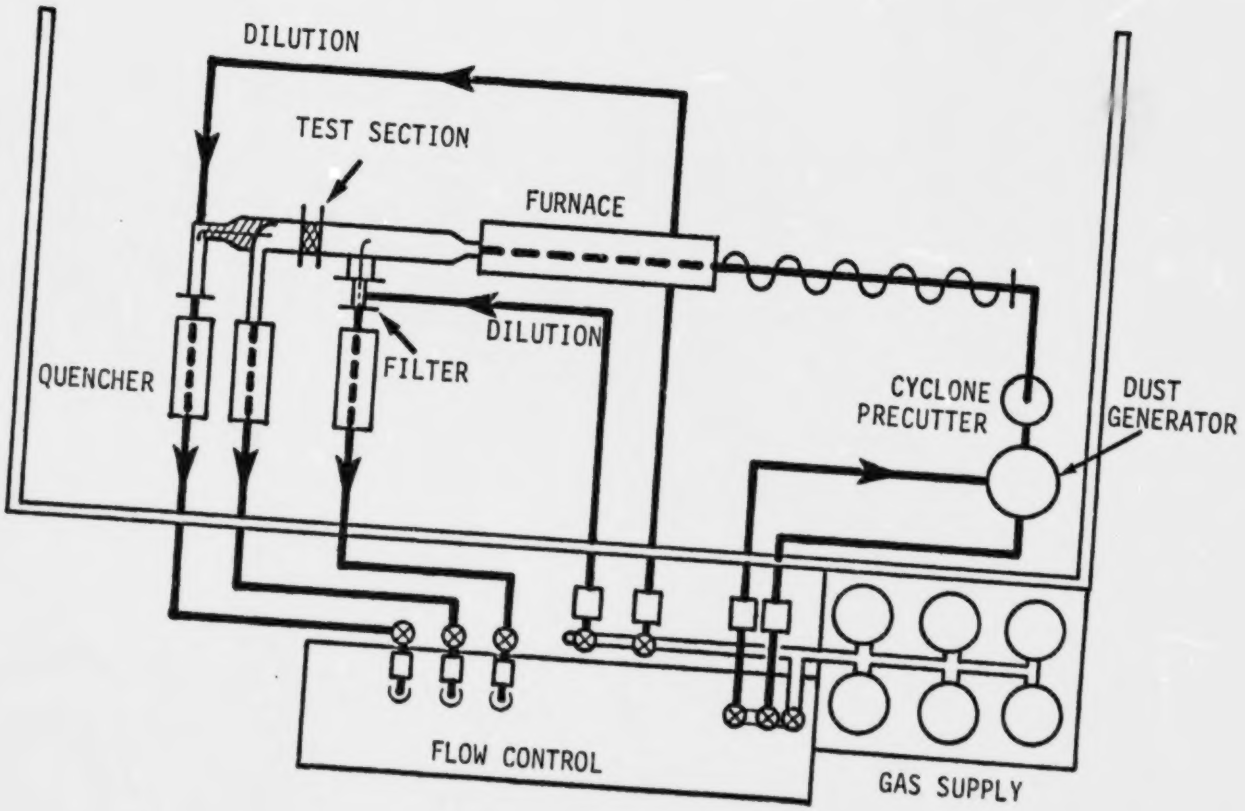
DILUTION
TEST SECTION
FURNACE
DILUTION
QUENCHER
FILTER
CYCLONE
PRECUTTER
DUST
GENERATOR
FLOW CONTROL
GAS SUPPLY

Figure 7. Test apparatus.

sample flow outlets were operated at room temperature and pressure. Other rotameters were at system pressure. All rotameters were calibrated at their operating pressure using a standard wet gas meter.

After leaving the final rotameters, the gas was vented.

Instrumentation

All temperatures, pressures, flow rates, and electrical power were monitored and controlled at the control panel located outside the protective barricade. The general setup is illustrated in Figure 7.

Temperatures were measured using type "K" thermocouples located on the pipe surface under each heating tape and furnace as well as in the gas stream at the inlets and outlets to the test section and sample filters. An 18-point dot recorder quasi-continuously monitored temperatures during heatup. A more accurate reading of the test section temperature was obtained using a digital multimeter.

Pressures were measured using gauges calibrated for the appropriate ranges. A photograph of the control panel is shown in Figure 8.

Protective Barricade

Because design codes for small high temperature and pressure piping were not available, it was necessary to design a protective barricade behind which all the high temperature and pressure components would be kept. No personnel access to the high temperature components was allowed during a test.

Various barricade structures were considered including wire rope blasting mats, concrete walls, and steel walls. For maximum safety and ease of fabrication 0.48 cm (3/16-inch) thick carbon steel walls were selected.

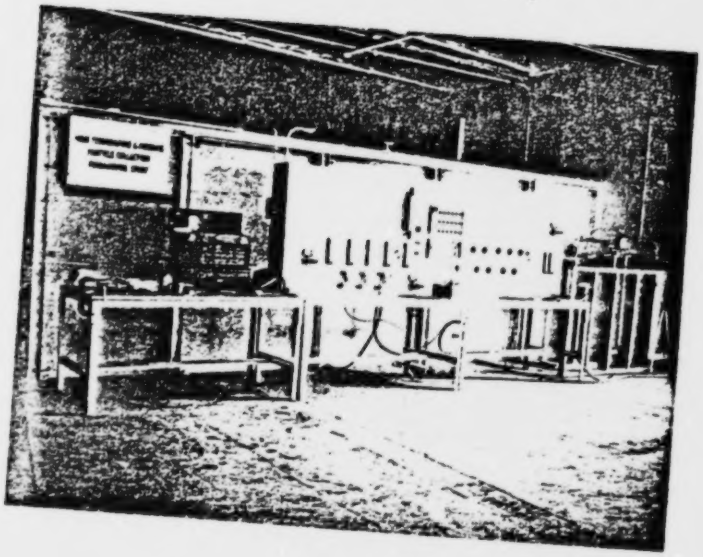

Figure 8. Control panel.

The maximum energy that would be released by failure of the test apparatus was assumed to be equal to the energy released by an isentropic expansion of the gas from the maximum temperature and system pressure to atmospheric pressure.

Using this information, estimates for total system volume and mass, and design equations presented by Moore (1972), it was determined that 0.48 cm 3/16-inch thick carbon steel would be sufficient to stop a missile resulting from pressure vessel failure.

The barricade, made of 0.48 cm thick carbon steel sheets was supported by 10 cm (4 in.) square "H" beams. It surrounded the test setup with three walls and a ceiling. The fourth wall was the concrete wall of the building. The barricade is effectively a steel-walled room inside which the experiment was conducted. All controls for the experiment were located outside the barricade (Figure 8) so that no one needed to be inside the barricade during a test.

Dust Generator

Two dust generator designs were used to redisperse fine fly ash dust at high pressure. The first design is illustrated in Figure 9. Fly ash and nickel spheres were loaded, batch-wise, into a steel pipe which had a blender blade mounted at the bottom and was heated to 150°C-200°C to remove moisture. The blade was coupled to an external electric motor through a graphite packing gland. When the motor was started the dust was dispersed into a cloud. A small flow of nitrogen was then used to blow the redispersed fly ash into the main gas stream.

The main gas stream passed through a Po^{210} ionizer before the fly ash was introduced into it. The positive and negative ions from the ionizer neutralized the static charge on the dust particles. A cyclone removed particles larger than 10 μm in diameter and the remainder of the particles and gas flowed to the

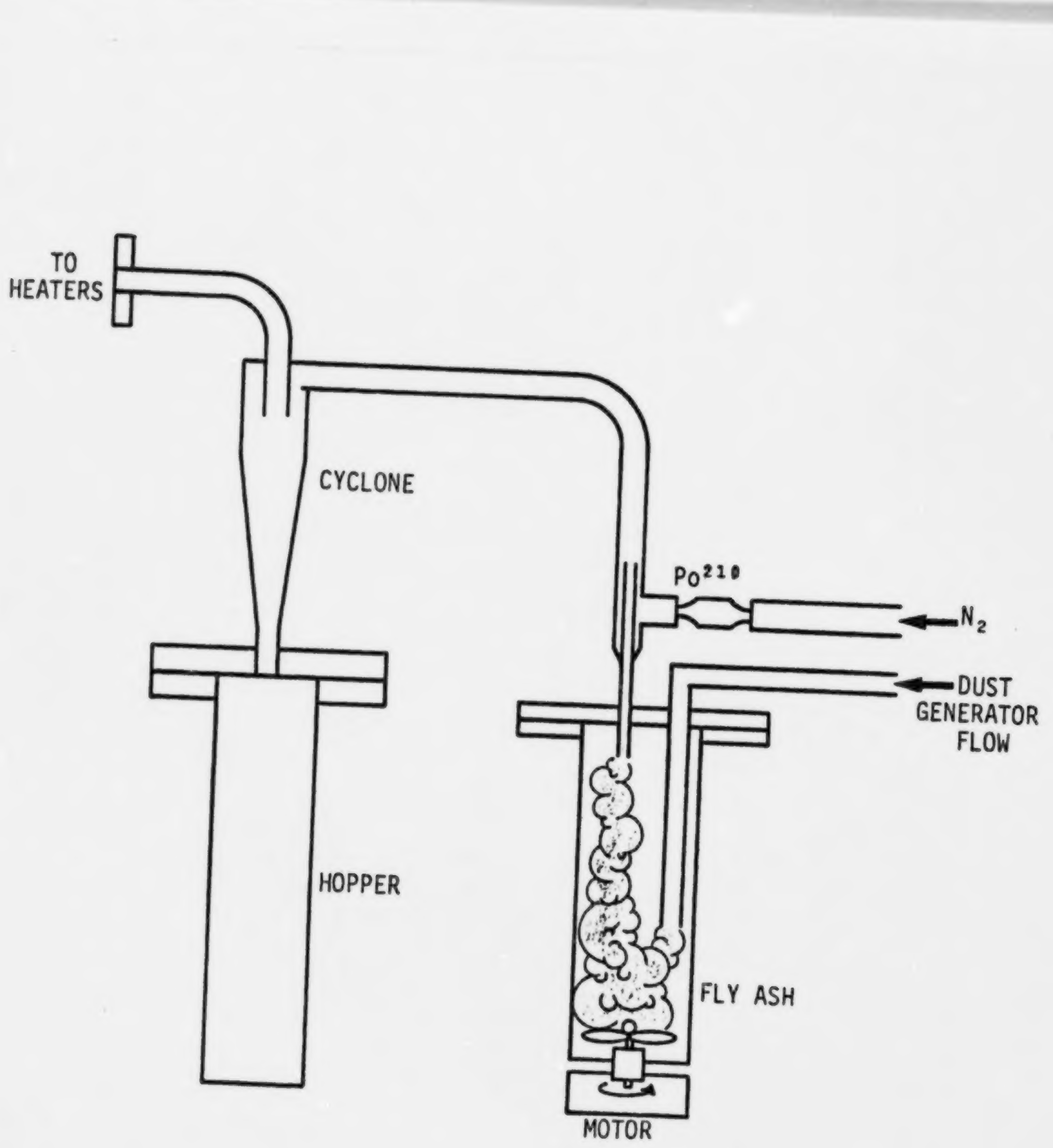
TO HEATERS
CYCLONE
HOPPER
Po^{210}
N_2
DUST GENERATOR FLOW
FLY ASH
MOTOR

Figure 9. Blender dust generator.

heater sections.

The dust generator put out a relatively steady flow of deagglomerated fly ash particles for periods of up to a few hours. However, this dust generator was later abandoned because of problem with the rotary blade shaft which seized repeatly during runs. The major cause of shaft seizure was fly ash working its way in between the shaft and the bearing. An air-purged bearing was tried but without much more success.

The second dust generator design is shown in Figure 10. It was a heated, batch-wise, fluidized bed of nickel spheres and fly ash. Fly ash was loaded into the bed before the start of each run. A portion of the total flow was used to fluidize the nickel bed. The bed movement deagglomerated fly ash particles which were then elutriated from the bed at a fairly steady rate. A Po^{210} ionizer and scalping cyclone were used in a similar way to that described for the blender dust generator.

The fly ash was from the baghouse of a pulverized coal-fired power plant. The particle density which was determined with a pycnometer (ASTM D153) was 2.3 g/cm^3.

Sampling System

The basic approach was to remove isokinetic samples at the inlet and outlet of the test section. The gas samples were then diluted, filtered and passed through flow monitoring and measurement instruments.

Details of the sampling arrangement are shown in Figure 11. The gas expanded from the secondary heater (1.37 cm diameter) to the main test section (5 cm diameter). The inlet sample probe was located approximately 50 cm downstream from the expansion and just upstream from the test section. The outlet probe was located 50 cm downstream from the test section. The probe was welded to the blind flange to prevent leakage. Another disk was welded to the probe near the branch "tee" entrance to minimize

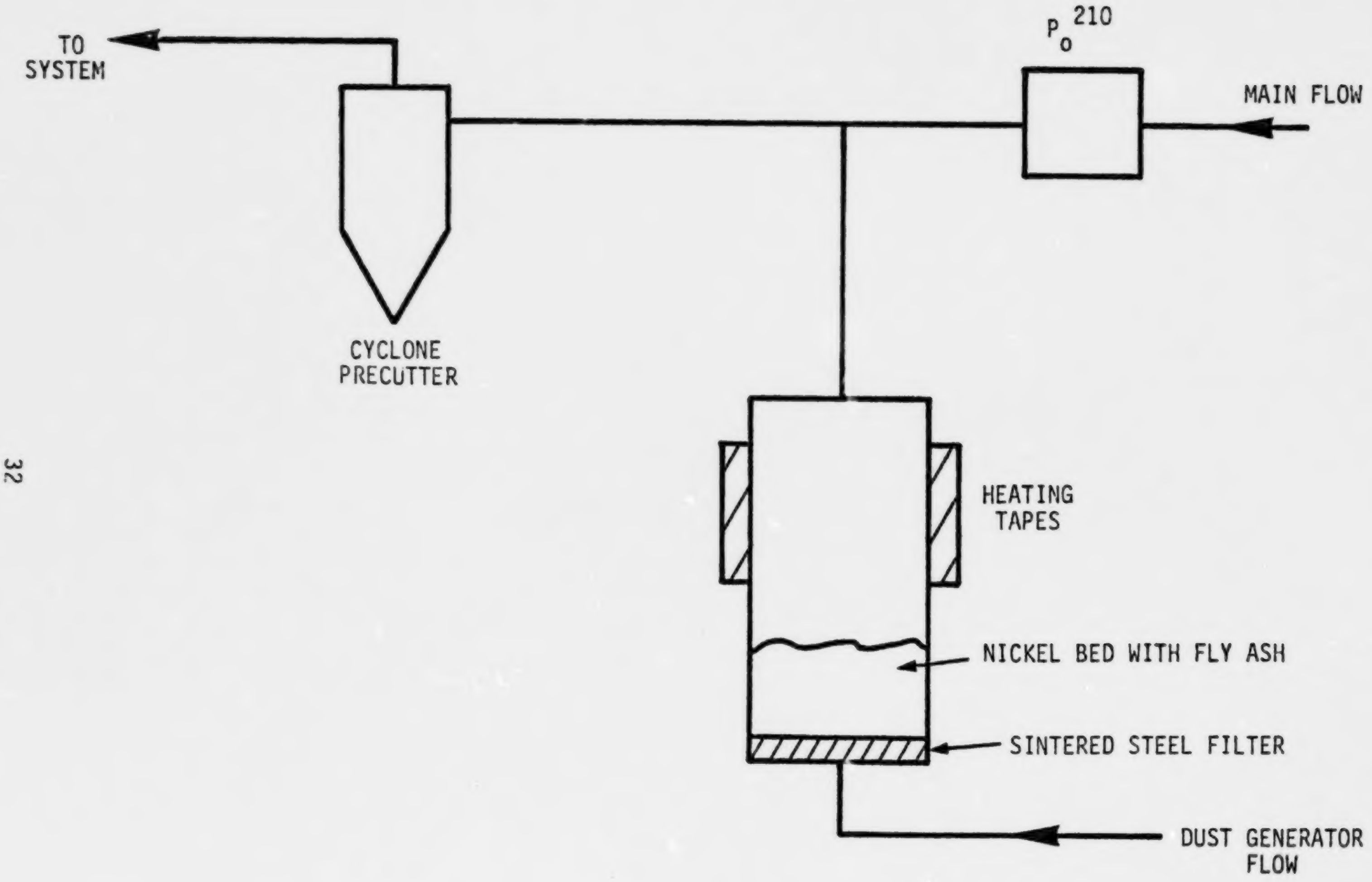
TO SYSTEM
P_o^{210}
MAIN FLOW
CYCLONE PRECUTTER
HEATING TAPES
NICKEL BED WITH FLY ASH
SINTERED STEEL FILTER
DUST GENERATOR FLOW

Figure 10. Batch-wise fluidized bed dust generator.

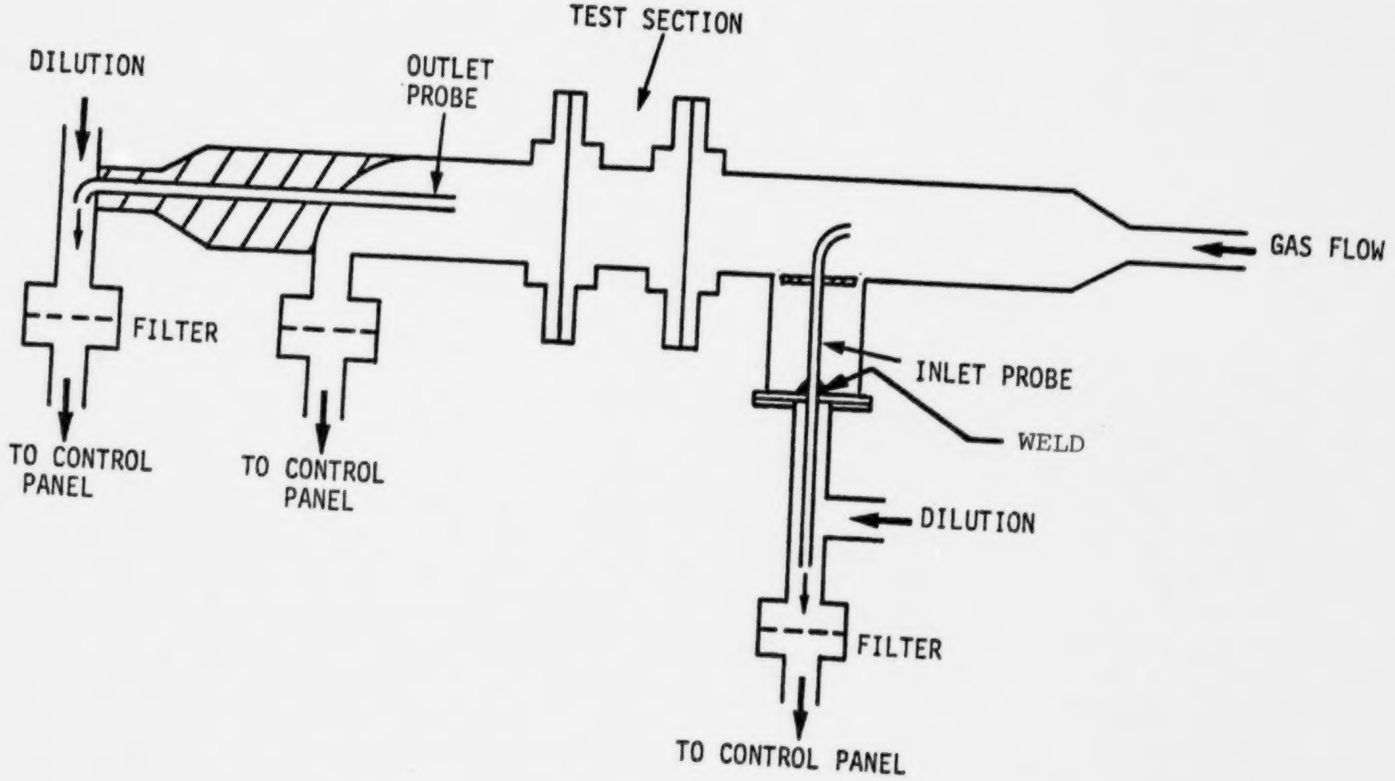
DILUTION
OUTLET PROBE
TEST SECTION
GAS FLOW
FILTER
TO CONTROL PANEL
TO CONTROL PANEL
INLET PROBE
WELD
DILUTION
FILTER
TO CONTROL PANEL

Figure 11. HTP sampling apparatus.

the disturbance and flow of gas into the branch "tee". After each test the probes and piping between the probe and filter were washed with acetone to remove any particles deposited there.

A number of ceramic and sintered metal filters were considered and tested for use at high temperature. Table 6 shows the measured penetration of 0.5 μm diameter monodisperse polystyrene latex particles through ceramic filter paper. The type H880J paper is by far the most efficient collector.

Sintered stainless steel filters also were able to collect better than 98% of 0.5 μm diameter particles. Both the ceramic and sintered steel filters presented analytical problems. When the filter was cleaned to remove the collected fly ash particles, it released a high level of background particles which masked the sample particles. The background from the sintered steel filter was somewhat reduced by prewashing in acetone, however the background could not be reduced sufficiently.

To overcome this problem, collecting a much larger sample was considered so that the majority of the collected dust would be in a surface cake and could be removed from the filter easily. This approach, however, would have required runs lasting 5 to 6 hours which could not be completed in a day because of the long heatup and cooldown times. Also, the impactor substrate overloaded after about 30-45 minutes and thus would have to have been replaced numerous times during the test. This would have impractically lengthened the time required to conduct an experiment.

The final approach selected was to use Nuclepore membrane filters for collecting particle samples. These filters must be kept below 100°C and therefore dilution gas was required for the hot tests.

Table 6. FILTER MATERIAL TEST RESULTS

FILTER	CONDITIONS	FILTER WEIGHT, mg/cm^2	ΔP, cm W.C. (in W.C.)	PENETRATION, %
BLANK (w/o Filter)	10 ℓ/min 12.5 ℓ/min	---	33.3 (13.1) 46.5 (18.3)	--- ---
GELMAN (61631 AE-Type)	10 ℓ/min 12.5 ℓ/min	7.7	55.7 (21.9) >64 (>25)	1.4 1.25
FIBERFRAX (970A Paper) (1/32 inch thick)	10 ℓ/min 12.5 ℓ/min	18.0	37.8 (14.9) 52.1 (20.5)	27 20
FIBERFRAX (H880A Paper) (1/32 inch thick)	10 ℓ/min 12.5 ℓ/min	17.9	40.4 (15.9) 54.4 (21.4)	2.7 2.5
FIBERFRAX (H880J Paper) (1/8 inch thick)	10 ℓ/min 12.5 ℓ/min	56.5	64 (25) >64 (>25)	<0.1 <0.1
FIBERFRAX (550F Paper) (1/16 inch thick)	10 ℓ/min 12.5 ℓ/min	35.3	42 (16.5) 56.6 (22.3)	25 16.3

Test Sections

Four different test sections were used in this project:

1. Inertial impactor
2. Cyclone separator
3. Screen diffusion battery
4. Electrical precipitator

Each section had a slightly different sampling arrangement. They will be discussed in detail in later sections of this report.

ANALYTICAL PROCEDURES AND DATA ANALYSIS

System Operation

The operation, sampling, and analytical procedures varied somewhat depending on the test sections being used. The general procedures described in the following were for the inertial impaction tests. Variations from these procedures for the cyclone separator, Brownian diffusion, and electrical migration work will be discussed later in the appropriate sections of this report.

An experiment was started by heating all piping up to the test temperature, then turning on the main gas flow and allowing the gas temperature to come to equilibrium. Small adjustments were made with the heaters to provide the proper test temperature. The test pressure was regulated when the gas flow was turned on. When the main gas flow had steadied out to the proper temperature and pressure, the sample flow lines were opened sufficiently to assure isokinetic samples were being taken. When all flows, temperatures and pressure were steady, sampling was started by turning on the dust generator. After the experiment had been completed (sampling duration varied from 15 minutes to 2 hours), the system was cooled down and disassembled.

The sample filters were removed and replaced with new filters, the impactor substrate was removed and replaced with a clean substrate, and the probes were removed and washed. The system was then reassembled and made ready for the next experiment.

Sample Handling

The probes were thoroughly rinsed with acetone and the rinse solution was then poured into a glass beaker. The beaker was heated to about 40°C in a water bath and the acetone was allowed to evaporate. The sample filter (inlet or outlet as appropriate) was added to the residue particles from the probe wash and the entire sample was redispersed in 200 ml of 3% NaCl electrolyte solution which had been filtered and prepared for Coulter counter analysis. An ultrasonic bath was used for redispersion along with 2-3 drops of an anionic dispersing aid (Coulter Type II A).

Aliquots of the dispersed, concentrated solutions were taken and further diluted to concentrations suitable for Coulter counter analysis. Generally two dilutions were required. The inlet and outlet samples were handled and diluted identically.

Coulter Analysis

A model TAII Coulter Counter was used for quantitative analysis of the size distribution and number of particles collected at the inlet and outlet. The Coulter counter was used in the manometer mode so that it counted and sized particles in a specific sample volume. The particles were separated into 16 size ranges with average particle diameters as listed in Table 7. Because of electrical interference, channel 1 reading was not reliable. There were also not enough particles in channels 11-16 to obtain reliable results. Therefore, analysis were concentrated on channels 2-10 (approximately 0.5 to 4 μm).

TABLE 7. SAMPLE TEST RUN #28-32

TEMPERATURE: 25°C

PRESSURE: 1 atm

Ch.	Average Particle Diameter, μm	Inlet Count "I"	Outlet Count "O"	Pt, fraction
1	0.45	---	---	--
2	0.57	104,500	107,300	1.0
3	0.71	84,900	87,300	1.0
4	0.90	81,700	80,900	1.0
5	1.13	95,300	91,300	0.95
6	1.43	84,700	78,000	0.92
7	1.80	67,800	60,100	0.89
8	2.26	38,700	33,000	0.85
9	2.85	18,400	14,700	0.80
10	3.60	4,830	3,660	0.76
11	4.52			
12	5.70			
13	7.18			
14	9.04			
15	11.39			
16	>12.7			

Four blank (without the test section) tests were run to check that the sampling system was working properly. The data from the four runs are shown in Tables 7 through 10. There was only open pipe between the inlet and outlet samples so that ideally the penetration should have been 100% for all particle sizes. The mean penetration measured was 96% with a standard deviation of 8%. Thus on average our sampling system is adequate (within 4%) however there is some uncertainty from run to run.

One potential problem in Coulter counter analysis is that particles which were agglomerates in the gas stream may be redispersed and then detected as single particles. To investigate this problem particles were sampled simultaneously with cascade impactor and filter. The filter sample was analyzed with Coulter counter as described above. Figure 12 shows the measured particle size distributions for the two methods. The Coulter counter results had been converted to mass distribution with the measured particle density of 2.3 g/cm³. It can be seen from Figure 12 that the measured size distribution with the two instruments were close to each other. Deagglomeration by the Coulter counter did occur. However, the amount of fly ash deagglomeration was small. It seems the fluidize bed particle generator was effective in deagglomerating the fly ash and producing individual fly ash particles for test purpose. For the size range of interest (0.4 to 4 µm diameter), the difference between cascade impactor and Coulter counter measurements was small. Therefore, Coulter counter was used for all experiments.

Data Reduction

The Coulter Counter data were used to obtain fractional penetration or fractional efficiency curves by two methods. The first method used the total particle count in each channel and divided the outlet data by the inlet data to get a penetration corresponding to that channel mean diameter. The second method used the Coulter Counter size distribution expressed as a cumula-

TABLE 8. SAMPLE TEST RUN #28-34

TEMPERATURE: 25°C

PRESSURE: 1 atm

Ch.	Average Particle Diameter, μm	Inlet Count "I"	Outlet Count "O"	Pt, fraction
1	0.45	---	---	--
2	0.57	212,900	219,800	1.03
3	0.71	166,200	170,400	1.02
4	0.90	134,000	134,100	1.00
5	1.1	123,200	123,800	1.00
6	1.4	82,800	80,400	0.97
7	1.8	53,200	49,600	0.93
8	2.3	26,200	24,000	0.91
9	2.8	12,100	11,600	0.96
10	3.6	3,100	3,100	1.00
11	4.5			
12	5.7			
13	7.2			
14	9.0			
15	11.4			
16	>12.7			

TABLE 9. SAMPLE TEST RUN #28-35

TEMPERATURE: 25°C

PRESSURE: 1 atm

Ch.	Average Particle Diameter, μm	Inlet Count "I"	Outlet Count "O"	Pt, fraction
1	0.45	---	---	--
2	0.57	130,600	126,600	0.97
3	0.71	105,600	97,900	0.93
4	0.9	97,100	89,100	0.92
5	1.1	109,200	99,900	0.91
6	1.4	89,800	83,700	0.93
7	1.8	69,700	64,900	0.93
8	2.3	39,100	35,700	0.91
9	2.8	19,500	17,300	0.89
10	3.6	5,200	4,400	0.84
11	4.5			
12	5.7			
13	7.2			
14	9.0			
15	11.4			
16	>12.7			

TABLE 10. SAMPLE TEST RUN #28-36

TEMPERATURE: 25°C

PRESSURE: 1 atm

Ch.	Average Particle Diameter, μm	Inlet Count "I"	Outlet Count "O"	Pt, fraction
1	0.45	---	---	--
2	0.57	93,300	94,100	1.01
3	0.71	73,900	76,400	1.03
4	0.9	67,200	69,900	1.04
5	1.1	72,900	76,500	1.05
6	1.4	57,300	60,500	1.06
7	1.8	40,200	42,600	1.06
8	2.3	20,300	21,700	1.07
9	2.8	9,400	9,500	1.01
10	3.6	2,600	2,400	0.91
11	4.5			
12	5.7			
13	7.2			
14	9.0			
15	11.4			
16	>12.7			

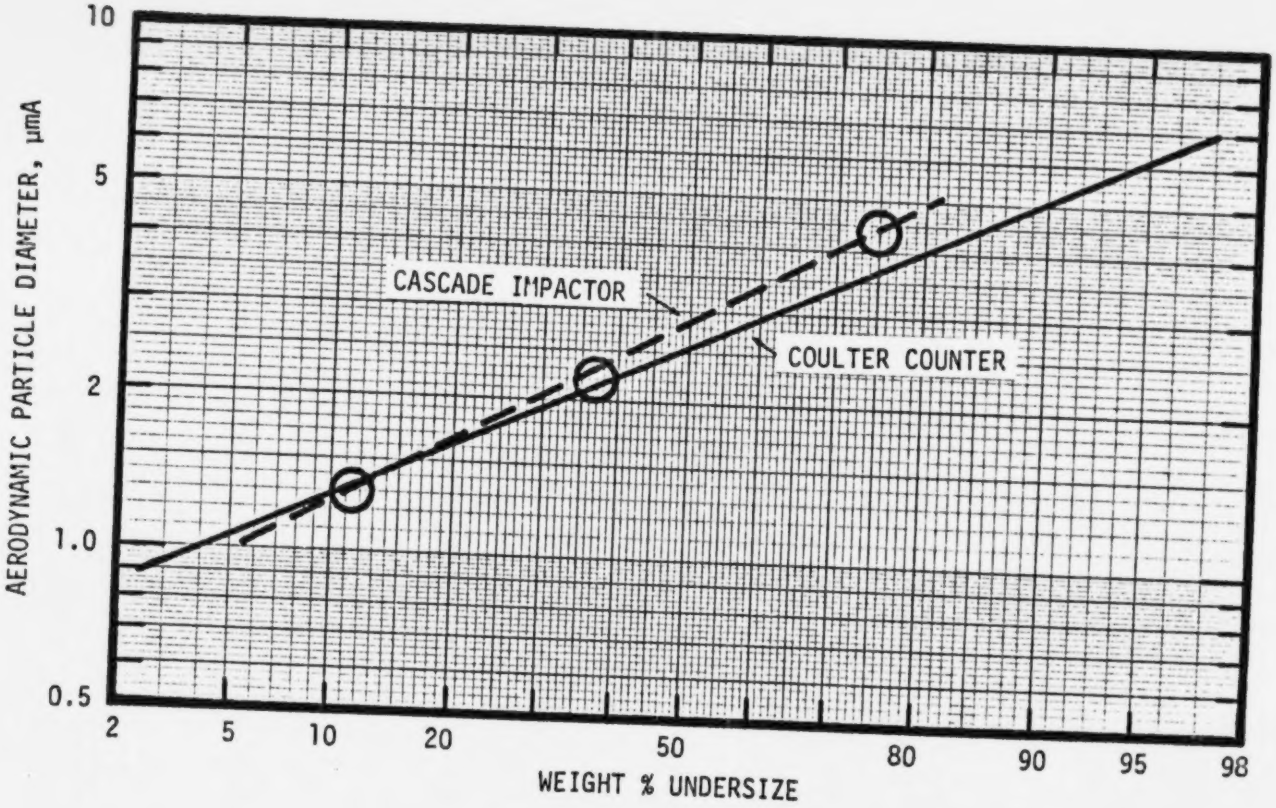

Figure 12. Fly ash size distribution.

tive volume concentration for the inlet and outlet. These data were used as input to a computer routine which fits a spline curve to the data and calculates "$dV/d(\log d_p)$" for several particle diameters (Lawless, 1978). The penetration was then calculated by dividing the outlet "$dV/d(\log d_p)$" by the inlet "$dV/d(\log d_p)$" at the same diameter. The resulting grade penetration curves by these two methods are close to each other as can been in Figure 13.

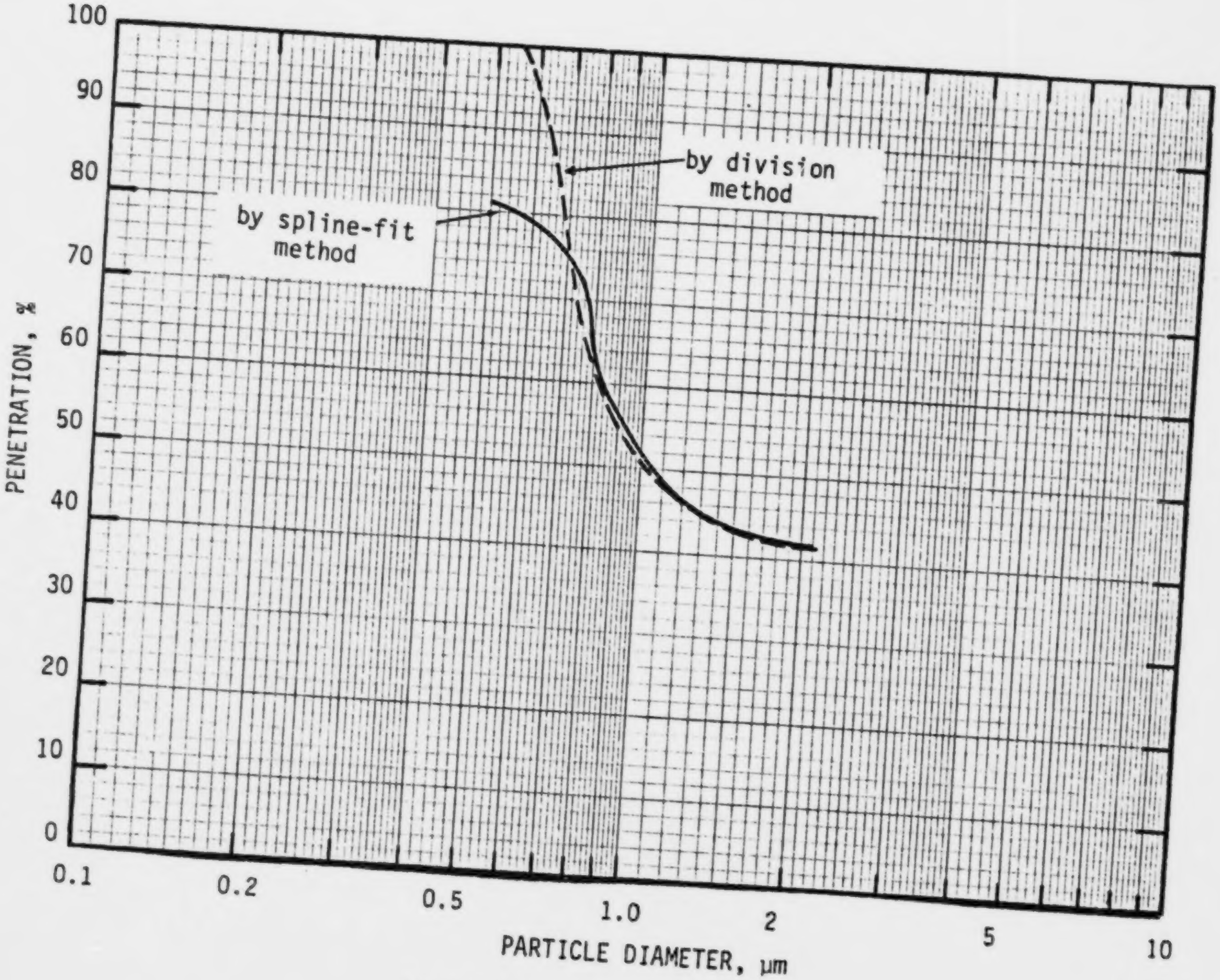

Figure 13. Hot Test: 300°C, 1 atm

SECTION 4
INERTIAL IMPACTION

Inertial impaction is the term used to describe the separation of solid particles from a gas by impingement against a target. Large particles impact the target while the fine particles and gas are diverted around it. The driving force for collection is the particle inertia. Therefore collection by inertial impaction will increase with the particle velocity, diameter, and density.

Inertial impaction is the mechanism responsible for particle separation in sizing instruments such as cascade impactors and very small cyclones. It also is one of the primary collection mechanisms in gas cleaning equipment for particles larger than a few tenths of a micrometer in diameter.

In this study, the theoretical basis for predicting the collection efficiency of inertial impaction devices at high temperatures and pressures has been studied and evaluated experimentally. The preliminary theoretical review was reported by Calvert and Parker (1977). In this section, an elaboration on the earlier theoretical work as well as the results of the experimental program are presented.

THEORY

Stokes' Law

The major difference between the collection of particles at normal conditions and at high temperature and pressure is in the resistance force of the gas. For a rigid spherical particle moving through a continuous viscous gas at constant relative velocity, and for negligible inertial effects arising from the gas being displaced by the particle, the resistance force, F_r, is given by Stokes' Law:

$$F_r = - 3\pi \mu_G d_p u_r \qquad (1)$$

where "μ_G" is the gas viscosity, "d_p" is the particle diameter, and "u_r" is the relative velocity between the particle and the gas. The negative sign indicates that the drag force is opposite to the direction of motion of the particle.

Equation (1) must be modified for non-continuum effects when the mean free path of the gas molecules becomes significant in comparison with the particle diameter. The modified Stokes' Law becomes:

$$F_r = \frac{-3\pi \mu_G d_p u_r}{C'} \qquad (2)$$

The correction factor, C', is referred to as the "Cunningham slip correction factor" and will be discussed in more detail later.

Equations (1) and (2) are valid only for Reynolds numbers, N_{Re}, smaller than one. That is,

$$N_{Re} = \frac{d_p u_r \varrho_G}{\mu_G} < 1 \qquad (3)$$

where "ϱ_G" is the gas density.

For larger "N_{Re}", the drag force may be calculated as:

$$F_r = -C_D \frac{\pi d_p^2 \varrho_G u_r^2}{8 C'} \qquad (4)$$

where "C_D" is the drag coefficient for spheres. The relationship between the drag coefficient and N_{Re} is illustrated in Figure 14. Figure 14 also shows comparison between the drag coefficient corresponding to Stokes' Law and experimental data (from Fuchs,

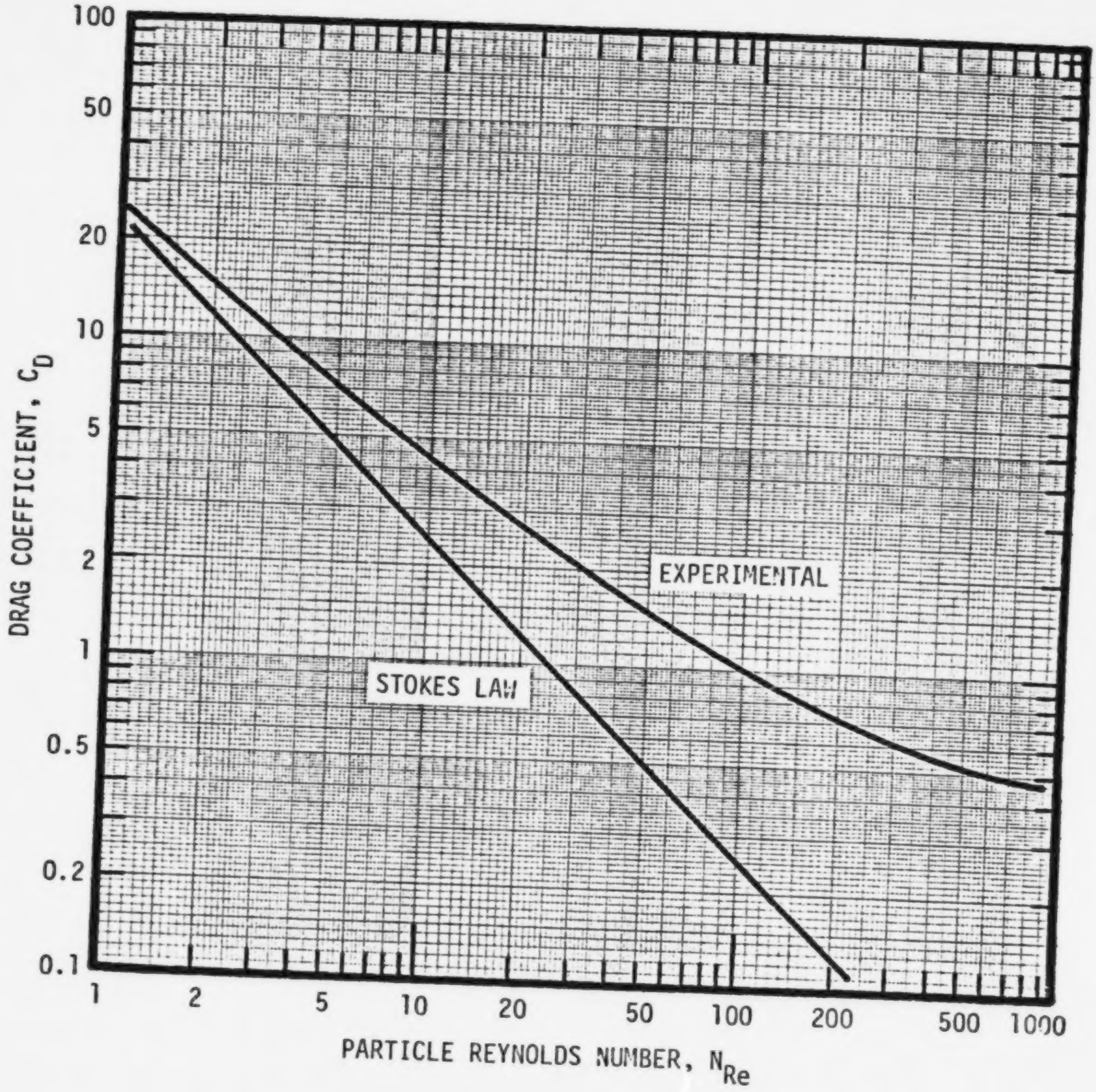

Figure 14. Drag coefficient as a function of particle Reynolds number.

1964) for large Reynolds numbers. In most high pressure situations, "N_{Re}" is larger than one and equation (4) should be used to predict the drag force rather than equation (2).

Inertial Impaction

The dimensionless parameter which characterizes the extent to which particles are removed by inertial impaction is the inertial impaction parameter, K_p. It is defined as the ratio of the particle stopping distance to the characteristic dimension of the collector. Derivations of this dimensionless number have been presented by many authors in the field of aerosol science, including Fuchs (1964), and Hidy and Brock (1970).

For any particle Reynolds number, the inertial impaction parameter may be expressed by this general formula.

$$K_p = \frac{8\ d_p\ \varrho_p\ C'}{3\ \varrho_G\ d_c}\ f(N_{Re}) \qquad (5)$$

where

$$f(N_{Re}) = \frac{3\ \varrho_G\ K_p\ d_c}{8\ d_p\ \varrho_p\ C'} = \frac{3\ \varrho_G\ x_s}{4\ d_p\ \varrho_p} \qquad (6)$$

"d_c" is any characteristics length of the collector and "x_s" is the particle stopping distance.

Using the drag coefficient data of Lapple and Shepherd (1940), a graphical solution for $f(N_{Re})$ was obtained (Figure 15).

For low Reynolds numbers, $f(N_{Re})$ reduces to the familiar form: $N_{Re}/24$ and,

$$K_p = \frac{C'\ d_p^2\ \varrho_p\ u_r}{9\ \mu_G\ d_c} \qquad (7)$$

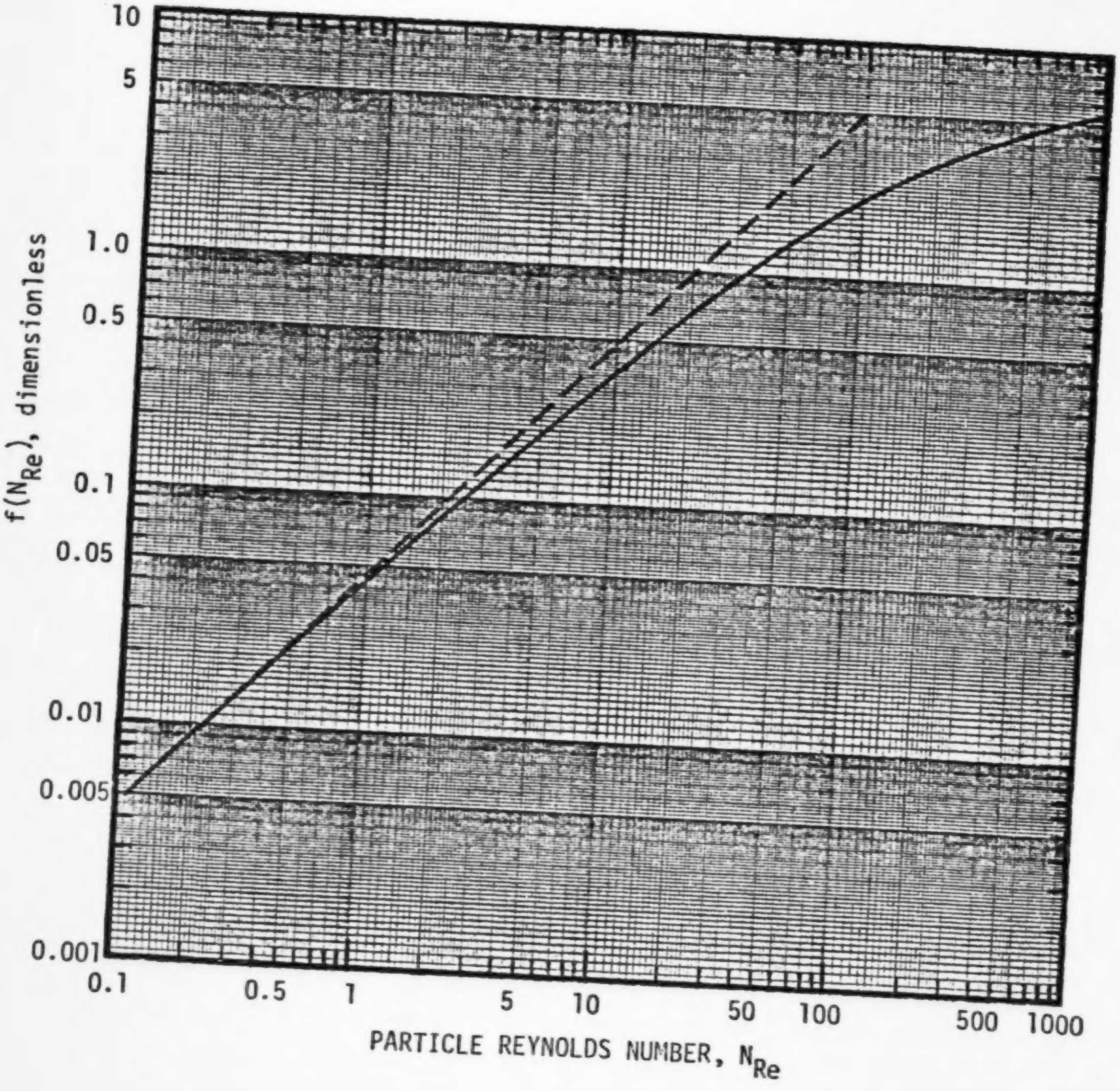

Figure 15. Stopping distance for particle Reynolds numbers beyond the Stokes region.

Slip Correction Factor

The major uncertainty in the application of equation (2) at high temperatures and pressures is in the Cunningham slip correction factor, C', used to modify Stokes' Law. It is an empirical factor first proposed by Cunningham (1910), later evaluated using the data of Millikan (1923a, b). The form used here was presented by Davies (1945) as:

$$C' = 1 + N_{Kn} \left[1.257 + 0.400 \exp\left(-1.10/N_{Kn}\right)\right] \qquad (8)$$

where "N_{Kn}" is the Knudsen number, defined by:

$$N_{Kn} = \frac{2\, l_f}{d_p} \qquad (9)$$

and where "l_f" is the mean free path of the gas molecules. The temperature and pressure dependence of the mean free path is shown in equation (10) where the subscript "o" denotes values at some known conditions, and where temperature and pressure are expressed in absolute units.

$$\frac{l_f}{l_{fo}} = \frac{\mu_G}{\mu_{Go}} \frac{P_o}{P} \left(\frac{T}{T_o}\right)^{1/2} \qquad (10)$$

At 293°K and 1 atm the mean free path for air molecules is 0.065 μm (Calvert and Parker, 1977).

The constants in equation (8) are based on experimental data for Knudsen numbers from 0 to greater than 100 (Millikan, 1923b). The experiments were at low pressure (about 0.003 atm) and room temperature (20°C to 25°C). Therefore consideration must be given to their applicability at high temperatures and pressures.

Equation (8) may be written in the general form:

$$C' = 1 + N_{Kn} \left| A + B \exp\left(-c/N_{Kn}\right) \right| \qquad (11)$$

Equation (11) may then be broken down into the two cases:

$$C' = 1 + A\, N_{Kn} \qquad (12)$$

for small "N_{Kn}"; and

$$C' = 1 + (A + B) N_{Kn} \qquad (13)$$

for large "N_{Kn}". The constant "c" in equation (11) is used to interpolate between equations (12) and (13) for intermediate Knudsen numbers.

The theoretical basis for equation (12) was discussed by Millikan (1923a). He found that for air and oil drops at 23°C:

$$A = 0.998 \left(\frac{2}{a_m}\right) - 1 \qquad (14)$$

where "a_m" is the fraction of molecules that are diffusely reflected from the particle surface. The constant "0.998" was obtained using the Chapman and Enskog definition of the mean free path as presented by Davies (1945). Millikan stated that equation (14) is valid as long as the term "$2/a_m$" is not very large compared to unity.

At large Knudsen numbers, the gas molecules are independent of each other and the particle is in the free molecular regime. The drag force on the particle depends on the momentum transfer between the gas molecules and the particle surface. Millikan (1923b) showed that equation (13) is also a function of "a_m" and determined bounds for the constant "A+B". That is,

$$(A + B) = 2.455 \qquad \text{for } a_m = 0 \qquad (15)$$

$$(A + B) = 1.612 \qquad \text{for } a_m = 1 \tag{16}$$

Therefore, the constants in equation (11) are a function of the momentum transfer between the gas molecules and the particle surface, and most likely are bounded by equations (14), (15), and (16). The effects of temperature and pressure on the constants in equation (11) will come in through the factor "a_m", which is the momentum accomodation coefficient.

Willeke (1976) discussed the temperature dependence of particle slip in a gaseous medium. He considered temperature up to 727°C (1,000°K). He assumed that Millikan (1923a) had recorded the maximum range of reflection coefficients (momentum accommodation), and estimated that the maximum error in the drag force (and hence slip correction) resulting from a lack of knowledge of the exact degree of accommodation would be ± 3%.

The maximum range of reflection coefficients found by Millikan was from 0.75 (air-fresh shellac) to 1.00 (air-mercury). These measurements were at room temperature. It is possible that at extreme temperatures, the degree of accommodation could be even lower than that measured by Millikan.

Wachman (1962) reviewed the theory and experimental data for momentum transfer between free molecules and surfaces. He showed that the drag coefficient is proportional to the square root of the energy (thermal) accommodation coefficient, "a_t", where "a_t" generally can be expressed by:

$$a_t = \frac{T_r - T_g}{T_s - T_g} \tag{17}$$

and where "T_g" is the absolute temperature of the incident gas molecule, "T_r" is the temperature of the reflected gas molecule, and "T_s" is the temperature at the particle surface.

The experimental data reviewed by Wachman (1962) generally showed "a_t" decreasing with increasing gas temperature. This would imply that the drag coefficient, and hence "a_m" would also decrease with increasing temperature and thereby influence the constants in equation (11). The accommodation coefficient was found to be independent of gas pressure.

Other authors have also found the accommodation coefficients to decrease with increasing temperature, including: Stickney (1962), Wachman (1966), Goodman and Wachman (1967), Byers and Calvert (1967), Goodman (1969), and Ramesh and Marsden (1974).

Ramesh and Marsden (1974) obtained the following empirical equation for the slope of the "a_t" versus surface temperature curve, for nitrogen impinging on a surface.

$$\frac{d\,a_t}{d\,T_s} = (-13.7 + 0.09\,M_s) \times 10^{-4} \qquad (18)$$

where "M_s" is the molecular weight of the surface material. From equation (18), it can be predicted that "a_t" will decrease with increasing temperature for any surface material whose molecular weight is less than about 150. If it is assumed that fly ash is 50% SiO_2, 25% Fe_2O_3, and 25% Al_2O_3, then the average molecular weight will be approximately 100.

From the above discussion, it appears that high temperature drag forces should be smaller than would be predicted by using equations (2) and (8). The constants in equation (8) should increase with temperature to account for the less efficient momentum transfer between the molecules and the surface observed at high temperatures. These observations, however, are based on data taken with clean, pure surfaces and gases. Wachman (1962) notes that the accomodation coefficient can increase significantly with the buildup of an absorbed gas layer on the surface. Therefore it is not possible to infer any quantitative information concerning the accommodation coefficient of effluent gases on fly ash particle surfaces.

If the constants in equation (11) are bounded by equations (15) and (16), the maximum increase in "C'" would probably be smaller (because N_{Kn} is smaller) but equation (14) is not valid as "a_m" approaches zero, so the maximum allowable size of the constant "A" in equation (11) cannot be determined.

In summary, inertial impaction is expected to be somewhat less effective at high temperature than would be predicted by accounting for the effects of temperature on gas viscosity and mean free path. In terms of cut diameters, the inertial impaction cut diameters are expected to be slightly higher than predicted at high temperature. The high pressure data is not expected to be noticeably different from the predictions.

APPARATUS

The experimental apparatus was described in detail in an earlier section of this report. The details of the sampling arrangement are shown in Figure 16. The gas and fly ash particles were sampled isokinetically upstream and downstream from the impactor. The impactor was sandwiched between two flanges so that all the gas flows through it.

The impactor test section is shown in detail in Figure 17. For most of the runs, a jet plate which had 12 jet holes of 1.4 mm in diameter was used. Run Number 33-25 used a jet plate with 12 holes, 2.6 mm in diameter.

Particles were collected on ceramic fiber paper substrates (Fiberfrax grade 970-C) in order to minimize particle bounce at the impaction plate and to facilitate sample removal and analysis. The substrates were pretreated by baking for 30 minutes at 200°C. This treatment burns off the organic binder so that a stable substrate weight can be maintained for high temperature tests. One consequence of the pretreatment is that without the binder, the substrate tears very easily and is

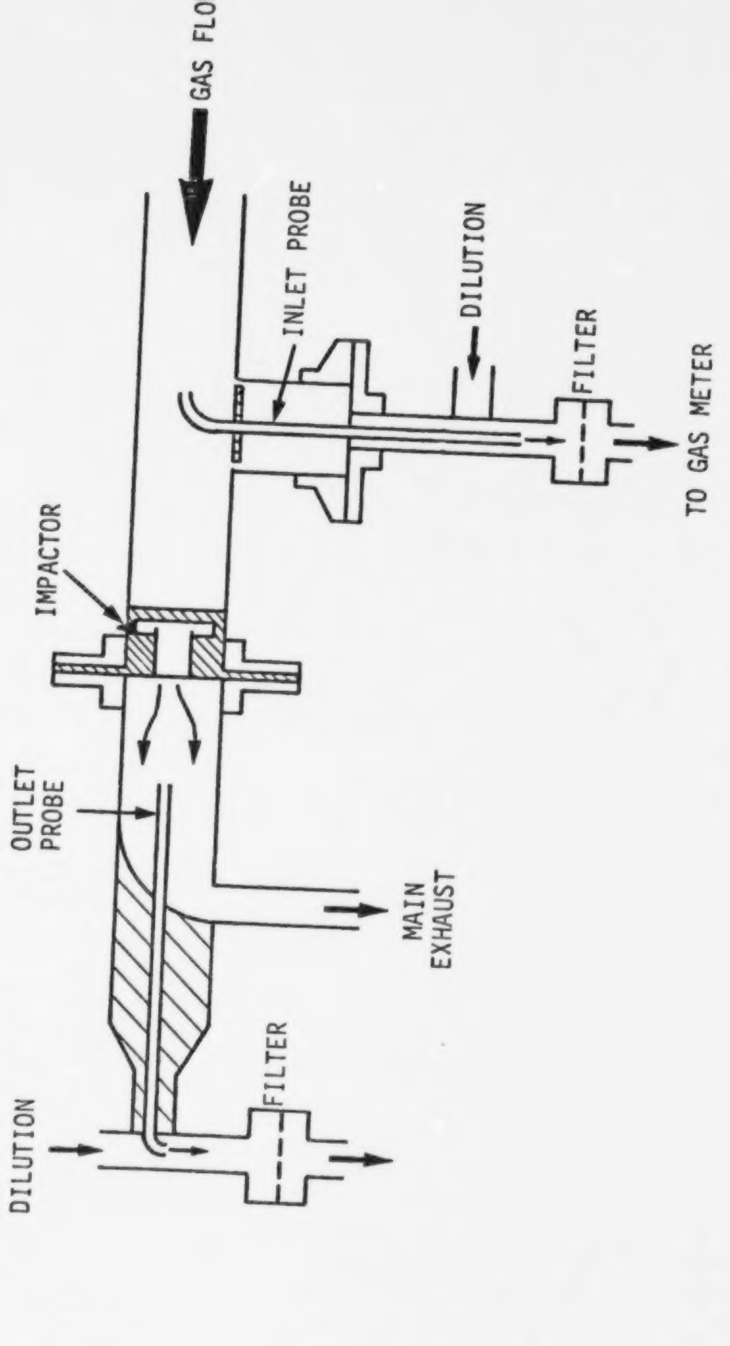
GAS FLOW
INLET PROBE
DILUTION
FILTER
TO GAS METER
IMPACTOR
OUTLET PROBE
MAIN EXHAUST
FILTER
DILUTION

Figure 16. HTP sampling apparatus, for impaction studies.

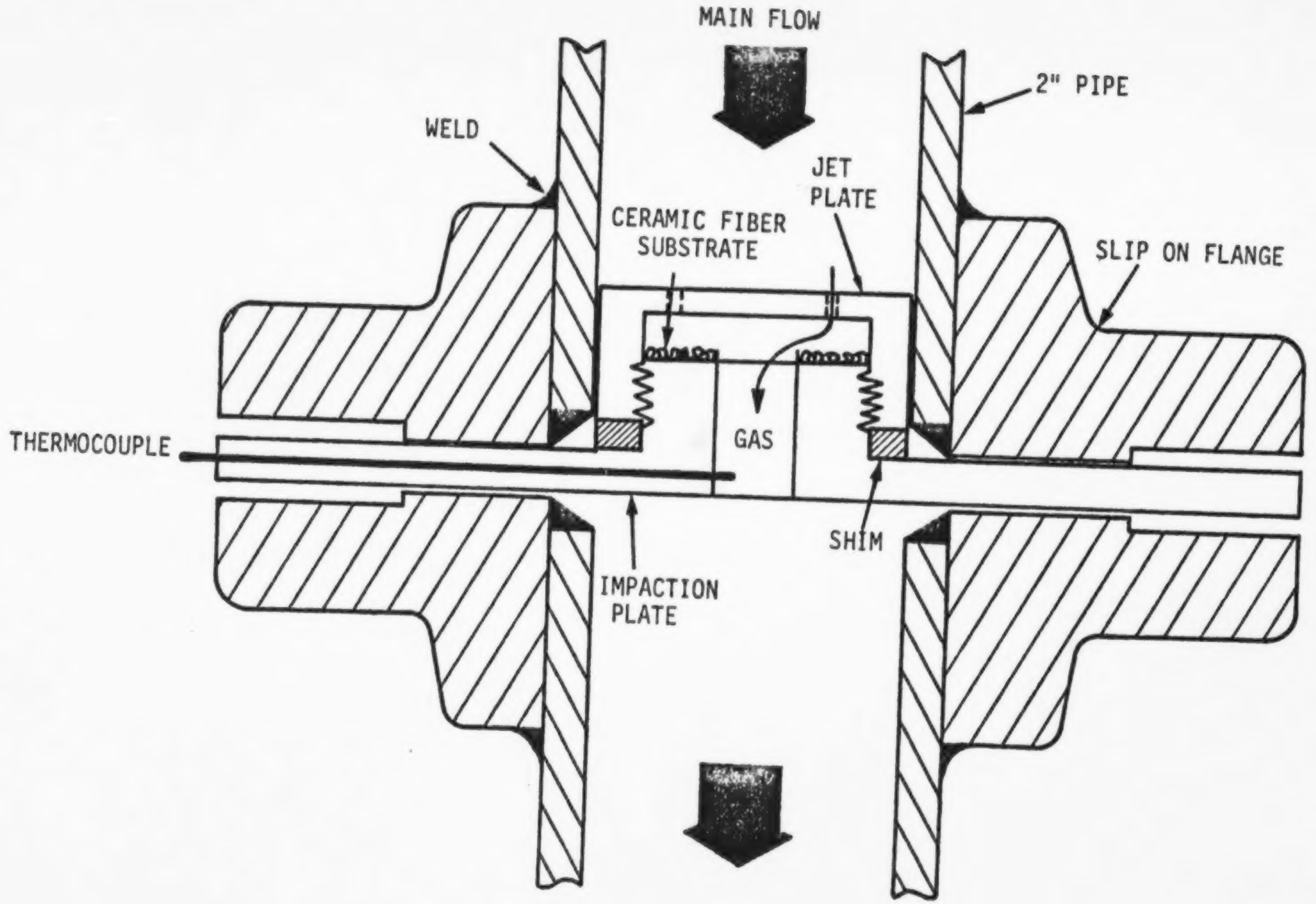
MAIN FLOW
WELD
2" PIPE
JET
PLATE
CERAMIC FIBER
SUBSTRATE
SLIP ON FLANGE
THERMOCOUPLE
GAS
SHIM
IMPACTION
PLATE

Figure 17. Inertial impaction test section.

difficult to handle.

Bare metal substrates were tried as substrates but they resulted in excessive particle bounce for high temperature runs. No useful cut diameter data were obtained with bare metal substrates operating at high temperatures. Jet velocities for these experiments ranged from 900 to 1,200 cm/s.

Calibration

In order to properly characterize the impactor cut diameter, it was necessary to perform a calibration. The calibration was conducted with a method similar to that reported by Calvert et al. (1976).

The calibration was done at room temperature and pressure in the laboratory using 1.1 μm monodisperse, polystyrene latex particles. The particle concentration entering and leaving the impactor was measured with an optical particle counter. The impaction plate was lined with ceramic fiber paper (0.25 mm thick) which was the same type used in the test section.

The experimental particle penetration was plotted against inertial impaction parameter which was calculated from the following equation:

$$K_p = \frac{4\ d_p^2\ \rho_p\ C'\ Q}{9\ \pi\ \mu_G\ d_h^3\ N} \qquad (19)$$

where: d_p = particle diameter, cm
ρ_p = particle density, g/cm³
C' = slip correction factor, dimensionless
Q = total volumetric flow rate, cm³/s
μ_G = gas viscosity, g/cm-s
d_h = jet hole diameter, cm
N = number of jet holes, dimensionless

The penetration curve obtained from the calibration (Figure 18) was used to determine the inertial impaction cut parameter "K_{p50}" which is the value of "K_p" at 50% penetration. From Figure 18, $K_{p50} = 0.22$.

"K_{p50}" is used to characterize the impactor and is assumed to be a constant. The basic assumption here is that the calibrated value of "K_{p50}" is a function of impactor geometry and is independent of gas temperature and pressure. Maximum thermal expansion of the jet nozzles was less than 0.15% of the jet diameter, and therefore was negligible.

RESULTS

The results of the inertial impaction tests are summarized in Table 11. Tests were run at temperatures from 26 to 816°C, pressures from 110 to 149 kPa, and jet velocities from 3.7 to 28.7 m/s.

The Coulter counter data were reduced into grade penetration curves. Figure 19 shows the curves for several runs. The penetration data for other runs are presented in Appendix A. The penetation curves were in "S" shape and were similar and close to those reported in the literature for glass fiber substrates in conventional cascade impactors (Rao and Whitby, 1979).

Cut diameter, the particle diameter collected at 50% efficiently, was obtained from the experimental penetration curve and is shown in the last column of Table 11.

The predicted cut diameters, based on Stoke's Law (equation 7) and the general formula (equation 5), are also shown in Table 11. The difference between the two predictions becomes significant at high pressure.

The predicted (from the general formula) and experimental cut diameters are plotted in Figure 20. There is a considerable

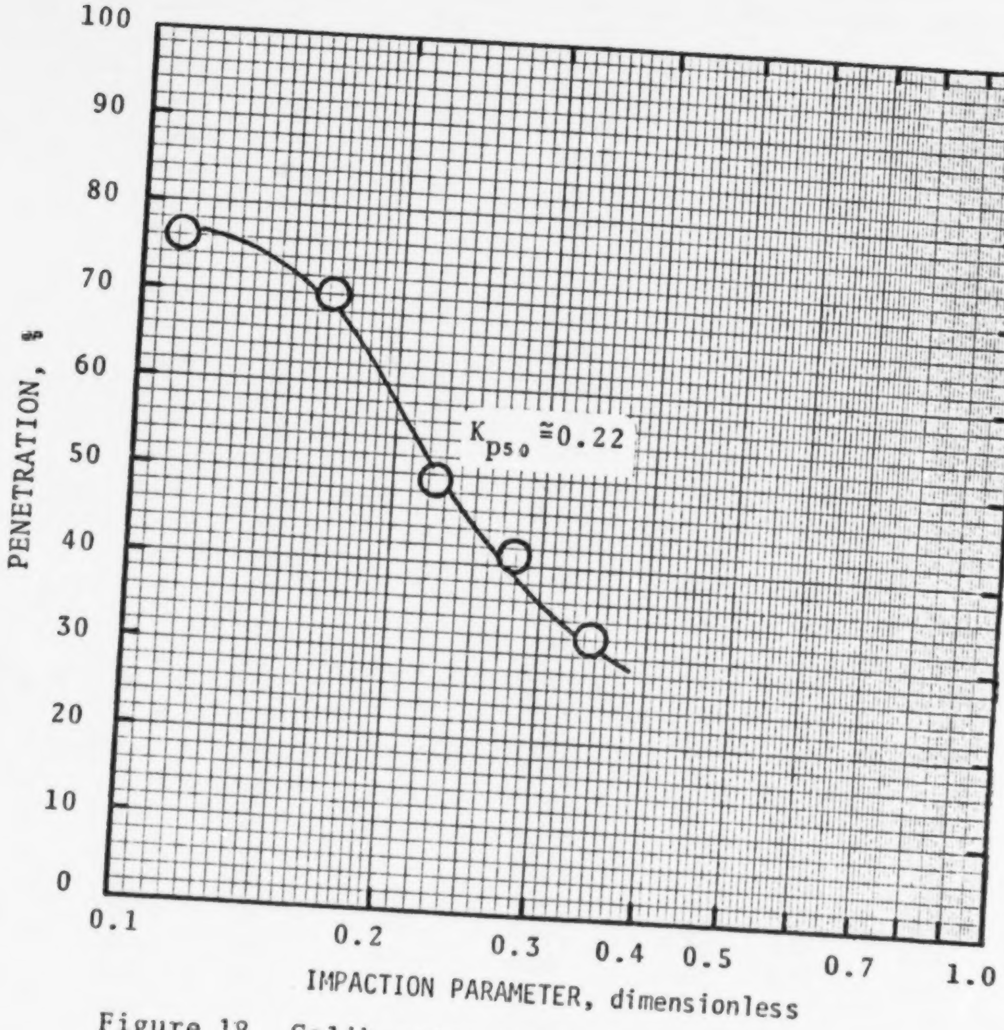

Figure 18. Calibration curve for impactor test section.

TABLE 11. INERTIAL IMPACTION TEST CONDITIONS AND RESULTS

Run #	Temperature, °C	Pressure, atm	Jet Velocity, cm/s	Cut Diameter, μm		
				Stokes' Law	General Formula	Experiment
30-12	26	1.4	2,631	0.85	0.93	1.08
30-6	27	1.4	2,610	0.86	0.93	1.15
34-16	29	1.5	1,149	1.33	1.41	1.30
34-11	30	1.2	1,448	1.17	1.25	1.12
33-24	30	1.4	1,260	1.27	1.34	1.08
33-26	31	1.4	1,258	1.27	1.34	1.19
33-27	31	1.4	1,233	1.28	1.35	1.05
33-25	32	1.4	374	3.25	3.49	3.11
33-10	33	1.2	1,191	1.30	1.37	0.73
33-9	33	1.2	1,197	1.29	1.36	0.74
33-7	33	1.2	1,302	1.24	1.32	0.92
32-28	102	1.3	1,318	1.32	1.36	1.31
31-31	104	1.2	1,319	1.31	1.36	1.29
31-6	106	1.3	2,582	0.92	0.98	1.11
34-13	107	1.2	1,177	1.40	1.42	1.43
31-15	112	1.4	2,433	0.96	1.03	0.98
34-19	124	1.5	1,192	1.43	1.50	1.40
31-25	202	1.3	2,621	0.97	1.02	1.20
34-3	208	1.2	1,315	1.41	1.45	1.70
31-16	313	1.4	2,669	1.02	1.06	1.01
35-2	491	1.6	1,222	1.69	1.70	2.20
35-3	500	1.4	1,256	1.65	1.65	2.25
31-17	504	1.3	2,693	1.06	1.09	1.00
33-1	514	1.4	1,194	1.70	1.70	1.61
34-19	535	2.0	932	2.02	2.04	2.60
30-11	699	1.1	2,607	1.08	1.09	1.26
31-18	797	1.2	2,870	1.05	1.04	0.82
30-13	816	1.1	2,601	1.10	1.10	1.32
34-12	96	3.0	1,362	1.34	1.45	1.12
34-6	28	5.1	1,241	1.32	1.50	1.20
34-4	30	5.1	1,249	1.31	1.52	1.51
34-5	31	5.1	1,254	1.31	1.48	1.69
33-15	34	5.1	384	1.29	1.46	1.40
33-16	34	5.1	1,309	1.29	1.46	1.33
31-1	103	5.1	2,438	1.00	1.15	1.45
31-4	106	5.1	2,508	1.00	1.14	0.95
35-6	119	5.1	1,471	1.33	1.49	2.18
36-14	26	10.2	556	1.98	2.33	2.02
36-16	27	10.2	558	1.98	2.33	1.72
36-12	31	10.2	564	1.98	2.30	2.04
31-2	100	9.8	1,760	1.20	1.47	1.31
35-7	127	10.0	1,458	1.35	1.61	2.60
31-3	100	14.9	1,510	1.30	1.64	1.15

*The jet diameter for Run #33-25 was 0.258 cm. All other runs used 0.140 jets.

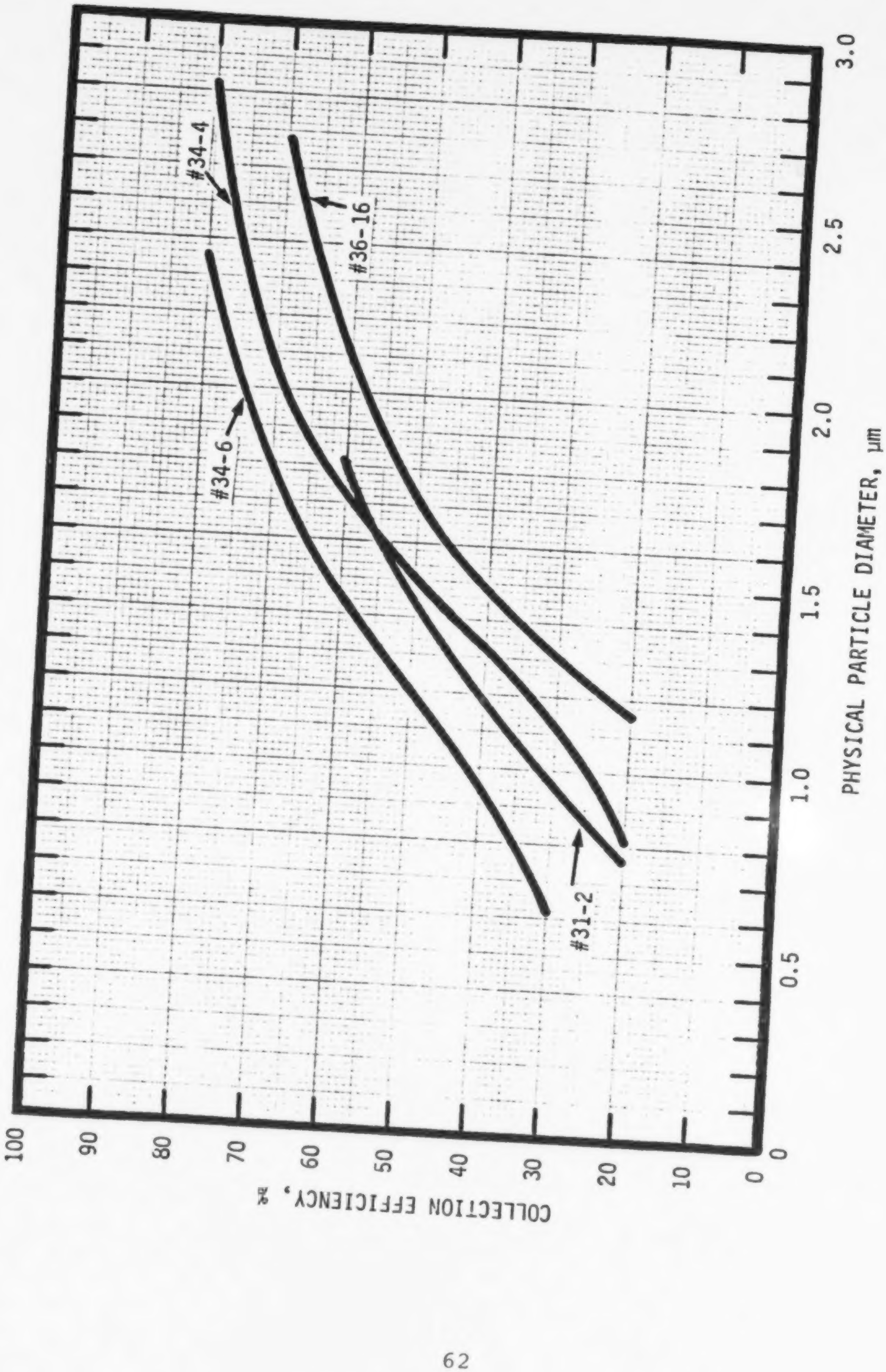

Figure 19. Experimental efficiency curves.

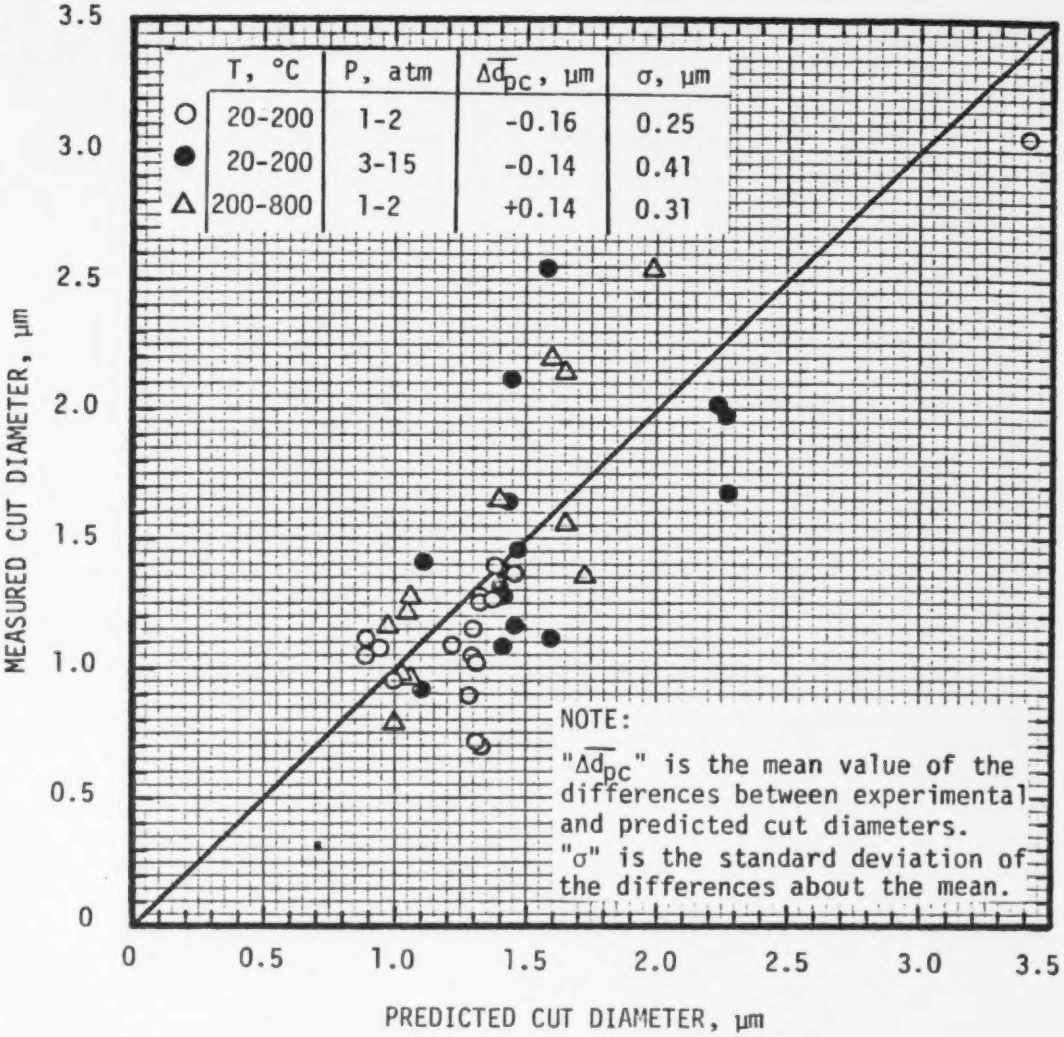

Figure 20. Comparison between experimental and predicted cut diameters.

amount of scatter in the data which reflects the difficulty of obtaining precise, repeatable results with high temperature and pressure apparatus. One of the major uncertainties encountered is the question of particle bounce at impact. Normally inertial impaction devices use a greased substrate to ensure adhesion of the particles to the surface upon impact. This is not possible at high temperature. Many substrate materials had been evaluated, including bare metal foil (copper, stainless steel, Inconel 600) and ceramic fiber paper. As mentioned earlier the ceramic paper worked best, however its impaction characteristics were far from ideal.

The mean difference, $\overline{\Delta d_{pc}}$, between the experimental cut diameter and the cut diameter predicted from the general formula has been calculated for three test categories; low temperature and pressure (20-200°C, 1-2 atm), high temperature (200-800°C), and high pressure (3-15 atm). The mean differences and their standard deviations, σ, are presented in Figure 20 along with the comparison of experimental and predicted cut diameters.

The low temperature data average about 0.15 μm below the predictions. The high temperature data average about 0.14 μm over the predictions. Thus the experimental cut diameters at high temperature seem to be slightly larger than the predicted values. This is consistent with the result obtained based on the theoretical evaluation of accommodation coefficients discussed earlier. Similarly, no difference was observed between the low pressure and high pressure comparison between data and predictions. In both cases the experimental cut diameter average slightly less than the predicted values.

For all test conditions the standard deviations are larger than the mean differences. Therefore, the observed trends with temperature and pressure are not statistically significant and much more data would be needed to complete any quantitative evaluation. The most valuable result from these experiments is that we were able to predict cut diameters at high temperature and high pressure with approximately the same accuracy and precision as we could at normal temperatures and pressures using ceramic fiber substrates.

CONCLUSIONS

There does not appear to be any major deviation from theoretical predictions when working with impaction devices at high temperature and pressure. The major difficulty will more likely be a practical one rather than a fundamental, theoretical one. High temperature substrate materials are difficult to find and at best seem to be unreliable. Also problems with high temperature and pressure seals, and material corrosion pose severe design problems for impactors.

Particle collection equipment which depend on the inertial impaction mechanism should perform as predicted based on the results of our tests. Devices which fall into this category include granular filters, dry scrubbers, molten salt scrubbers, and to a lesser extent fiber and membrane filters (before cake filtration becomes dominant). The performance-limiting problems are likely to be particle adhesion and reentrainment, granule attrition, corrosion, and other problems which are not directly related to the primary particle collection efficiency.

SECTION 5

CYCLONE SEPARATION

In recent years there has been a renewed interest in the performance of cyclone dust collectors at high temperature and pressure. This interest is related to the need for reliable sampling and particulate control equipment for advanced coal conversion and combustion processes. Applications at temperatures up to 1,200°C and pressures up to 5,000 kPa are being considered.

Only very limited experimental data have been reported, and these are insufficient for evaluating the effects of temperature and pressure on the mechanisms responsible for particle deposition in cyclones. An understanding of these fundamental mechanisms is essential in order to evaluate and develop design models for high temperature and pressure cyclones.

BACKGROUND

Parent (1946) and Yellott and Broadley (1955) reported cyclone performance data for temperatures up to 600°C and pressures up to 500 kPa. Their data confirm the expected decrease in overall efficiency with increasing gas temperature. They do not present any data on the effect of gas pressure. They do not present any fractional efficiency data and their results are insufficient for evaluating theoretical performance models.

Smith et al. (1979) studied small scale sampling cyclones at temperatures from 25 to 204°C. Particle cut diameters of the cyclones ranged from 0.32 to 5.9 μm. Cyclone diameters were 1.5, 2.5, 3.1, 3.7 and 4.5 cm. The largest cyclone they tested is comparable to the cyclone used in the present study and the data for these runs agree well with present data. Data for the smaller cyclones show smaller cut diameters than measured in the present study. Their data are compared with ours later in this report.

Knowlton and Bachovchin (1978) reported on a study of cyclones at pressures up to 5,500 kPa. Their results indicate that the overall efficiency and fractional efficiency (for particle diameters larger than 4 μm) are independent of system pressure. They tested a 4-inch diameter, tangential entry, reverse flow cyclone. The test aerosol was coke dust with a bimodal size distribution. The mass median diameters for the fine and coarse fractions were 15 μm and 110 μm, respectively. Their data are compared with ours later in this report.

Ernst et al. (1979) reported data from the tertiary cyclone at Exxon's pressurized fluidized-bed combustor Miniplant. Their data show much higher collection efficiency than could be accounted for theoretically. Test conditions were approximately 700 kPa and 635°C. The dust particles entering the cyclone had a mass median diameter of about 2 μm and a particle density of 1.5 g/cm^3.

The Exxon tertiary cyclone is a 15 cm (6 inch) diameter, rectangular inlet tangential entry, reverse flow cyclone with an inlet velocity of 36 m/s. The 5 cm diameter test cyclone used in the present study was similar in configuration to the Exxon cyclone and operated at inlet velocities from 1.8 to 5.2 m/s.

THEORY

There are a large number of cyclone models presented in the literature which may be used to predict particle collection efficiencies, cut diameter, critical diameters and pressure drops. These models have been presented and reviewed in the literature and therefore they will not be presented here. For more detailed information, refer to Leith and Mehta (1973), Strauss (1966), and the specific references as cited in Table 12.

Equations for the three collection efficiency models and five pressure drop models are presented below.

TABLE 12. CYCLONE PERFORMANCE MODELS

Collection Efficiency:	Leith and Licht (1972)
	Sproull (1970)
	Dietz (1981)
Cut Diameter:	Stairmand (1951)
	Lapple (1951)
	Barth (1956)
Critical Diameter:	Rosin (1932)
	Davies (1952)
	Strauss (1966)
Pressure Drop:	Stairmand (1949)
	Barth (1956)
	Shepherd and Lapple (1940)
	First (1950)
	Alexander (1949)

Efficiency

Leith and Licht Model -

Leith and Licht (1972) derived an equation for predicting cyclone efficiency from theoretical considerations. Their equation is:

$$E = 1 - \exp\left[- 2\ (C\ K)^{1/(2n+2)}\right] \qquad (20)$$

where "C" is a function of the cyclone's dimension ratios only (see Figure 22 for definition of symbols):

$$C = \frac{\pi D^2}{ab}\left[2\left(1 - \left(\frac{D_e}{D}\right)^2\right)\left(\frac{S}{D} - \frac{a}{2D}\right) + \frac{1}{3}\left(\frac{S + L - h}{D}\right) X \left(1 + \frac{d}{D} + \left(\frac{d}{D}\right)^2\right) + \frac{h}{D} - \left(\frac{D_e}{D}\right)^2 \frac{L}{D} - \frac{S}{D}\right] \qquad (21)$$

and where:

$$\frac{L}{D} = 2.3\ \frac{D_e}{D}\left(\frac{D^2}{ab}\right)^{1/3} \qquad (22)$$

and:

$$\frac{d}{D} = \frac{D - (D - B)((S + L - h)/(H - h)) -}{D} \qquad (23)$$

"L" is the farthest distance the vortex extends below the gas exit duct.

The pressure and temperature dependent terms are contained in the modified inertial parameter, K, and the vortex exponent, n, defined by:

$$K = \frac{C' \varrho_p d_p^2 u_c}{18 \mu_G D} (n + 1) \tag{24}$$

and:

$$n = 1 - \left(1 - \frac{(0.394D)}{2.5}^{0.14}\right)\left(\frac{T}{283}\right)^{0.3} \tag{25}$$

where C' = Cunningham slip correction factor, dimensionless
d_p = particle diameter, cm
ϱ_p = particle density, g/cm³
u_c = cyclone inlet velocity, cm/s
μ_G = gas viscosity, g/cm-s
T = gas temperature, °K
D = cyclone diameter, cm

Sproull Model -

Sproull (1970) presented a method for calculating cyclone efficiency by drawing a parallel between cyclone collection and the collection in an electrostatic precipitator. The efficiency equation presented is:

$$E = 1 - \exp - \left[\frac{w A_c}{Q_c}\right] \tag{26}$$

where "w"is the migration velocity of particles to the cyclone wall, given by:

$$w = \frac{C' \varrho_p d_p^2 u_c^2}{18 \mu_G D} \tag{27}$$

and "A_c" is the interior collecting surface of the cyclone;

$$A_c = \pi Dh + \frac{\pi}{2}(D+B)\left[(H-h)^2 + \left(\frac{D-B}{2}\right)^2\right]^{\frac{1}{2}} \tag{28}$$

"Q_c" is the actual flow rate in cm³/s at the cyclone inlet.

Dietz Model

Recently Dietz (1981) derived a theoretical model for cyclones which was used to predict the performance of cyclones operating at high temperature and pressure. His equations are presented below.

$$E = 1 - A \exp(b) \tag{29}$$

$$A = K_0 - (K_1{}^2 + K_2)^{\frac{1}{2}} \tag{30}$$

$$b = \frac{-2\pi\ R_c\ u_{pw}\ D}{Q_{vo}} \tag{31}$$

$$K_2 = \left(\frac{R_v}{R_c}\right)^{2m} \tag{32}$$

$$K_1 = \frac{1}{2}\left[1 - \left(\frac{R_v}{R_c}\right)^{2m}\left(1 + \frac{9\ \mu_G\ Q_{vo}}{4\pi\ L_n\ \varrho_p\ R_p^2\ u_{tw}^2}\right)\right] \tag{33}$$

$$K_0 = \frac{R_c\ u_{pw} + R_v\ u_r + R_v\ u_{pv}}{2\ R_v\ u_{pv}} \tag{34}$$

$$u_r = \frac{Q_{vo}}{2\pi\ R_v L_n} \tag{35}$$

$$u_{pv} = \frac{2}{9}\ \frac{\varrho_p\ R_p^2 u_{tw}^2}{\mu_G\ R_v} \tag{36}$$

$$u_{pw} = \frac{2}{9} \frac{\varrho_p R_p^2 u_{tw}^2}{\mu_G R_c} \qquad (37)$$

$$u_{tv} = u_{tw} \left(\frac{R_c}{R_v} \right)^m \qquad (38)$$

where: u_{tw} = tangential velocity at the wall, cm/s
u_{tv} = tangential velocity at the vortex, cm/s
u_{pw} = particle radial velocity at the wall, cm/s
u_{pv} = particle radial velocity at the vortex, cm/s
u_r = radial velocity in core region, cm/s
Q_{vo} = inlet volumetric flow rate, cm^3/s
m = cyclone vortex strength = 0.70.
R_p = particle radius, cm
R_v = radius of cyclone exit duct, cm
R_e = radius of cyclone cylinder, cm
L_n = effective cyclone length, cm

The effective cyclone length is the length of a cylinder such that the volume of this cylinder is equal to the volume of original cyclone that is below the average inlet position.

Pressure Drop

Cyclone pressure drop calculations were carried out with the theories presented by Shepherd and Lapple (1940); First (1950); Alexander (1949); Stairmand (1949); and Barth (1956). The equations are presented below. All express cyclone pressure loss as a number of inlet velocity heads, ΔH_v. Inlet velocity heads can be converted to pressure drop in terms of static pressure head, ΔP, by:

$$\Delta P = \frac{u_c^2 \varrho_G \Delta H_v}{2g \varrho_L} \qquad (39)$$

where ΔP = pressure drop across the cyclone, cm water column (W.C.)
ΔH_v = inlet velocity head, dimensionless
ρ_g = gas density, g/cm^3
V_c = cyclone inlet velocity, cm/s
ρ_L = density of water, g/cm^3
g = acceleration due to gravity, cm/s^2

Shepherd and Lapple -

Shepherd and Lapple (1940) correlated experimental pressure drop results with the following equation:

$$\Delta H_v = K_1 \frac{ab}{D_e^2} \tag{40}$$

where $K_1 = 16$ for a cyclone with standard tangential inlet, and $K_1 = 7.5$ for cyclone with an inlet vane, i.e. where the inner wall of the tangential entry extends past the cyclone inner wall to a point halfway to the opposite wall.

First -

First (1950) presented the following expression for cyclone pressure loss, which while similar to the Shepherd and Lapple equation, takes into consideration the additional factors of cyclone diameter, D, plus cone and cylinder height, (H-h) and h, respectively:

$$\Delta H_v = \frac{ab}{D_e^2} \left[\frac{12/Y}{[h(H-h)/D^2]^{1/3}} \right] \tag{41}$$

"Y" is a constant which is equal to 0.5 for a cyclone with no inlet vane, 1.0 for a neutral inlet vane, and 2.0 for an inlet vane that expands the entering gas stream and touches the gas outlet duct.

Alexander -

Alexander (1949) derived the following expression for pressure drop, assuming all pressure losses are due to kinetic energy losses in the gas stream. His equation is:

$$\Delta H_v = 4.62 \frac{ab}{DD_e}\left[\left(\left(\frac{D}{D_e}\right)^{2n} - 1 \right) \frac{1-n}{n} + f\left(\frac{D}{D_e}\right)^{2n}\right] \qquad (42)$$

where

$$n = 1 - 1 - \left(\frac{(0.394\ D)^{0.14}}{2.5}\right)\left(\frac{T}{283}\right)^{0.3} \qquad (43)$$

and

$$f = 0.8\left[\frac{1}{n(1-n)}\left(\frac{4-2^{2n}}{3}\right) - \left(\frac{1-n}{n}\right)\right] + 0.2\left[(2^{2n}-1)\left(\frac{1-n}{n}\right) + 1.5\ (2^{2n})\right] \qquad (44)$$

"D" is the diameter of cyclone in centimeter and "T" is the absolute temperature in degrees K.

Stairmand -

Stairmand (1949) has presented a method of calculating the pressure drop through a cyclone by:

$$\Delta H_v = 1 + 2f_n^2\left(\frac{2(D-b)}{D_e} - 1\right) + 2\left(\frac{4ab}{\pi D_e^2}\right)^2 \qquad (45)$$

$$f_n = \frac{-\left(\frac{D_e}{2(D-b)}\right)^{\frac{1}{2}} + \left(\frac{D_e}{2(D-b)} + \frac{4GA}{ab}\right)^{\frac{1}{2}}}{\frac{2GA}{ab}} \qquad (46)$$

"G" is a friction factor approximately equal to 0.005 and "A" is the inside surface of the cyclone exposed to the spinning gas. "A" can be calculated from:

$$A = \frac{\pi}{4}(D^2-D_e^2) + \pi Dh + \pi D_e S + \frac{\pi}{2}(D+B)\left[(H-h)^2 + \left(\frac{D-B}{2}\right)^2\right]^{\frac{1}{2}} \qquad (47)$$

Stairmand assumes that the total energy loss is due to losses in the cyclone vortex, plus entrance and exit losses.

Barth -

Barth (1956) expresses cyclone pressure drop as a function of the sum of two factors, "e_e" and "e_i". The factor "e_e" reflects losses due to entrance to the cyclone and internal friction and kinetic energy losses. The factor "e_i" results from losses at the gas outlet.

$$\Delta H_v = \left(\frac{u_i}{v_i}\right)^2 \left(\frac{4ab}{\pi D_e{}^2}\right)^2 [e_e + e_i] \qquad (48)$$

where

$$e_e = \frac{D_e}{D}\left[\frac{1}{[1-(u_i/v_i)\ (H-S)\ (2/D_e)\ f_f]^2} - 1\right] \qquad (49)$$

$$e_i = \frac{4.4}{(u_i/v_i)^{2/3}} + 1 \qquad (50)$$

$$\frac{u_i}{v_i} = \frac{(D_e/2)\ (D-b)\pi}{2abx + (H-S)\ (D-b)\pi f_f} \qquad (51)$$

$$x = 1 - 1.2\ b/D \qquad (52)$$

"f_f" is a friction factor approximately equal to 0.02.

APPARATUS AND TEST METHODS

Apparatus

The high temperature and pressure test facility is illustrated in Figure 21. High pressure nitrogen was supplied from a manifold of gas cylinders. Some of the gas passed through a batch fluidized-bed dust generator and the rest bypassed the bed and was used for dilution. The fluidized bed contained 100 to 150 μm diameter nickel spheres which had been mixed with fly ash. A Polonium-210 air ionizer was used to ionize the dilution air and neutralize the electric charge on the particles.

The gas and fly ash particles passed through a long heating section and into the test cyclone. The gas and uncollected particles left the cyclone, and were cooled and filtered. The clean gas then flowed back to the control panel for metering and venting. A sample probe and filter were also provided upstream from the cyclone for collecting samples of the fly ash at the cyclone inlet.

Three test cyclones were used. Their design geometry and dimensions are presented in Figures 22 and 23. Preliminary data were obtained with Model C1 (plexiglas) and Model C2 (stainless steel with circular inlet). The majority of the data and analyses were for the high temperature and pressure (HTP) cyclone

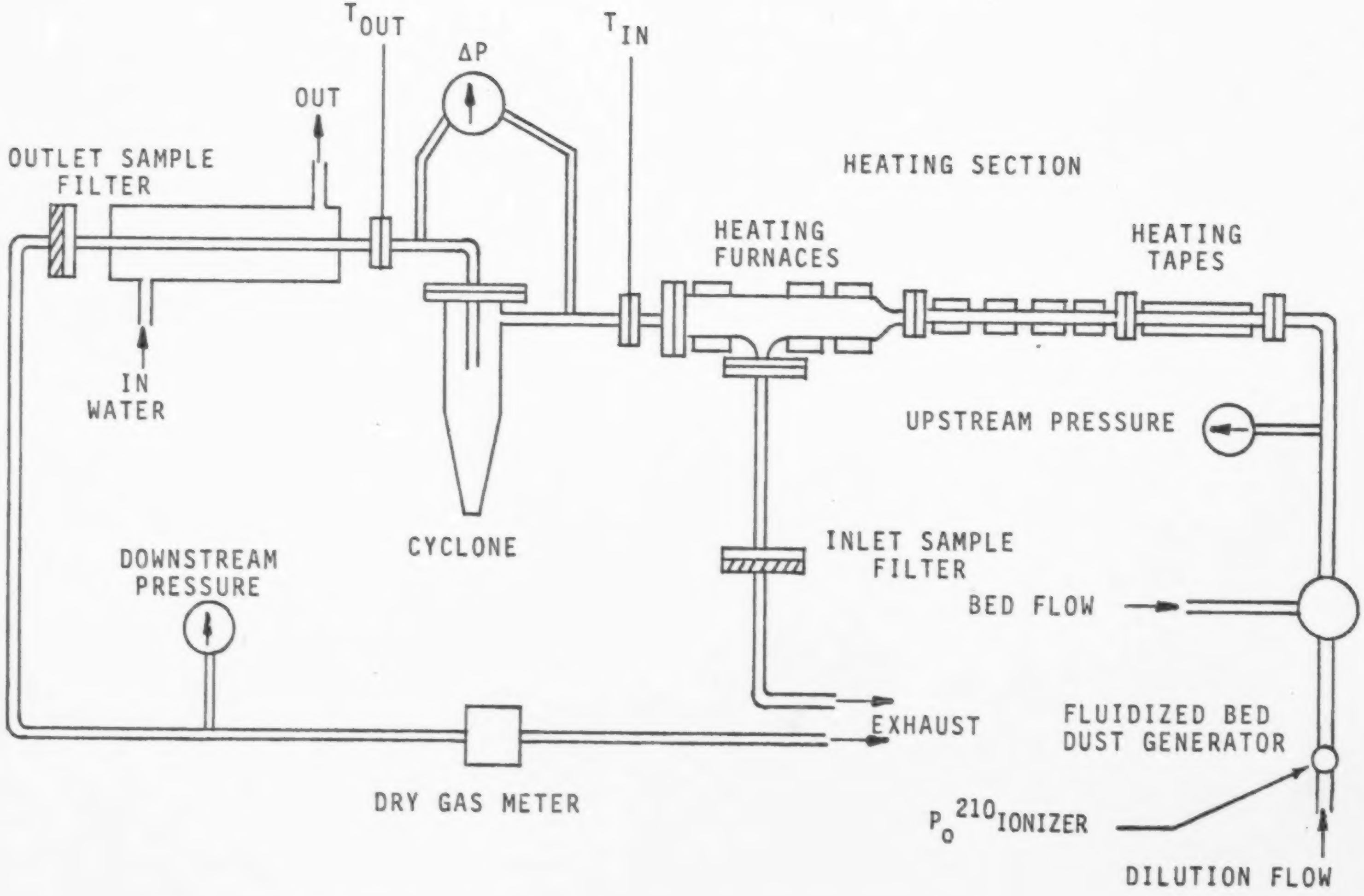
OUTLET SAMPLE FILTER
OUT
T_{OUT}
ΔP
T_{IN}
HEATING SECTION
HEATING FURNACES
HEATING TAPES
IN WATER
UPSTREAM PRESSURE
CYCLONE
DOWNSTREAM PRESSURE
INLET SAMPLE FILTER
BED FLOW
EXHAUST
FLUIDIZED BED DUST GENERATOR
DRY GAS METER
P_o^{210} IONIZER
DILUTION FLOW

Figure 21. Schematic diagram of experimental setup for HTP tests.

MODEL C1 and C3

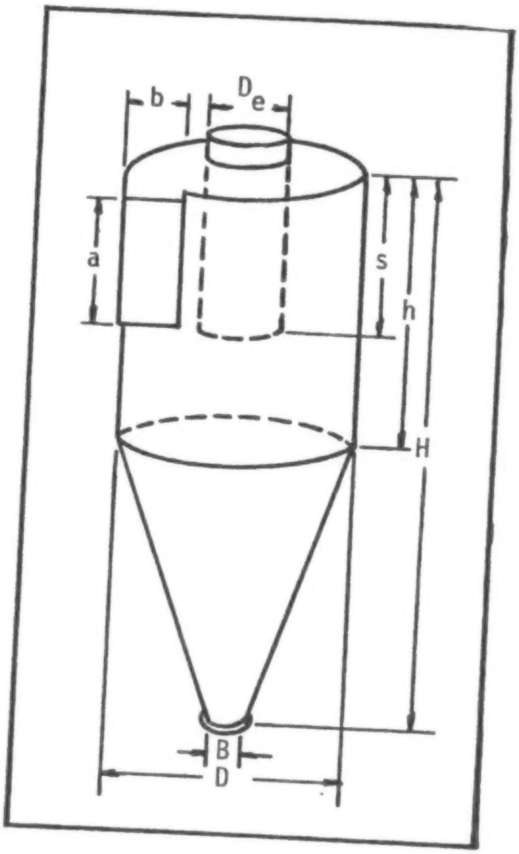

a = 0.75 in. = 1.905 cm
b = 0.375 in. = 0.953 cm
D_e = 0.625 in. = 1.588 cm
D = 2.0 in. = 5.08 cm
S = 2.25 in. = 5.715 cm
h = 3.625 in. = 0.208 cm
H = 8.625 in. = 21.908 cm
B = 0.75 in. = 1.905 cm

Figure 22. Dimensions for plexiglas cyclone(C1) and HTP cyclone (C3).

MODEL C2

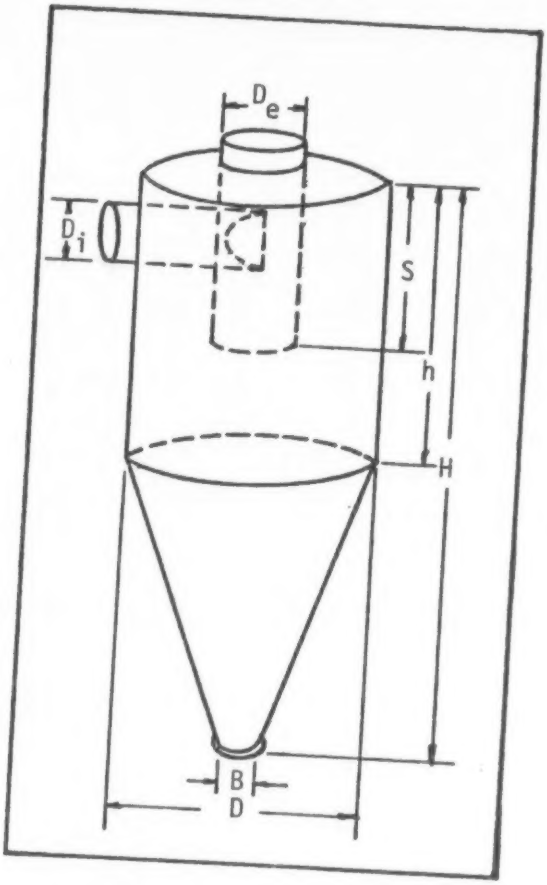

D_e = 0.493 in. = 1.25 cm

D_i = 0.493 in. = 1.25 cm

S = 1.50 in. = 3.81 cm

h = 3.0 in. = 7.62 cm

H = 8.0 in. = 20.32 cm

B = 0.75 in. = 1.905 cm

D = 2.0 in. = 5.08 cm

Figure 23. Dimensions for circular inlet cyclone (C2).

(Model C3). The HTP cyclone was fabricated out of type 316 stainless steel. High temperature heating tapes and ceramic blanket insulation were wrapped around the cyclone during the hot tests.

Data Collection and Analysis

After each run, the cyclone was washed with acetone to remove the collected particles. The outlet duct and final filter were also washed. The acetone was then evaporated from the sample and the fly ash particles were redispersed in a 3% NaCl electrolyte solution. The samples were then analyzed by Coulter counter to obtain the size distributions of dust captured in and penetrating the cyclone.

The analysis gives cumulative mass concentration data as a function of particle diameter (0.8 to 20 μm) for the cyclone catch and the particles that penetrate the cyclone. The particle density was measured to be 2.3 g/cm^3. The mass concentration data are used as input to a computer program which approximates the cumulative mass curves using a spline fit, as reported by Lawless (1978). The fractional penetration of particles was obtained by taking the ratio of the slopes of the outlet and inlet cumulative mass concentration curves at several particle diameters. The inlet data were obtained by summing the outlet and cyclone catch data.

RESULTS

Preliminary Experiments

Preliminary tests were run on a plexiglas cyclone and on a metal cyclone with a circular inlet while the high temperature and pressure cyclone was being fabricated. The plexiglas cyclone was also used to visualize the flow pattern through the cyclone to ensure that the particle deposition was a result of cyclone separation and not inertial impaction at the cyclone inlet.

The test conditions for the preliminary experiment are listed in Table 13. The results of the plexiglas cyclone (C1) runs (Tests 47/1 and 47/2) are presented in Figure 24 along with theoretical predictions based on the Leith-Licht and Sproull models. The data fall between the two predicted curves.

The results of the metal cyclone (C2) tests are presented in Figures 25 and 26 for room temperature and 300-350°C. The room temperature data follow Sproull's model fairly closely, however the high temperature collection efficiency is much lower than predicted.

The curves all show a minimum efficiency generally between 2 and 4 μm particle diameters. This could be an artifact introduced by the analytical technique used. In preparing particles for the Coulter counter, agglomerates of particles that were caught in the cyclone might be broken up. This problem was minimized by baking and hand grinding the fly ash before loading it into the dust generator.

The theoretical models appear to be fairly accurate for room temperature and pressure conditions.

HTP Cyclone Experiments

The main test program was done with the HTP cyclone (Model C3). Its dimensions and geometry are given in Figure 22. Tests were run at temperatures up to 693°C, pressures up to 2,530 kPa, and inlet velocities of approximately 1.8, 2.6, and 5.2 m/s. The dust concentration varied from 0.04 to 9.6 g/Am^3. The test conditions are listed in Table 14.

Also listed in Table 14 are the cyclone pressure drop, ΔP, and inlet Reynolds number. The Reynolds number is based on the average inlet velocity, u_c, and the cyclone diamter, D, and is defined as:

TABLE 13. TEST CONDITIONS FOR PRELIMINARY CYCLONE TESTS

Run No.	Test Cyclone	t, min.	T, °C	P, kPa	Qs, cm³/s	Qc, cm³/s	Vc, cm/s	ΔP, cm water	Comments
31/47/1	Plexiglas (C1)	45.0	27	170.7	15.7	369.0	202.7	1.27	Dust generator at room temperature.
31/47/2	Plexiglas (C1)	15.2	27	172.1	16.7	445.3	244.7	1.40	Dust generator at room temperature.
31/47/3	Metal (C2)	20.0	27	170.7	13.3	423.5	344.3	1.78	Dust generator at room temperature.
31/47/4	Metal (C2)	20.0	27	188.0	17.0	410.2	333.5	1.84	Dust generator at 360°C.
31/47/5	Metal (C2)	10.0	27	184.5	15.7	401.7	326.6	1.78	Dust generator at 360°C.
31/47/6	Metal (C2)	11.0	365	205.3	13.3	719.3	584.8	Not measured.	Fly ash was baked and hand ground before test.
31/47/7	Metal (C2)	10.0	303	174.2	6.3	491.8	399.9	Not measured.	Fly ash was baked and hand ground before test.

t = test duration, min.
T = gas temperature at the cyclone inlet, °C
P = system pressure, kPa
Q_s = inlet sampling flow rate, cm³/s
Q_c = gas flow rate at the cyclone inlet, cm³/s
V_c = gas velocity at the cyclone inlet, cm/s
ΔP = pressure drop across the cyclone, cm of water column

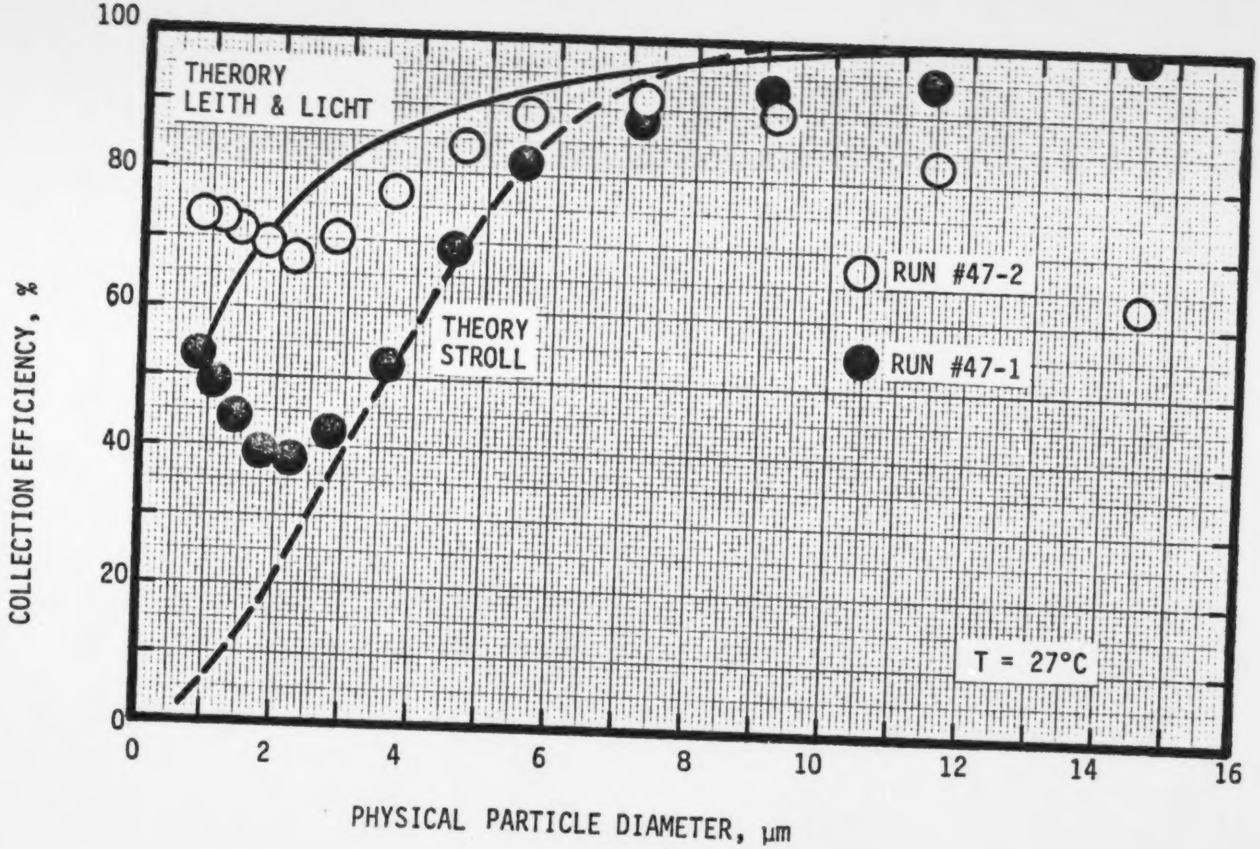

Figure 24. Experimental data for plexiglas cyclone (C1).

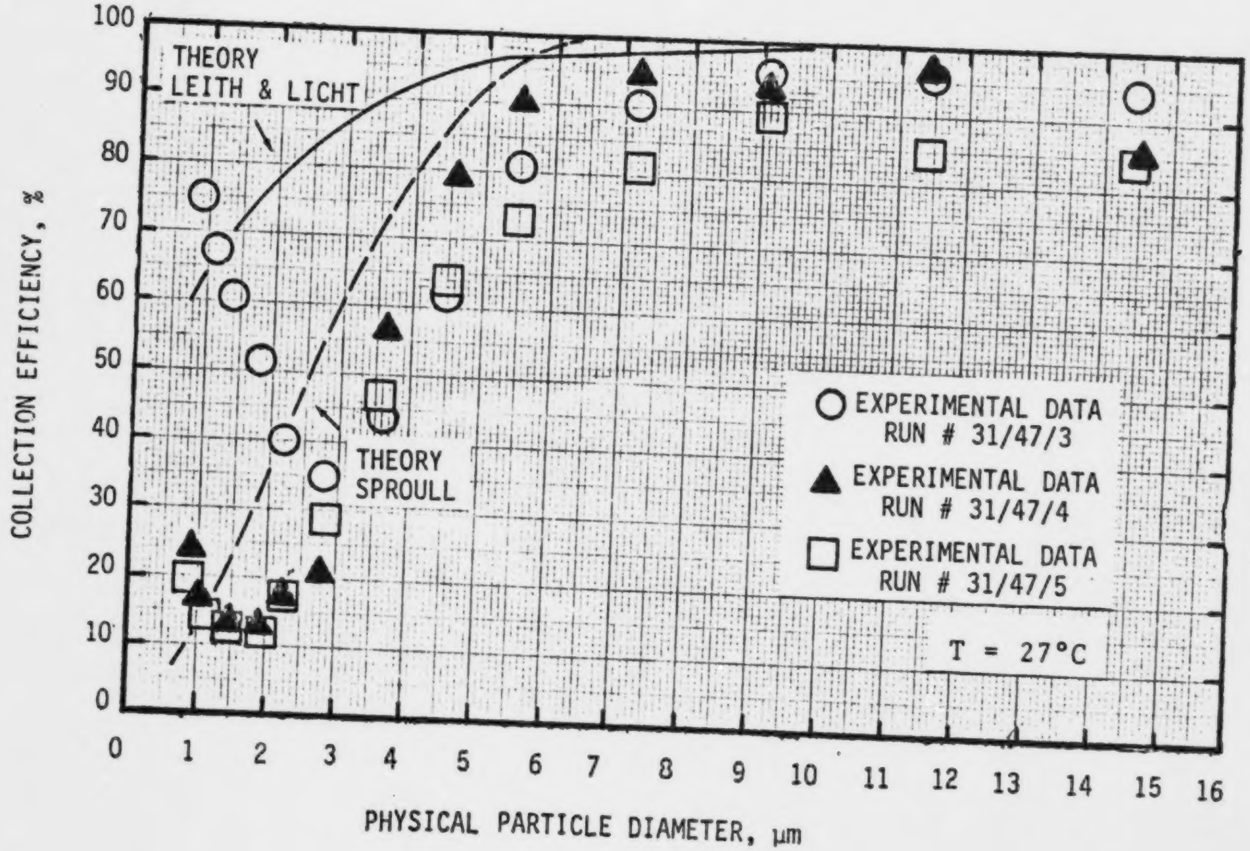

Figure 25. Experimental data for cicular inlet cyclone at low temperature.

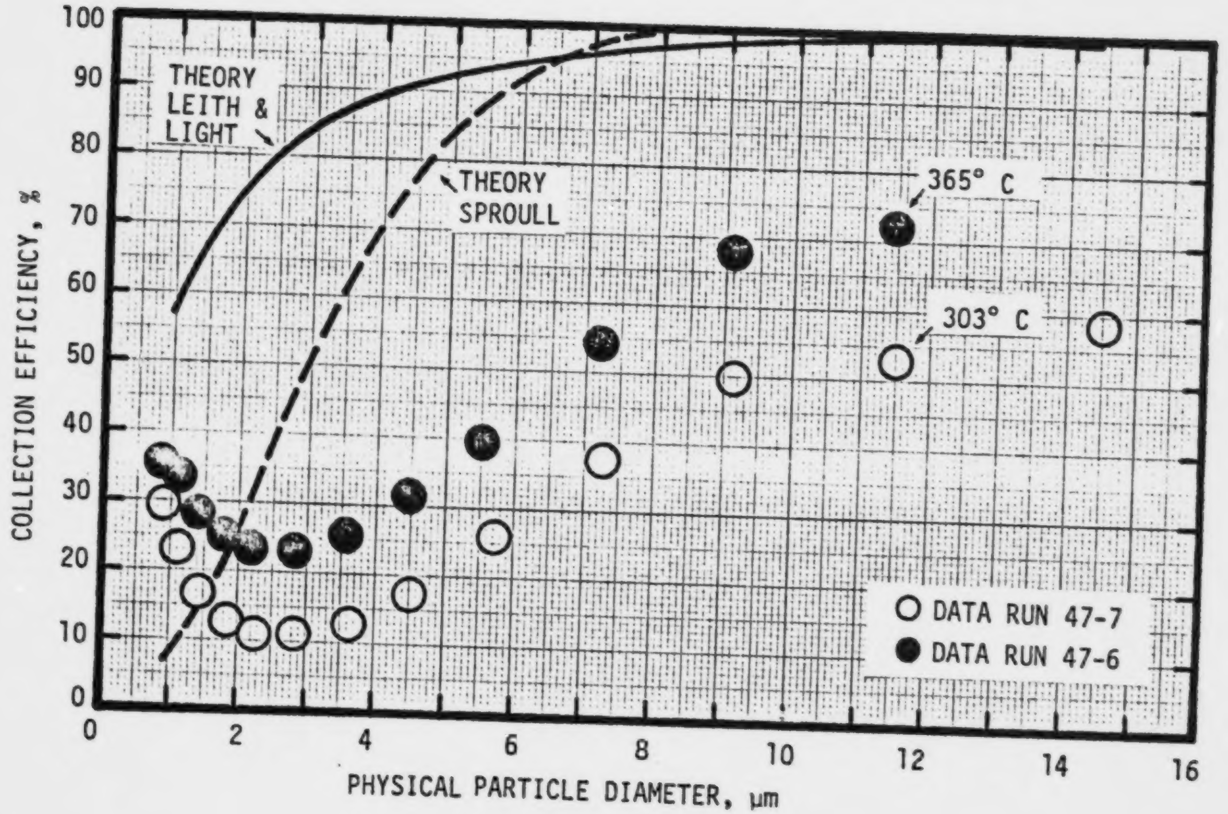

Figure 26. Experimental data for circular inlet cyclone (C2) at high temperature.

TABLE 14. TEST CONDITIONS FOR HTP CYCLONE RUNS

Test No.	Temperature, °C	Pressure, kPa	Inlet Velocity, cm/s	Inlet Dust Loading, g/m³	Pressure Drop, cm W.C.	Reynolds Number
48-01	22	192	264	3.17	0.64	16,600
48-02	20	190	266	0.18	0.64	16,700
48-03	130	200	254	0.22	0.46	9,700
48-04	209	192	275	0.48	0.30	7,400
48-05	375	192	236	1.15	0.19	3,900
48-06	352	192	252	0.77	0.20	4,400
48-07	410	192	243	0.15	0.15	3,700
49-01	155	141	226	1.85	0.23	5,500
49-02	22	157	181	2.22	0.20	9,300
49-03	20	516	188	0.97	0.76	32,200
49-04	20	931	183	1.30	2.29	56,800
49-05	20	1,310	182	0.79	4.57	79,000
49-06	20	516	260	2.17	2.41	44,500
49-07	20	931	260	0.56	6.35	80,700
49-08	20	1,220	253	1.63	9.91	102,600
49-09	495	516	256	1.73	0.51	8,700
50-01	512	516	262	0.42	0.51	8,600
50-02	502	516	262	1.49	0.51	8,700
50-03	693	205	288	1.47	0.25	2,700
55-02	30	1,560	253	0.32	5.59	124,000
55-03	40	1,540	256	9.56	4.19	117,000
55-04	22	2,030	521	0.44	*	348,000
55-05	21	2,030	523	0.23	*	350,000
55-06	29	2,030	523	4.55	19.1	334,000
55-07	30	2,520	522	0.26	37.5	413,000
55-08	25	2,530	521	0.46	39.6	425,000
55-09	22	2,520	524	0.04	35.6	433,000
55-10	42	2,520	265	0.52	7.62	195,000
55-11	49	2,030	261	0.82	6.35	149,000
55-12	45	2,510	263	0.91	8.13	140,000
55-13	41	2,030	261	0.73	8.00	156,000

* No Data

$$N_{Re} = \frac{D\, u_c\, \rho_G}{\mu_G} \qquad (53)$$

where ρ_G and μ_G are the gas density and viscosity.

The fractional efficiency data from all 31 runs are presented in Appendix B. Selected runs are presented here to illustrate the major temperature and pressure effects observed.

The effect of temperature on cyclone efficiency is illustrated in Figure 27. The efficiency decreases dramatically as temperature increases from 20°C to 700°C. This decrease is much greater than expected from theoretical considerations.

The effect of pressure on cyclone efficiency is shown in Figure 28. The efficiency clearly increases with increasing gas pressure. This is surprising because theory indicates that pressure should have no noticeable effect on efficiency.

Figure 29 shows the combined effects of high temperature and pressure. The effects of high temperature and pressure tend to cancel each other out. Therefore the effect is likely to be related more to gas density than to pressure or temperature alone.

Comparison With Theory

Many cyclone performance models have been reported in the literature. None of these models adequately predicts the effects of temperature and pressure observed in this study.

Present experimental data fall within the models of Leith and Licht (1972) and Sproull (1970) for low temperature and pressure runs. However, these theories do not adequately predict the effect of changes in temperature and pressure.

Figure 30 compares the model of Leith and Licht with experimental curves for selected runs. The theory predicts no pressure effect and much smaller temperature effects than were observed.

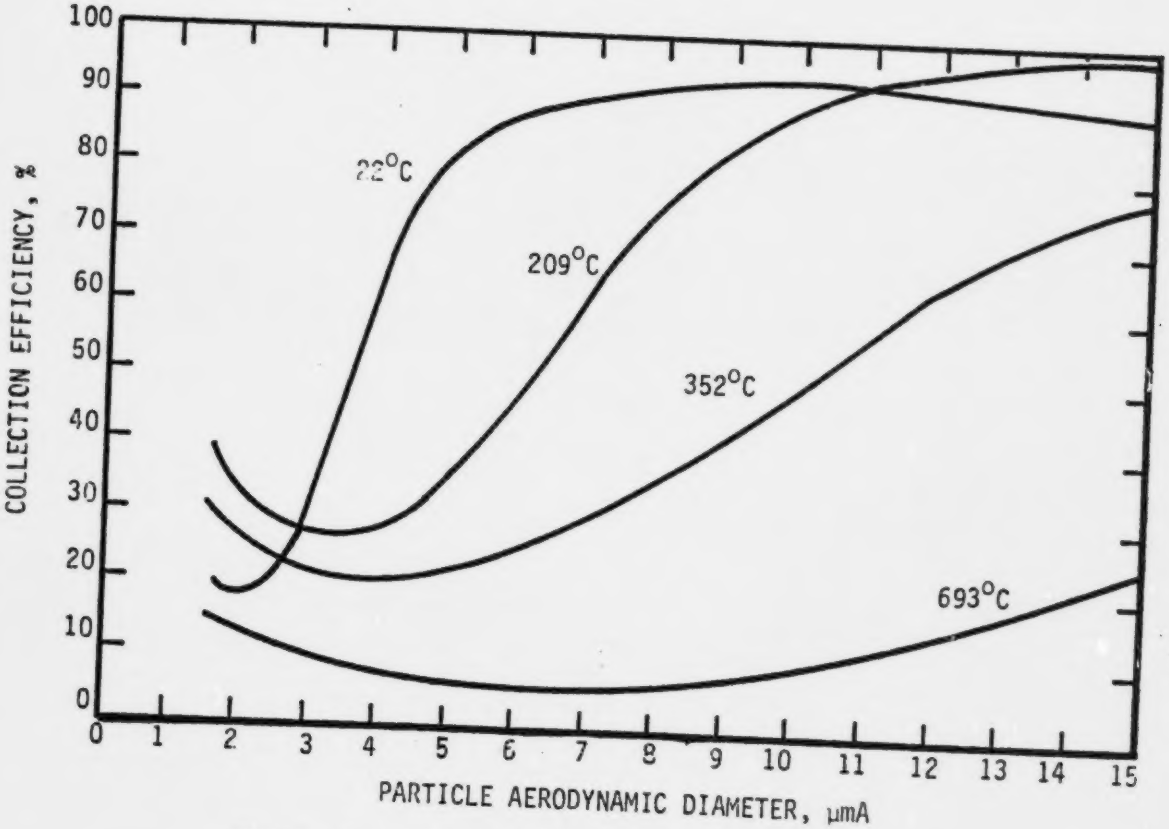

Figure 27. Effect of temperature on cyclone efficiency.

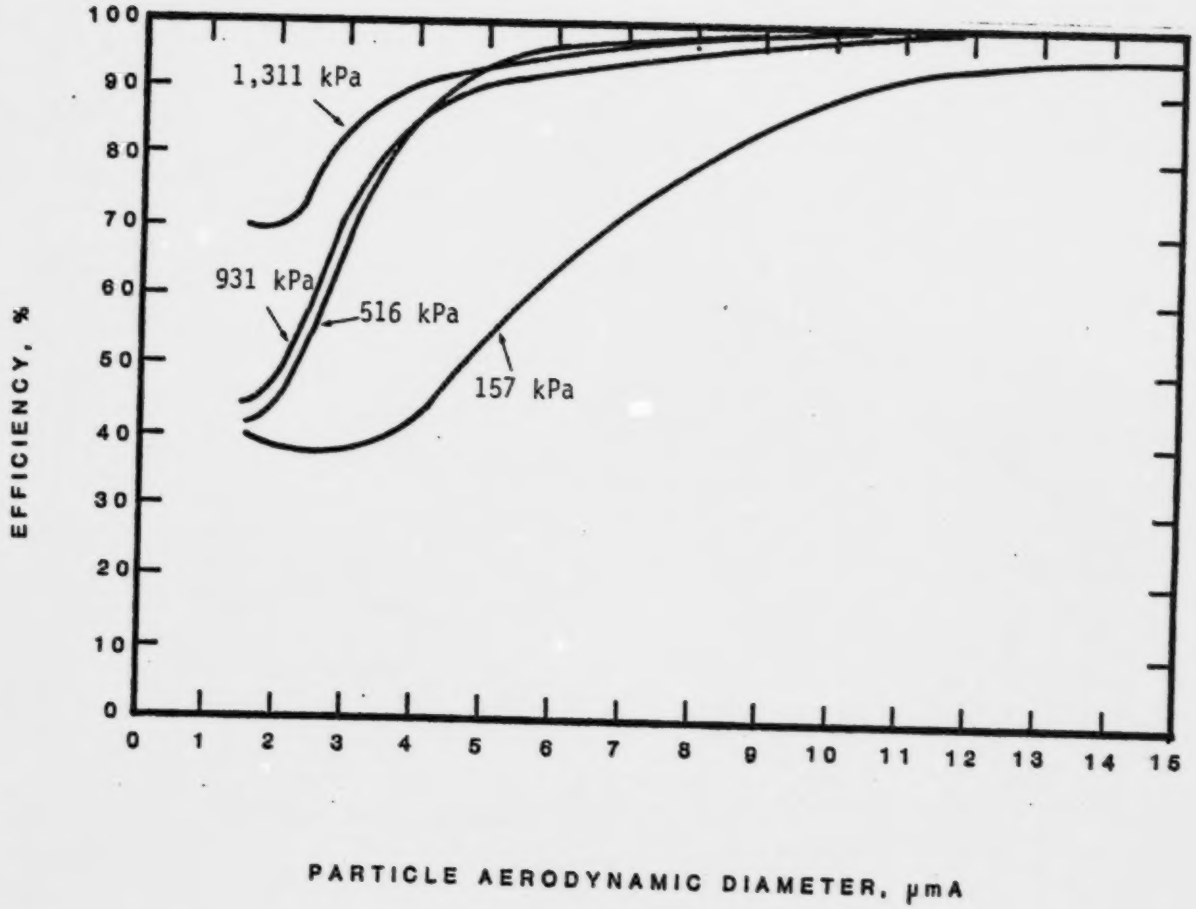

Figure 28. Effect of pressure on cyclone efficiency.

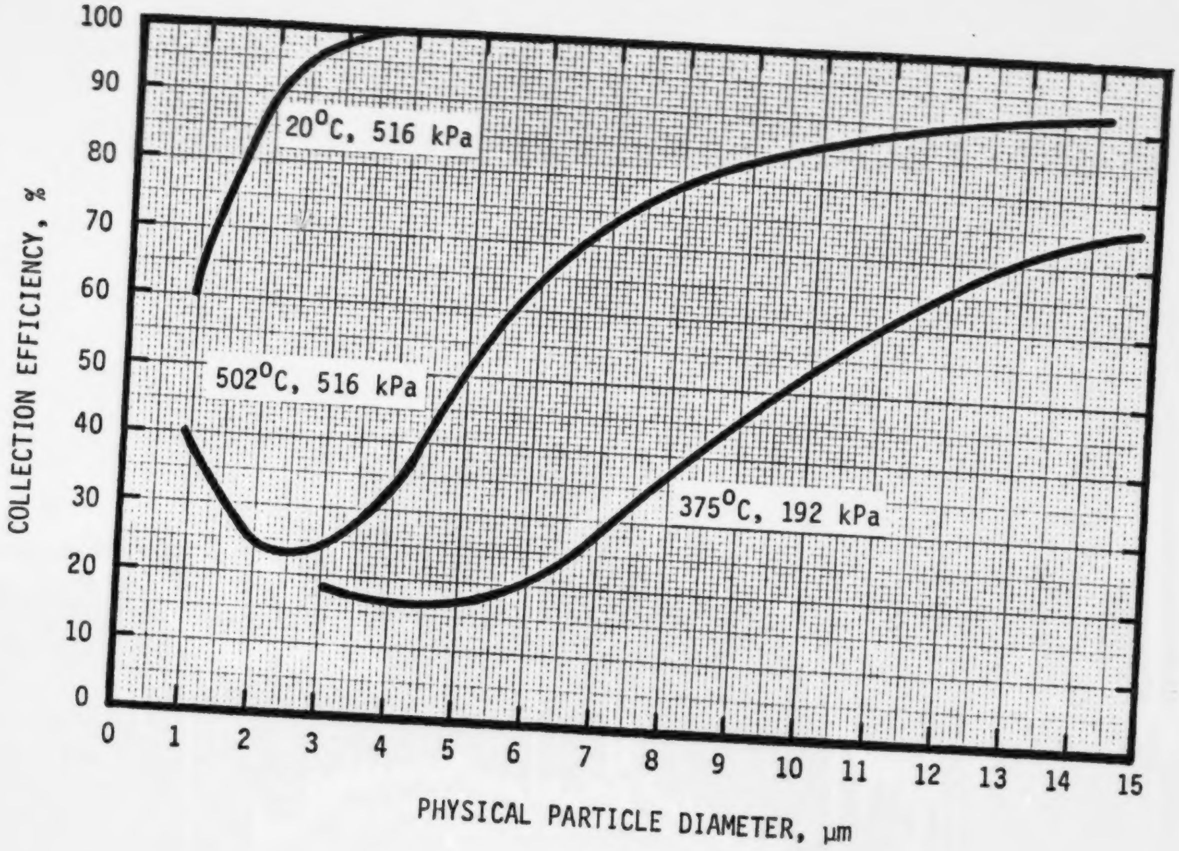

Figure 29. Combined effects of high temperature and pressure.

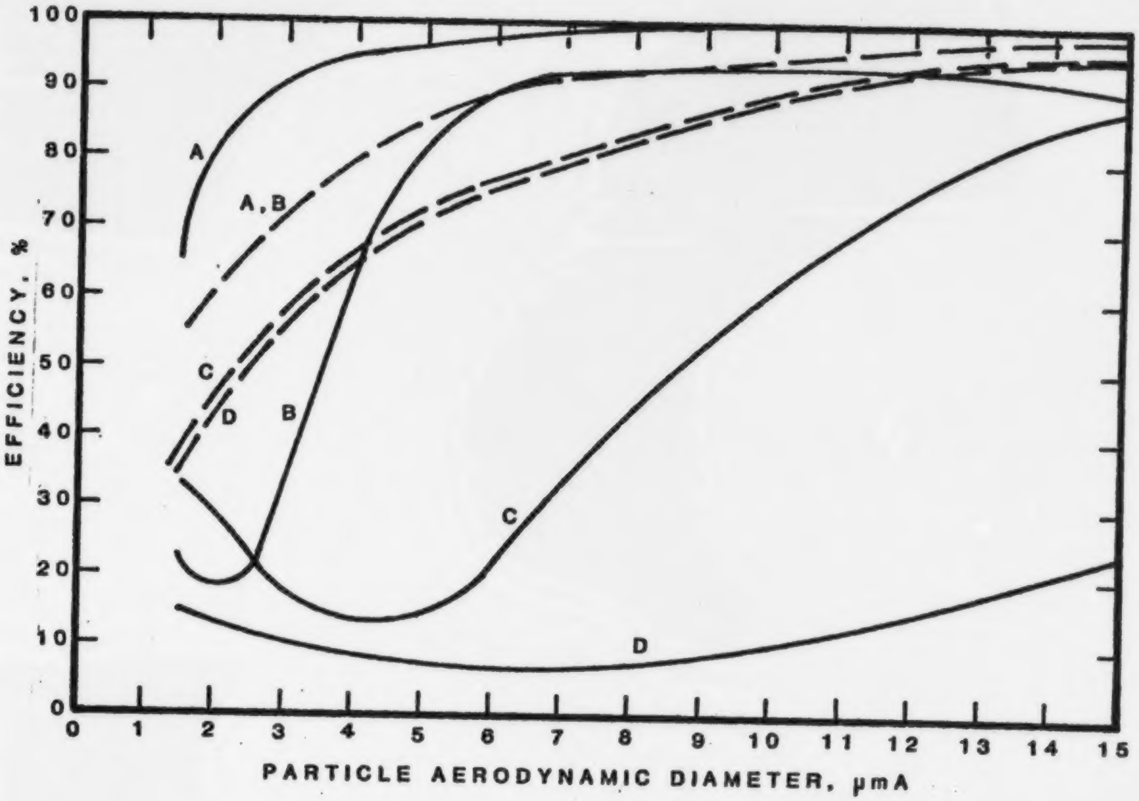

	T, °C	P, kPa	U_c, cm/s
A	20	1,221	253
B	22	192	264
C	512	516	262
D	693	205	288

– – – – THEORY

——— DATA

Figure 30. Comparison with model of Leith and Licht (1972).

The same is true for the Sproull model (Figure 31) and for the Dietz model (Figure 32). The three models are directly compared for each temperature and pressure condition in Figures 33, 34, 35 and 36.

The other theoretical models cited in Table 13 have also been evaluated. The predicted 50% cut diameters and critical diameters (above which collection efficiency is 100%) are compared with measured 50% and 90% cut diameters in Table 15. Some of the models agree fairly well for certain test conditions; however, none of them adequately account for the effects of temperature and pressure.

Cyclone pressure drop data are compared with theory in Table 16. The theories predict the effects of temperature and pressure fairly well for most runs.

Empirical Correlation

In an attempt to correlate our data and discover how to account for the observed temperature and pressure effects, experimental cut diameters are plotted against Reynolds number and against pressure drop as shown in Figures 37 and 38. Surprisingly, the Reynolds number correlation gave a tight, experimental curve for a wide range of temperatures and pressures.

Beeckmans (1979) found that cyclone efficiency cannot be correlated in terms of the Stokes number alone, and that the Reynolds number must also be included in the correlation. He used the correlation that efficiency varies with ($N_{Re}^{b} N_{Stk}{}^{\frac{1}{2}}$), where "b" is an empirical constant.

This empirical approach was successfully used in correlating our data. The best correlation was obtained by basing "N_{Stk}" on the hydraulic diameter of the cyclone inlet and "N_{Re}" on the overall cyclone diameter. The exponent, "b", was taken to be 1.0

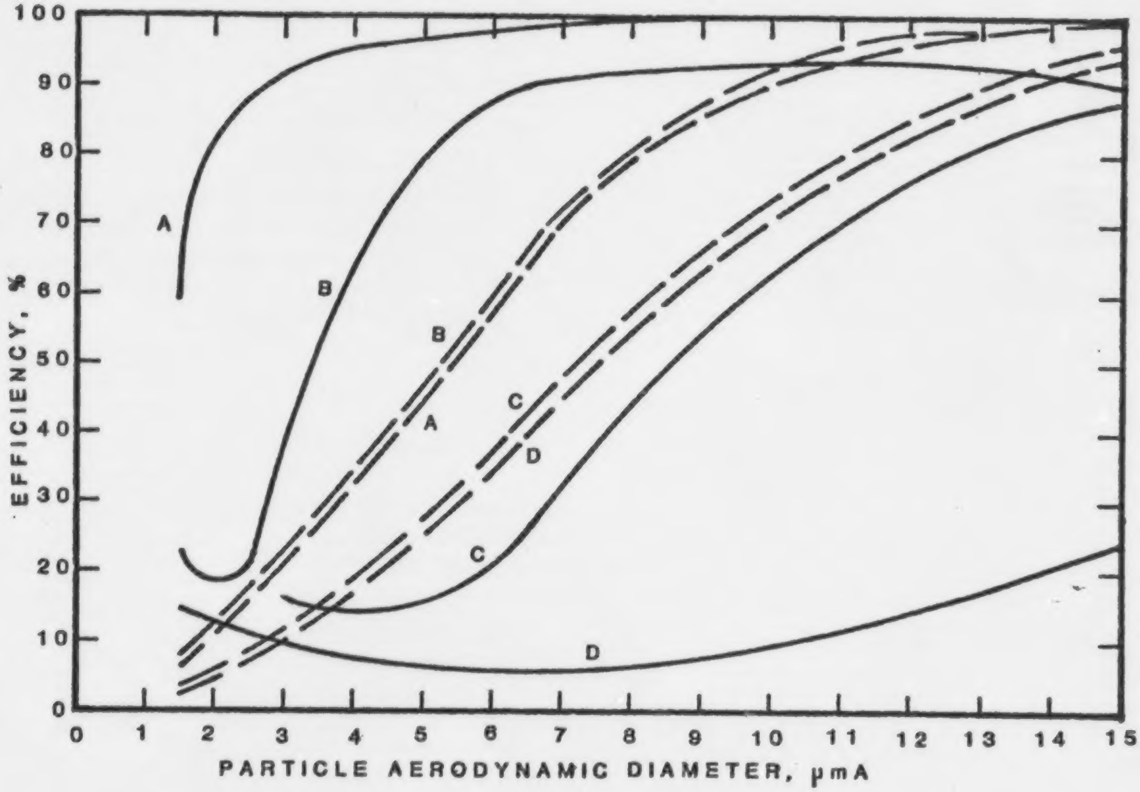

	T, °C	P, kPa	U_c, cm/s
A	20	1,221	253
B	22	192	264
C	512	516	262
D	693	205	288

---- THEORY

——— DATA

Figure 31. Comparison with model of Sproull (1970).

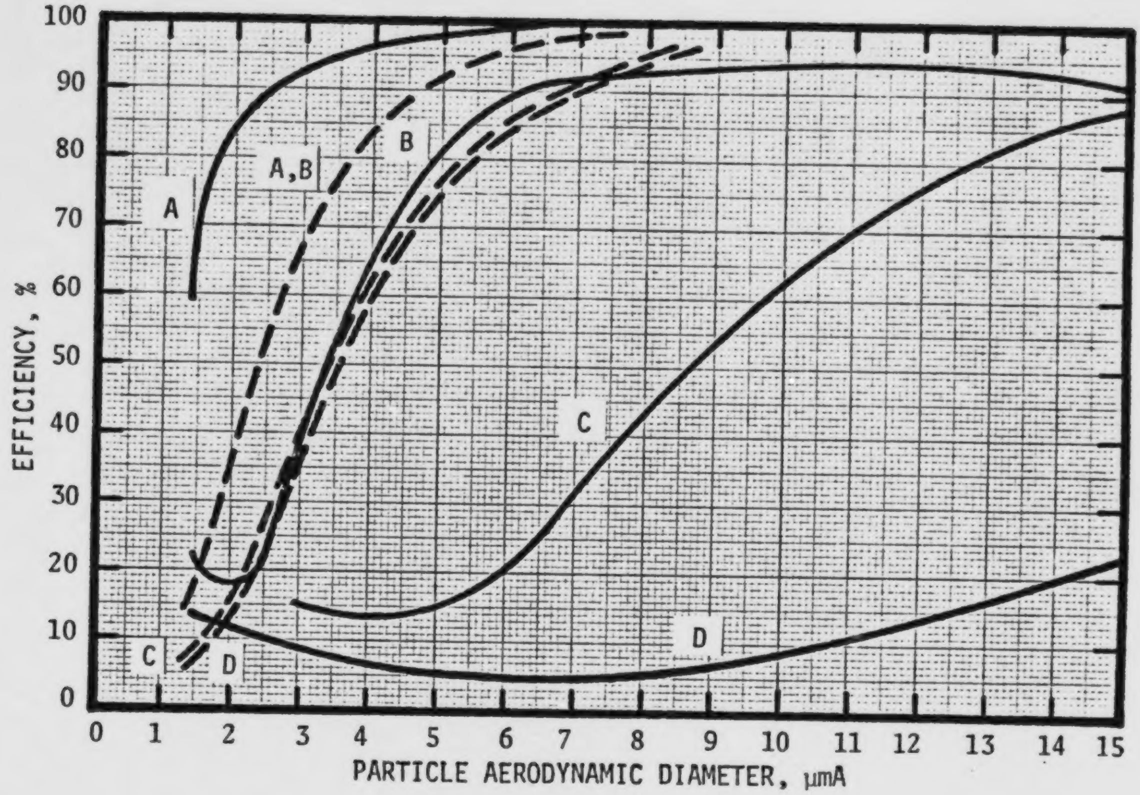

	T, °C	P, kPa	U_c, cm/s
A	20	1,221	253
B	22	192	264
C	512	516	262
D	693	205	288

Figure 32. Comparison with model of Dietz.

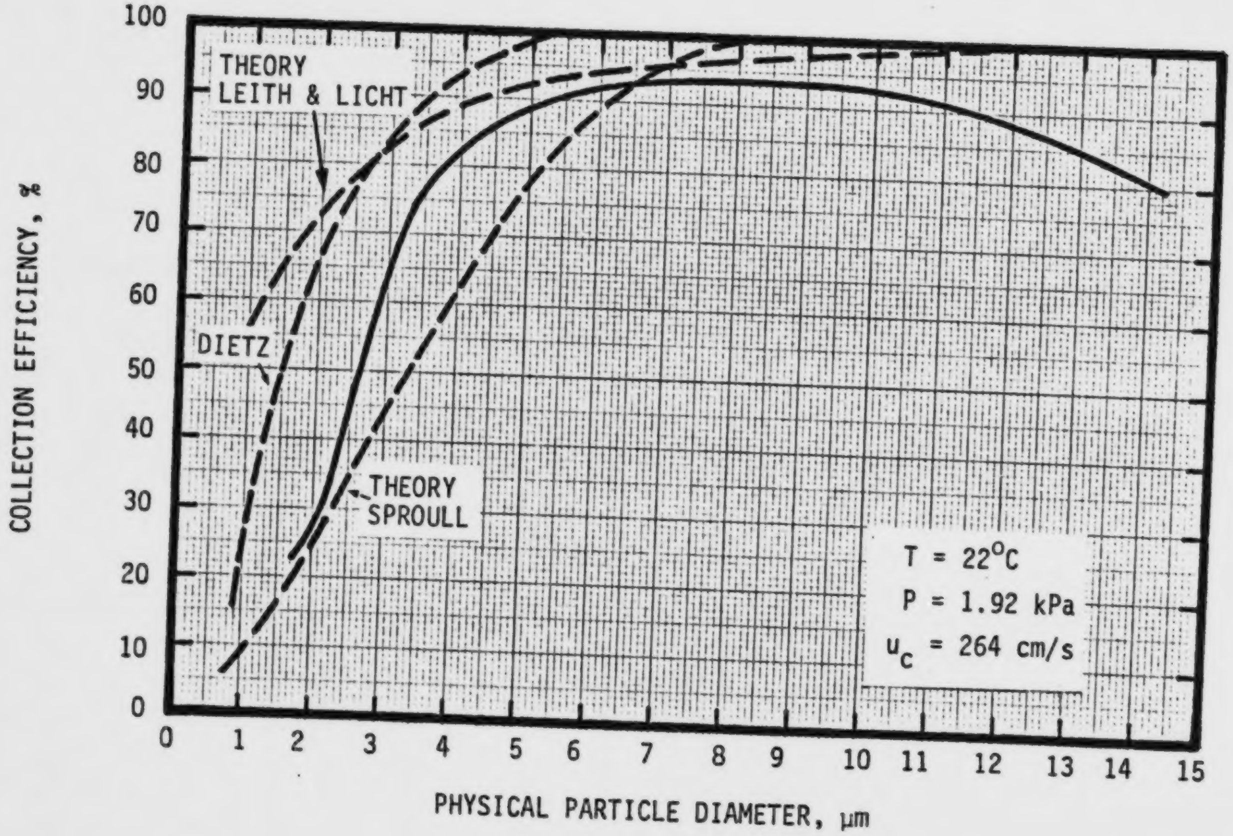

Figure 33. Comparison with models at low temperature and pressure; Test No. 31/48/1.

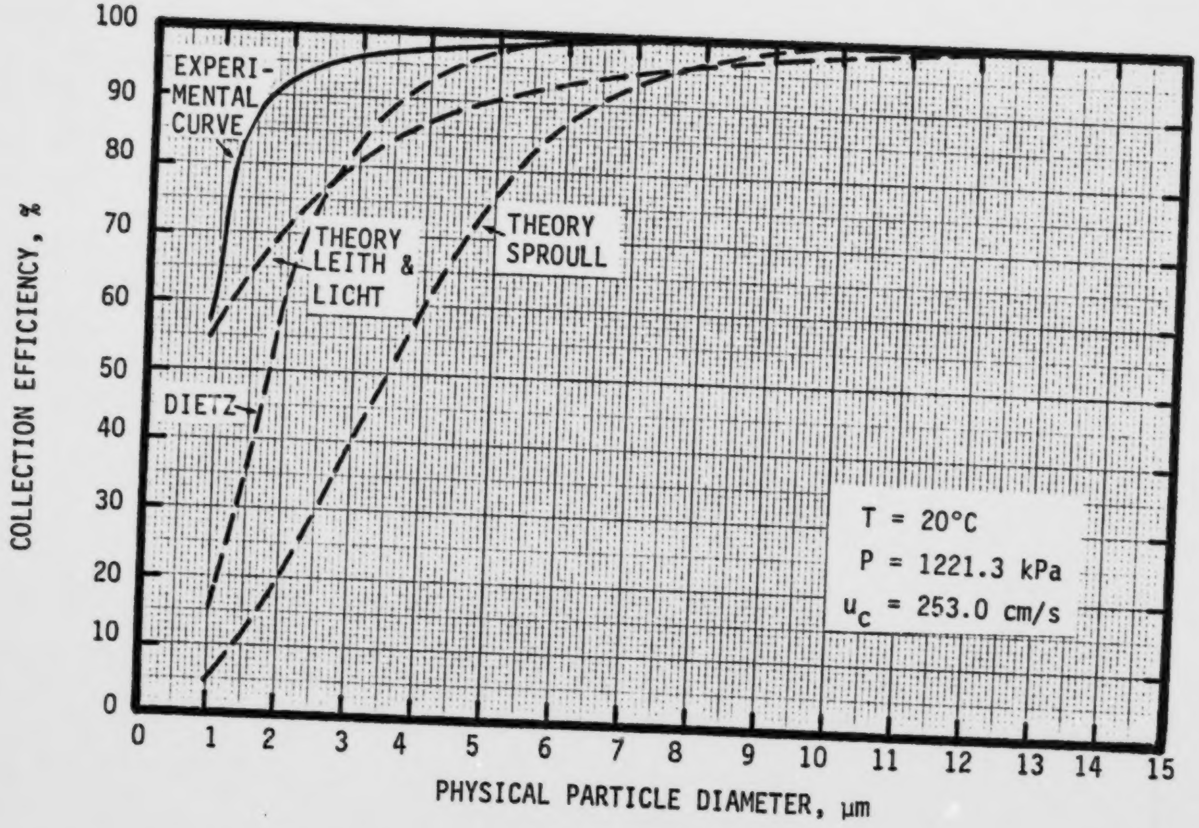

Figure 34. Compariton with models at high pressure; Test No. 31/49/8.

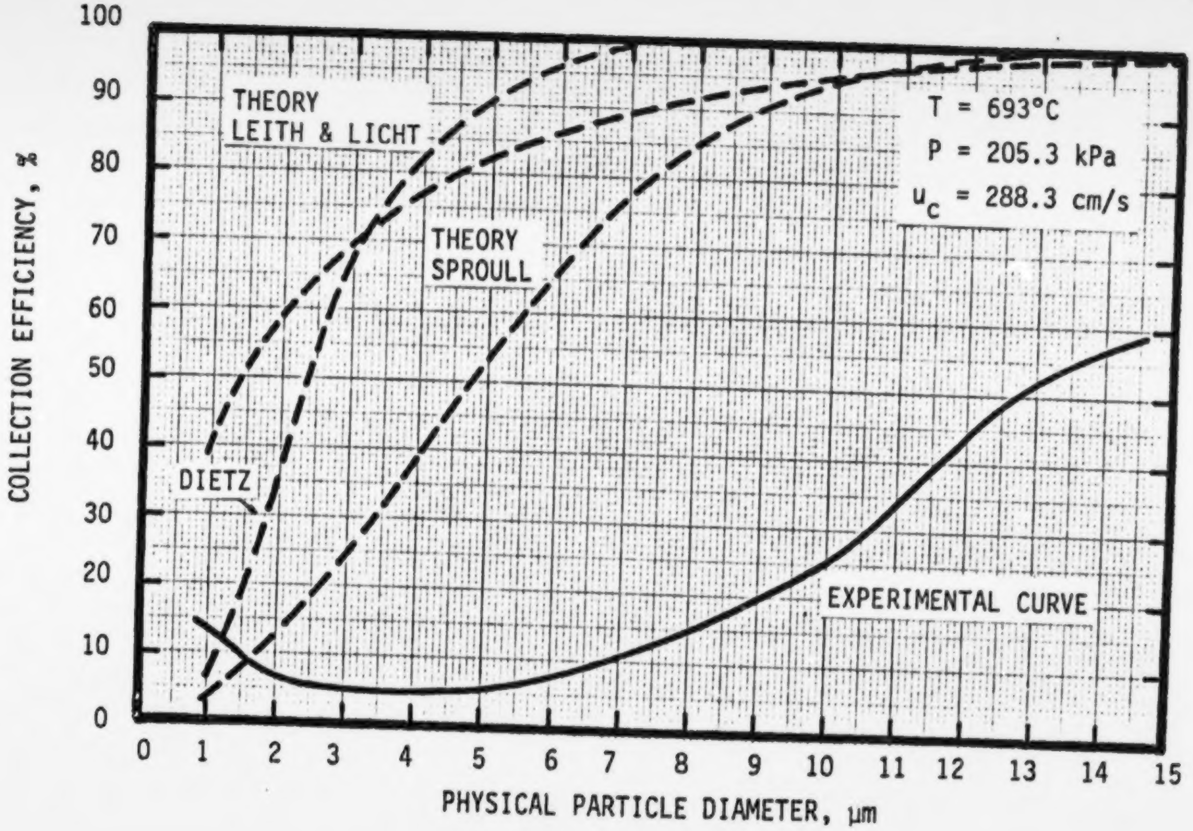

Figure 35. Comparison with models at high temperatures; Test No. 31/50/3.

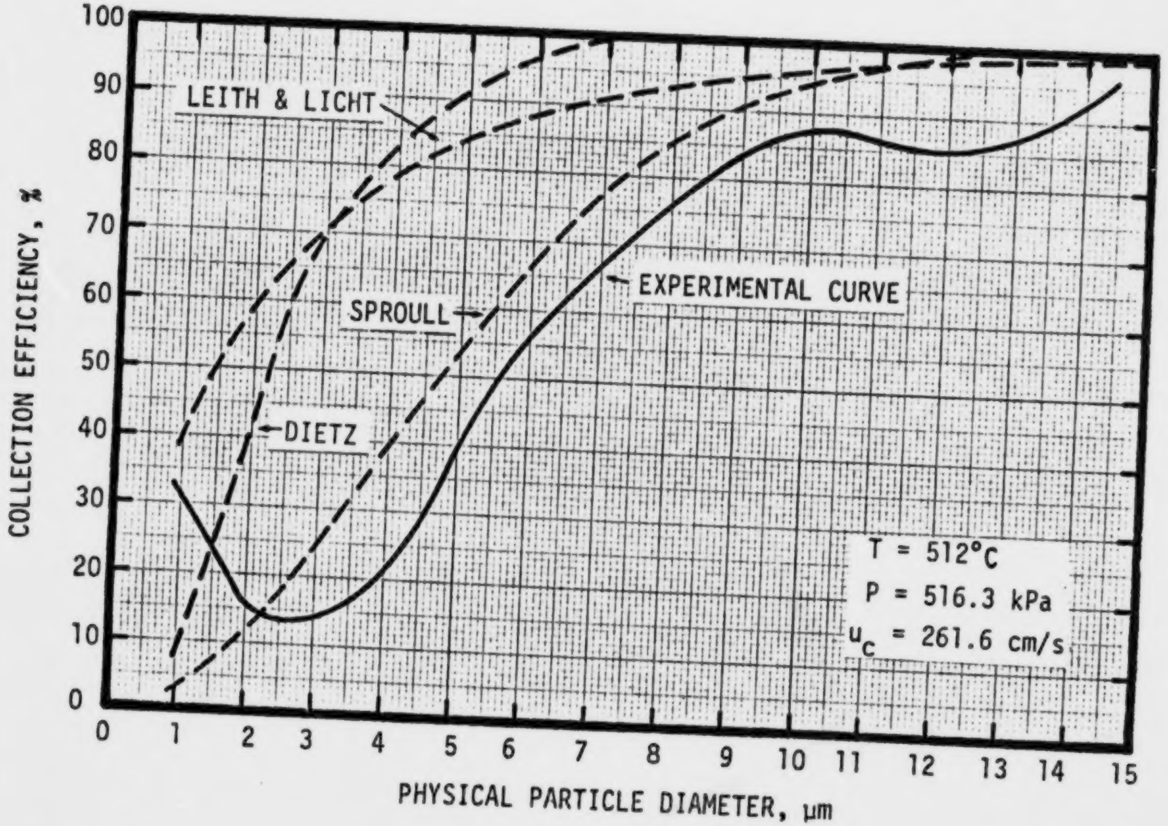

Figure 36. Comparison with models at high temperature and pressure; No. 31/50/1.

TABLE 15. EXPERIMENTAL AND THEORETICAL CUT DIAMETERS

Run No.	Aerodynamic Cut Diameters, µmA Experimental d_{p50}	Experimental d_{p90}	Rosin (10) d_{crit}	Davies (11) d_{crit}	Strauss (12) d_{crit}	Stairmand (13) d_{p50}	Barth (14) d_{p50}	Lapple (15) d_{p50}	Sproull (8) d_{p50}	Leith/Licht (7) d_{p50}
48-01	3.5	6.3	4.79	9.44	2.54	2.25	4.70	4.34	5.07	1.28
48-02	4.2	6.6	4.75	9.37	2.53	2.23	4.66	4.31	4.77	1.28
48-03	5.3	10.0	5.48	10.79	2.92	2.58	5.38	4.97	5.85	1.45
48-04	6.3	10.5	5.63	11.06	3.01	2.67	5.53	5.11	6.03	1.63
48-05	13.2	23.1	6.73	13.19	3.61	3.20	6.60	6.10	7.29	2.13
48-06	10.0	17.9	6.43	12.60	3.45	3.06	6.31	5.83	6.98	2.13
48-07	18.8	24.6	6.75	13.22	3.62	3.21	6.62	6.12	7.46	2.29
49-01	8.8	16.6	5.98	11.73	3.20	2.84	5.87	5.42	6.36	1.65
49-02	4.8	9.8	5.79	11.41	3.08	2.72	5.68	5.24	6.22	1.52
49-03	2.2	4.7	5.60	11.10	2.95	2.60	5.50	5.07	6.09	1.46
49-04	2.1	5.0	5.66	11.22	2.98	2.63	5.56	5.12	6.16	1.53
49-05	1.0	4.1	5.68	11.26	2.99	2.63	5.57	5.14	6.65	1.53
49-06	1.2	3.4	4.77	9.45	2.52	2.22	4.68	4.32	5.18	1.24
49-07	1.6	3.5	4.75	9.42	2.50	2.21	4.66	4.30	5.17	1.23
49-08	1.4	2.7	4.82	9.55	2.54	2.23	4.73	4.36	5.17	1.22
49-09	6.9	13.0	6.72	13.26	3.57	3.15	6.60	6.09	7.28	2.35
50-01	8.4	15.2	6.69	13.21	3.55	3.14	6.57	6.06	7.28	2.27
50-02	7.6	18.3	6.67	13.16	3.54	3.12	6.54	6.04	7.20	2.27
50-03	19.4	*	6.95	13.56	3.76	3.34	6.83	6.31	7.44	2.51
55-02	*	2.3	4.87	9.67	2.56	2.25	4.78	4.41	5.46	1.32
55-03	*	2.6	4.90	9.73	2.58	2.27	4.81	4.44	5.46	1.35
55-04	*	1.9	3.36	6.67	1.77	1.55	3.30	3.04	3.72	0.91
55-05	*	1.7	3.35	6.65	1.76	1.55	3.29	3.03	3.72	0.91
55-06	*	1.6	3.38	6.71	1.78	1.57	3.32	3.06	3.72	0.91
55-07	*	2.3	3.39	6.73	1.78	1.57	3.33	3.07	3.72	0.91
55-08	*	1.7	3.37	6.69	1.77	1.56	3.31	3.05	3.72	0.91
55-09	*	2.5	3.35	6.65	1.76	1.55	3.29	3.03	3.72	0.91
55-10	*	2.4	4.83	9.58	2.54	2.23	4.74	4.37	5.31	1.37
55-11	*	2.4	4.91	9.74	2.58	2.27	4.82	4.44	5.31	1.37
55-12	*	2.8	4.87	9.65	2.56	2.25	4.77	4.40	5.39	1.31
55-13	*	2.6	4.86	9.65	2.55	2.25	4.77	4.40	5.39	1.34

* No Data

TABLE 16. EXPERIMENTAL AND THEORETICAL PRESSURE DROP

				Theoretical Predictions (ΔP), cm water				
Run No.	Temp. °C	Pressure kPa	Measured Pressure Drop (ΔP), cm water	Shepherd/ Lapple (16)	First (17)	Alexander (18)	Stairmand (19)	Barth (14)
48.01	22	192	0.64	0.89	0.81	0.64	0.66	0.84
48-02	20	190	0.64	0.89	0.81	0.65	0.66	0.86
48-03	130	200	0.46	0.63	0.57	0.41	0.47	0.60
48-04	209	192	0.30	0.59	0.52	0.36	0.43	0.56
48-05	375	192	0.19	9.32	0.29	0.18	0.24	0.31
48-06	332	192	0.20	0.39	0.35	0.22	0.28	0.37
48-07	410	192	0.15	0.33	0.30	0.18	0.24	0.31
49-01	155	141	0.23	0.33	0.30	0.21	0.24	0.32
49-02	22	157	0.20	0.34	0.31	0.25	0.25	0.32
49-03	20	516	0.76	1.23	1.11	0.89	0.90	1.16
49-04	20	931	2.29	2.11	1.91	1.53	1.55	2.00
49-05	20	1,310	4.57	2.91	2.64	2.11	2.14	2.76
49-06	20	516	2.41	2.34	2.12	1.69	1.72	2.22
49-07	20	931	6.35	4.26	3.86	3.08	3.13	4.04
49-08	20	1,220	9.91	5.26	4.77	3.80	3.87	4.99
49-09	495	516	0.51	0.87	0.79	0.46	0.64	0.82
50-01	512	516	0.51	0.89	0.80	0.46	0.65	0.84
50-02	502	516	0.51	0.90	0.81	0.47	0.66	0.85
50-03	693	205	0.25	0.35	0.32	0.17	0.26	0.33
55-02	30	1,560	5.59	6.50	5.9	4.6	4.8	6.9
55-03	40	1,540	4.19	6.4	5.8	4.5	4.7	6.0
55-04	22	2,030	*	36.8	33.4	26.5	27.1	35.0
55-05	21	2,030	*	37.2	33.8	26.9	27.4	35.3
55-06	29	2,030	19.1	36.3	32.9	25.9	26.7	34.4
55-07	30	2,520	37.5	44.9	40.5	31.9	32.9	42.4
55-08	25	2,530	39.6	45.5	41.2	32.6	33.5	43.1
55-09	22	2,520	35.6	46.3	41.9	33.3	34.0	43.9
55-10	42	2,520	7.62	11.1	10.0	7.8	8.2	10.5
55-11	49	2,030	6.35	8.5	7.7	5.9	6.2	8.0
55-12	45	2,510	8.13	10.8	9.8	7.6	7.9	10.2
55-13	41	2,030	8.00	8.7	7.9	6.1	6.4	8.2

* No Data

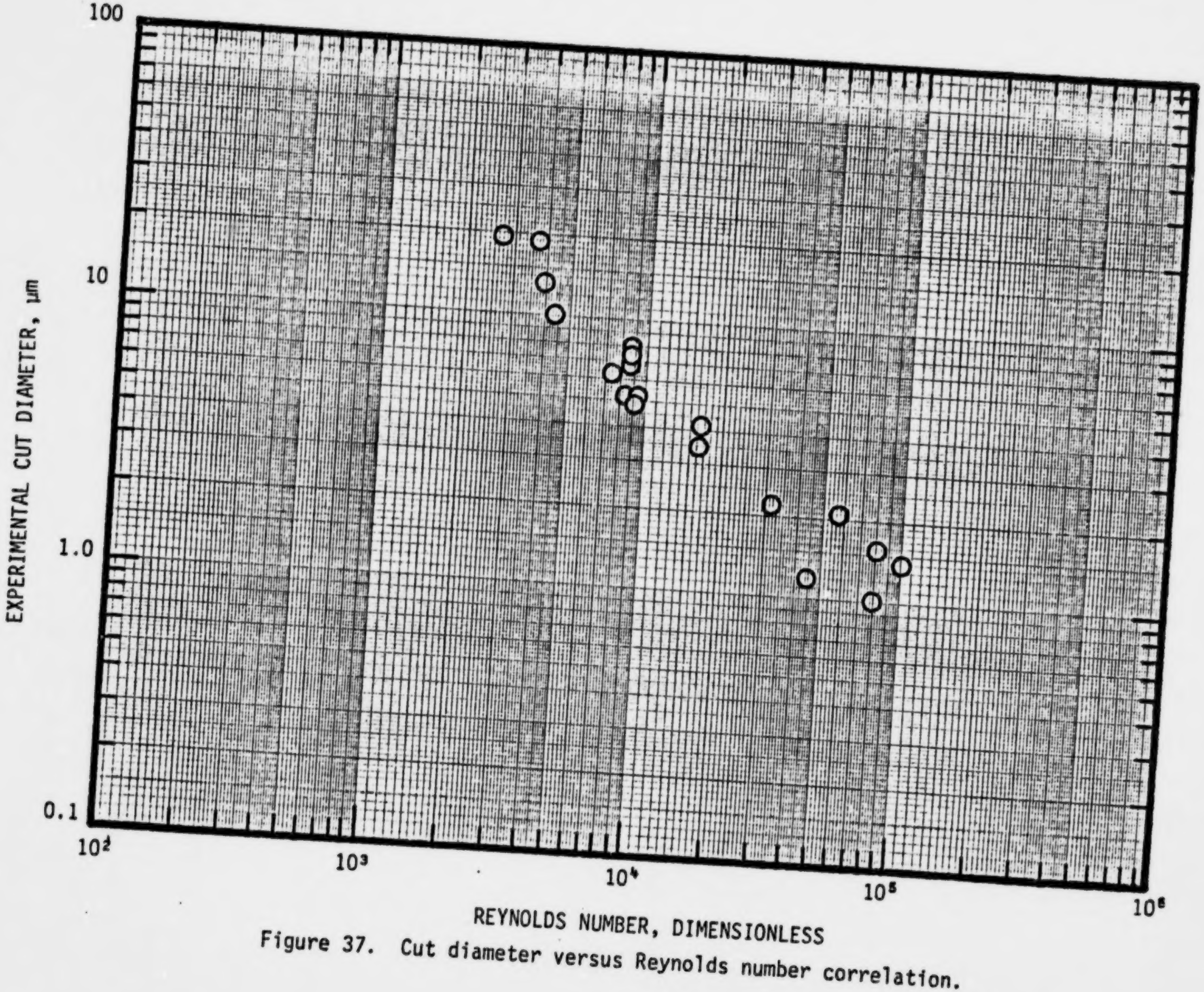

Figure 37. Cut diameter versus Reynolds number correlation.

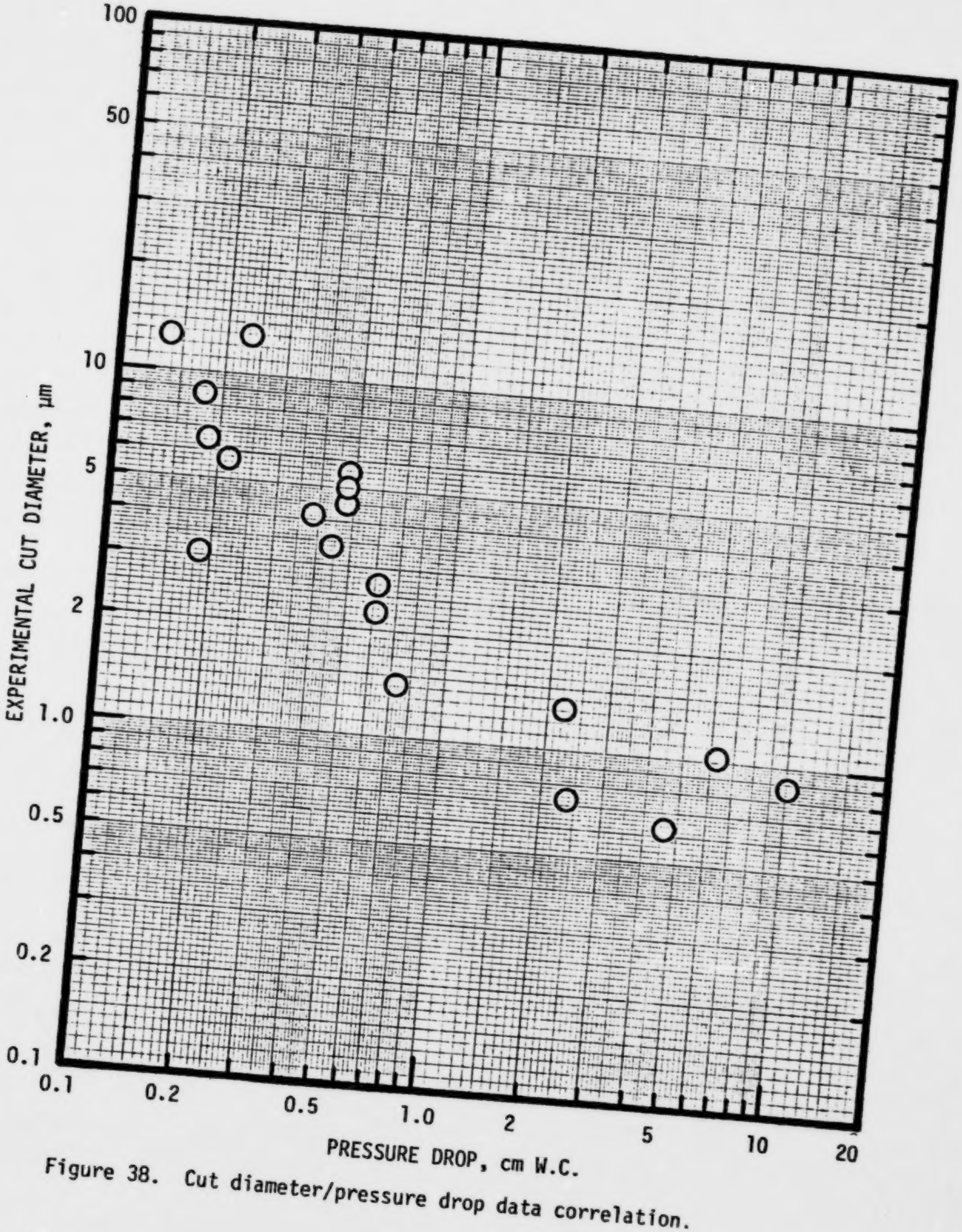

Figure 38. Cut diameter/pressure drop data correlation.

in the correlation. The Stokes number was defined in equation (54).

$$N_{Stk} = \frac{C' \, d_{pg}^2 \, \rho_p \, u_c}{9 \, \mu_G \, d_H} \tag{54}$$

where "d_{pg}" is the mass median diameter of the test aerosol.

The aerodynamic cut diameter is plotted versus the correlation parameter, "$N_{Re}N_{Stk}$" in Figure 39. The high temperature and pressure data fall on the same curve as the room temperature and low pressure data. Data from the Exxon Miniplant tertiary cyclone are also plotted in the same graph. The Exxon data agree well with the correlation.

Figure 40 shows the comparison between the correlation and the data of Smith et al. (1979). Their data show a similar functionality between cut diameter and "$N_{Re}N_{Stk}$"; however, their cut diameters are smaller, especially for the smaller cyclones. Apparently the cyclone size is an additional important parameter for small cyclones.

The high pressure data of Knowlton and Bachovchin (1978) do not extend low enough to give 50% cut diameters. Therefore, their data in terms of 90% cut diameters are plotted in Figure 41 along with present results. Their data fall at a higher "$N_{Re}N_{Stk}$" range than present study and show somewhat higher 90% cut diameters.

DISCUSSION AND CONCLUSIONS

The effects of temperature and pressure on cyclone performance are surprising when compared to cyclone performance models. The cut diameter correlation with "$N_{Re}N_{Stk}$" accounts for the observed temperature and pressure effects for our results.

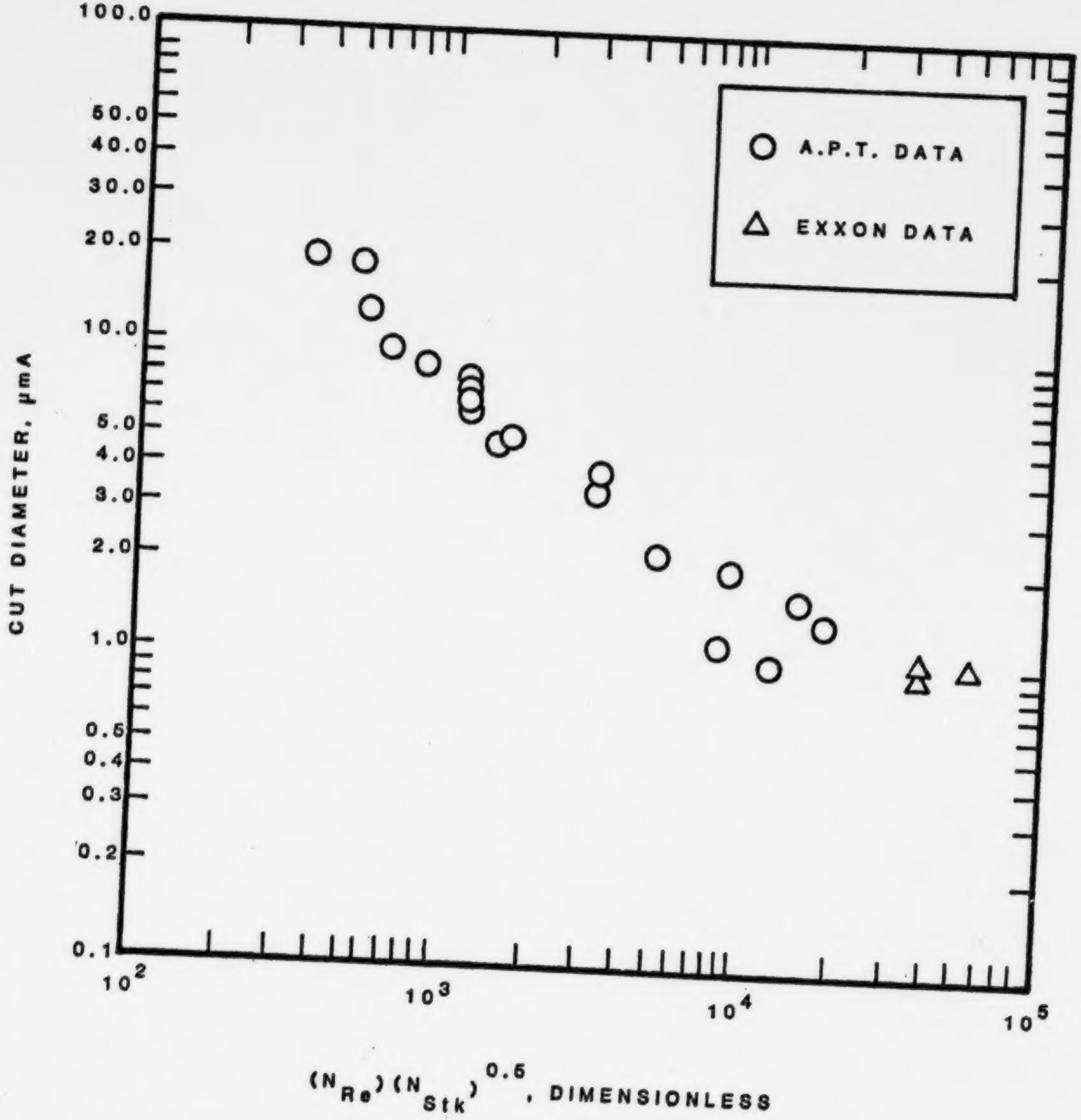

FIGURE 39. DATA CORRELATION WITH CUT DIAMETERS.

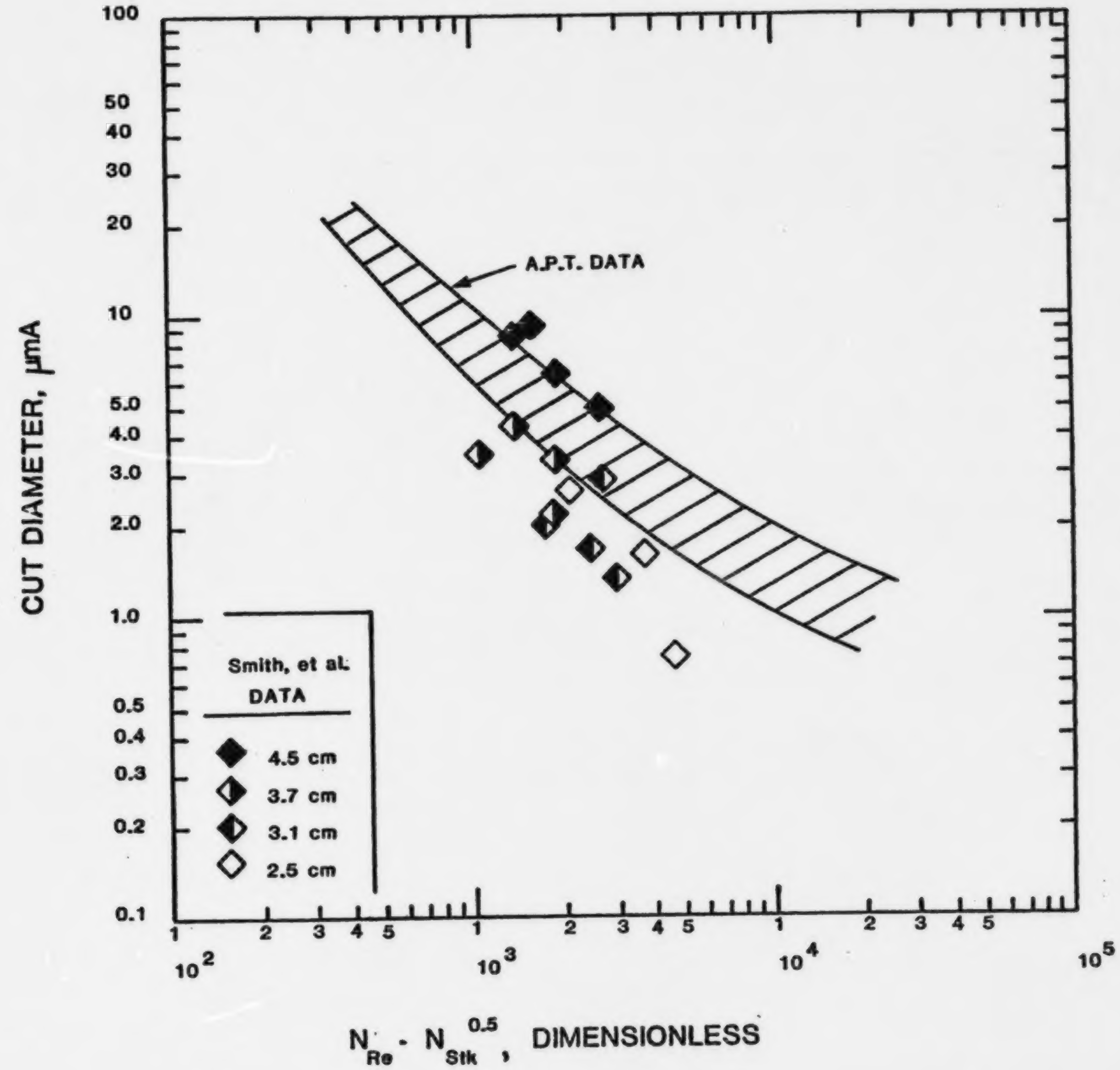

FIGURE 40. COMPARISON WITH DATA OF SMITH et al. (1979).

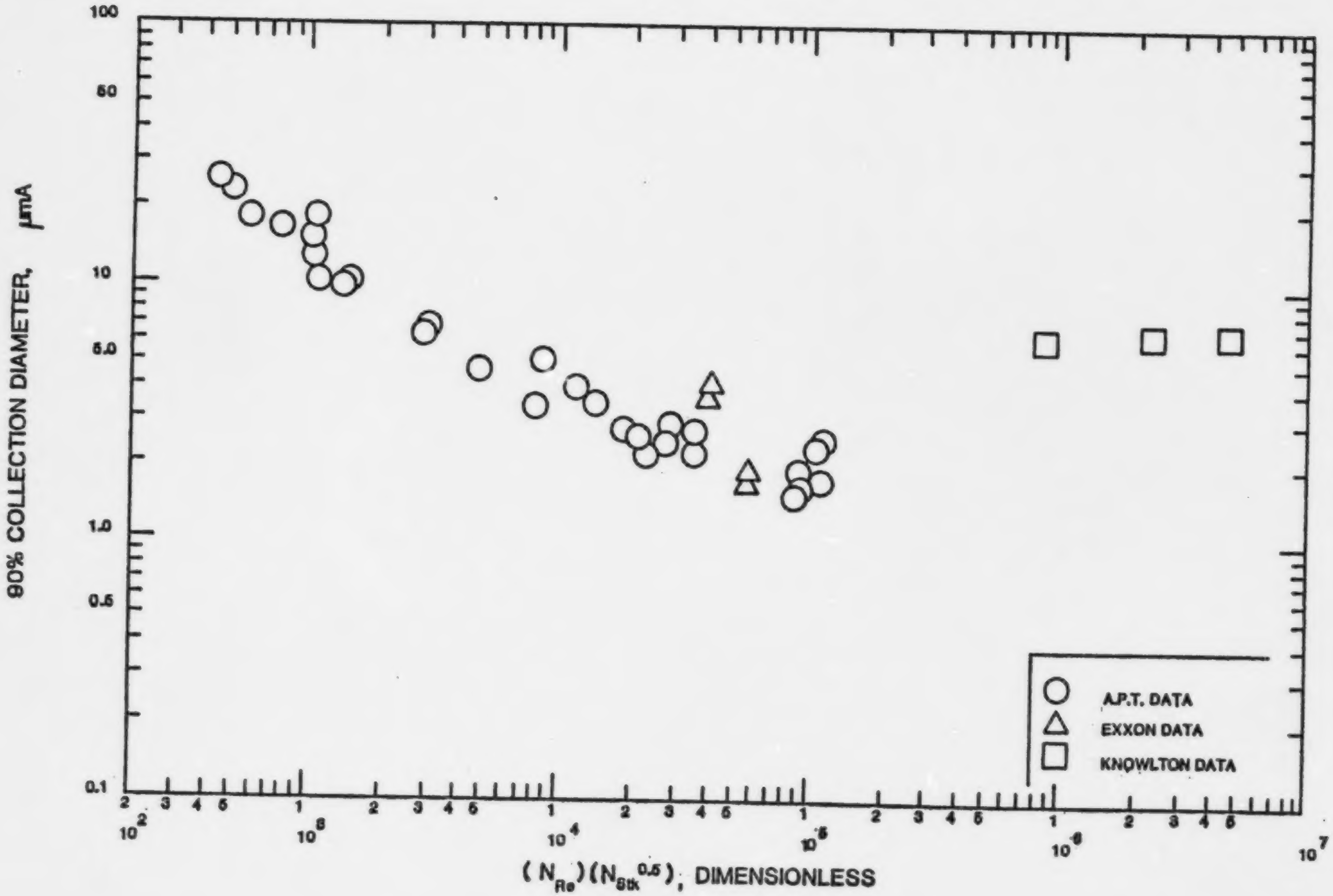

FIGURE 41. DATA CORRELATION WITH 90% CUT DIAMETERS.

This correlation also agrees with the Exxon Miniplant data where a larger cyclone (15 cm) was operated at much higher velocity (36 m/s). Apparently the Reynolds number, and hence the flow pattern in the cyclone, is very important in determining particle deposition.

The Knowlton and Bachovchin data show no effect of pressure on collection efficiency. Their data are at higher values of $N_{Re} \cdot N_{Stk}$ than presently studied. Their cut diameters also are somewhat larger than ours.

It may be that the gas flow is stabilized by the curved flow in the cyclone. It has been observed that the transition from laminar to turbulent flow occurs at "N_{Re}" as high as around 15,000 in flow through helical coils rather than at 2,100 as in straight pipes. If the two cases, in which the mean acceleration force on the particle is the same (i.e., same angular velocity of the gas streams), are compared, the particle deposition rate will be lower for turbulent flow than for laminar flow because the particle concentration gradient is decreased by the turbulent mixing.

Both the flow characteristics and the effect of high pressure on them need to be studied if a rational design basis is to be developed. Furthermore, present results are only for one cyclone geometry and are limited to relatively low velocities. More data at higher values of "$N_{Re}N_{Stk}$" would be useful. Also variations in cyclone dimensions and geometries should be investigated to determine how they affect this empirical correlation.

SECTION 6

BROWNIAN DIFFUSION

One important particle collection mechanism for very small particles is Brownian diffusion. Brownian diffusion is the random motion of particles resulting from collisions with the gas molecules. Particle collection by Brownian diffusion is only important for particles smaller than about 0.1 μm at normal temperatures and pressures. At high temperature, diffusion will increase and, depending on the particle size, may become significant for somewhat larger particles. A limited experimental investigation of Brownian diffusion at high temperature was done and the results are presented below.

Diffusion Battery

In the present work, a high temperature and pressure screen diffusion battery was used to study the effects of temperature and pressure on the particle collection efficiency when diffusion is the dominant collection mechanism.

The diffusion battery was exposed to fly ash aerosol in a well-defined laminar flow field. The diffusion battery consisted of a series of modules each containing 25 wire screens, 4.76 cm in diameter. Individual screens were separated by a triangular shaped Nichrome wire spacer. Each module was stiffened by end rings which were held together by pins. The modules are mounted in a pipe. The wire screens were made to fit snugly in the pipe to reduce the channeling of flow between the pipe wall and the modules. The precutter, diffusion battery, and final filter are arranged as shown in Figure 42.

THEORY

Fine particles in a gas stream undergo significant Brownian

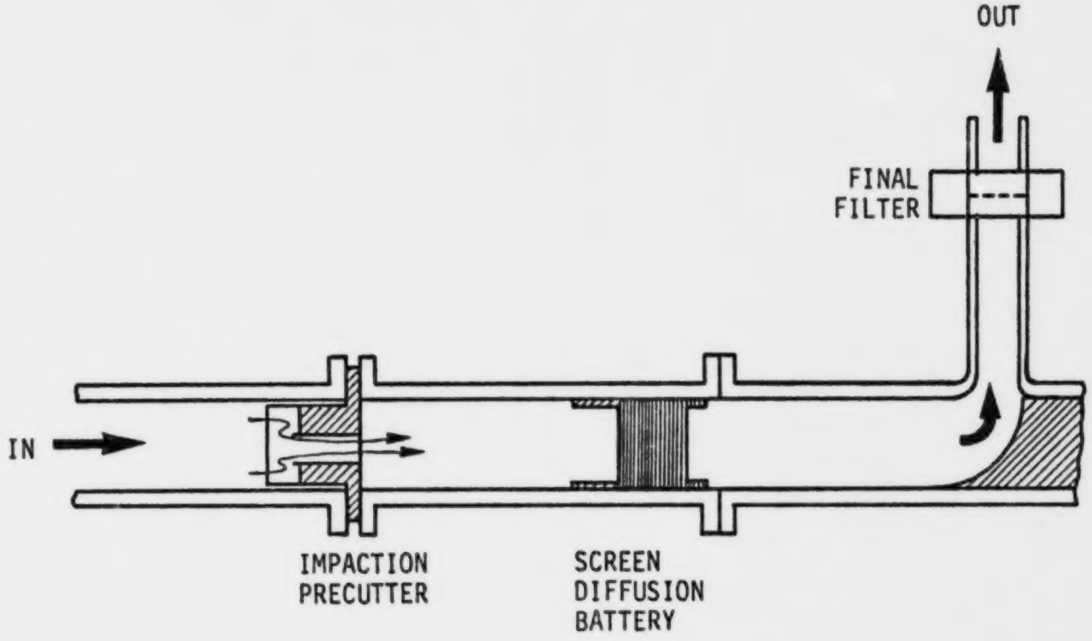
OUT
FINAL FILTER
IN
IMPACTION PRECUTTER
SCREEN DIFFUSION BATTERY

Figure 42. Diffusion battery and precutter setup.

motion resulting from the random bombardment of the particles by gas molecules. The rate of diffusion is characterized by the particle diffusivity, D_p, which is given by the Stokes-Einstein equation,

$$D_p = \frac{C' \; k \; T}{3 \; \pi \; \mu_G \; d_p} \tag{55}$$

where C' = Cunningham slip factor, dimensionless
k = Boltzman's constant, erg/°K
T = absolute temperature, °K
μ_G = gas viscosity, g/cm-s
d_p = particle diameter, cm

Particle diffusivity increases with increasing temperature but decreases with increasing pressure. It is often assumed that Brownian diffusion is not a significant collection mechanism for particles larger than about 0.1 μm. This may be true at standard conditions. At high temperatures the particle diffusivity is increased and thus the particle size for which diffusion is significant is increased.

Screen Diffusion Battery

The theory and data reduction method for screen diffusion battery have been presented by Patterson and Calvert (1978). The particle penetration through an array of wire cylinders is:

$$Pt_n = \frac{n_1}{n_2} = \exp \; (-S \; \eta) \tag{56}$$

where $S = 4 \; v_f \; x/\pi \; d_c$ is the solidity factor.
n_1, n_2 = the inlet and outlet particle number concentrations respectively, cm^{-3}

x = distance in the net flow direction, cm

v_f = volume fraction of wires, dimensionless

d_c = wire diameter, cm

η = single cylinder collection efficiency, dimensionless

For a "clean" single wire, collection due to diffusion is (Patterson and Calvert, 1978)

$$\eta_D = 6.0\ N_{Pe}^{\ -2/3} = 6.0\left(\frac{D_p}{u_G\ d_c}\right)^{0.67} \tag{57}$$

where N_{Pe} = Peclet number, dimensionless

By combining equations (56) and (57), the screen diffusion battery penetration is:

$$Pt_d = \frac{n_1}{n_2} = \exp\left[-6.0\ S\left(\frac{D_p}{u_G\ d_c}\right)^{0.67}\right] \tag{58}$$

where u_G is the superficial velocity.

It should be pointed out here that this equation applies to a "clean" diffusion battery. As the particles deposit they may collect on previously deposited particles to form chain-like structures or dendrites which can act as efficient collectors.

Predicted Screen Diffusion Battery Penetration

Particle deposition on wire screens can occur through any one or a combination of the following particle collection mechanisms.

1. Impaction
2. Interception
3. Sedimentation
4. Electrostatic forces
5. Diffusion

The wire screen is modelled as a geometric arrangement of single wires in space. The collection efficiency of a single wire can be used to calculate the overall efficiency of the wire mesh.

In order to estimate the contribution of each of the above mentioned deposition mechanisms, the single wire collection efficiency was calculated for the following conditions:

Pressure, $P = 1$ atm
Temperature, $T = 20°C$
Particle diameter, $d_p = 0.5$ μm
Particle density, $\varrho_p = 2.3$ g/cm^3
Gas density, $\varrho_G = 1 \times 10^{-3}$ g/cm^3
Gas viscosity, $\mu_G = 0.0018$ g/cm-s
Wire diameter, $d_c = 94$ μm
Superficial velocity, $u_G = 5.6$ cm/s

The collection efficiency, η_I, due to inertial impaction, is characterized by the inertial parameter, K_p.

$$K_p = \frac{d_p^2 \, C' \, \varrho_p \, u_G}{9 \, \mu_G \, d_c} \tag{59}$$

For the assumed conditions,

$$K_p = 0.0022$$

The inertial parameter, K_p, is very small so the inertial effects are negligible. At higher superficial velocities inertial effects would become more important.

The particle collection efficiency due to interception is characterized by,

$$K_R = \frac{d_p}{d_c} \tag{60}$$

For $K_R < 0.1$, collection due to interception, η_R, is (Davies, 1973):

$$\eta_R = \left(\frac{d_p}{d_c}\right)^2 / (2 - \ln N_{Re}) \qquad (61)$$

For the assumed conditions

K_R = 0.0053

N_{Re} = 0.263 (based on wire diameter)

η_R = 8.4×10^{-6}

The collection efficiency due to gravitational settling, η_G, is given by (Pich in Davies, 1966),

$$\eta_G = \frac{u_t}{u_G} \qquad (62)$$

where u_t = terminal settling velocity, cm/s

$$u_t = \frac{2\left(\frac{d_p}{2}\right)^2 (\varrho_p - \varrho_G)\ g}{9\ \mu_G} = 1.6 \times 10^{-3} \text{ cm/s} \qquad (63)$$

and $\eta_G = 2.8 \times 10^{-4}$

The collection efficiency, η_D, due to diffusion is given by equation (57). For the assumed conditions,

$$N_{Pe} = 7.86 \times 10^{4}$$
$$\eta_D = 3.3 \times 10^{-3}$$

Table 17 shows a summary of the calculations. As can be seen, diffusional collection is the most important mechanism for particles smaller than 0.5 μm diameter.

TABLE 17. INERTIAL, INTERCEPTION, GRAVITY SETTLING, AND DIFFUSION EFFICIENCIES FOR DIFFUSION BATTERY

$T = 20°C$, $P = 1$ atm

Particle Diameter	η_I	η_G	η_D
0.5 μm	8.4×10^{-4}	4.8×10^{-4}	1.47×10^{-3}
1.0 μm	2.9×10^{-3}	1.94×10^{-4}	8.4×10^{-4}
2.0 μm	1.3×10^{-4}	4.5×10^{-3}	1.13×10^{-3}

Equation (58) was used to predict the diffusion battery penetration for a gas velocity of 5.6 cm/s and a range of temperatures and pressures. The diffusion battery was assumed to consist of two modules of 25 screens each. The results are presented in Table 18.

APPARATUS AND EXPERIMENTAL PROCEDURE

A schematic diagram of the equipment is given in Figure 43. Fly ash particles were generated by the fluidized bed particle generator and particles larger than 2 μm diameter were removed from the aerosol with a cyclone and a precutter. The aerosol was then heated in the tubular section to 100°C and passed through a single stage impactor which had a cut diameter of 1.4 μm diameter. The aerosol was then passed through the diffusion battery where the fine particles were collected. The particles penetrating through the diffusion battery were collected at the exhaust filter. After 1 hour of operation, the diffusion modules were carefully removed from the pipe. The fly ash was removed by washing the modules in acetone. Each module was dismantled and washed in 80 ml of acetone in an ultrasonic bath for 15 minutes. The fly ash was recovered by evaporating the acetone and analyzed using a Coulter counter.

The number and volume size distributions of the fly ash particles collected on the exhaust filter were determoned by the same method described in the last section. The penetration, Pt_d, for a particular diameter, d_p, was calculated as follows:

$$Pt_d = \frac{N_2}{N_1 + N_2} \qquad (64)$$

Table 18. PREDICTED PENETRATION FOR SCREEN DIFFUSION BATTERY

a) 25 SCREENS

PARTICLE DIAMETER, µm	PENETRATION, Fraction 100°C 1 atm	300°C 1 atm	500°C 1 atm	800°C 1 atm	300°C 10 atm
0.56	0.985	0.982	0.978	0.972	0.986
0.71	0.988	0.985	0.983	0.979	0.988
0.89	0.990	0.988	0.986	0.983	0.990
1.12	0.992	0.990	0.989	0.986	0.992
1.41	0.993	0.992	0.991	0.989	0.993
1.78	0.994	0.993	0.992	0.991	0.994

b) 50 SCREENS

PARTICLE DIAMETER, µm	PENETRATION, Fraction 100°C 1 atm	300°C 1 atm	500°C 1 atm	800°C 1 atm	300°C 10 atm
0.56	0.970	0.964	0.957	0.946	0.973
0.71	0.976	0.971	0.966	0.958	0.977
0.89	0.980	0.976	0.972	0.966	0.980
1.12	0.983	0.980	0.977	0.973	0.983
1.41	0.986	0.984	0.981	0.978	0.986
1.78	0.988	0.986	0.985	0.982	0.988

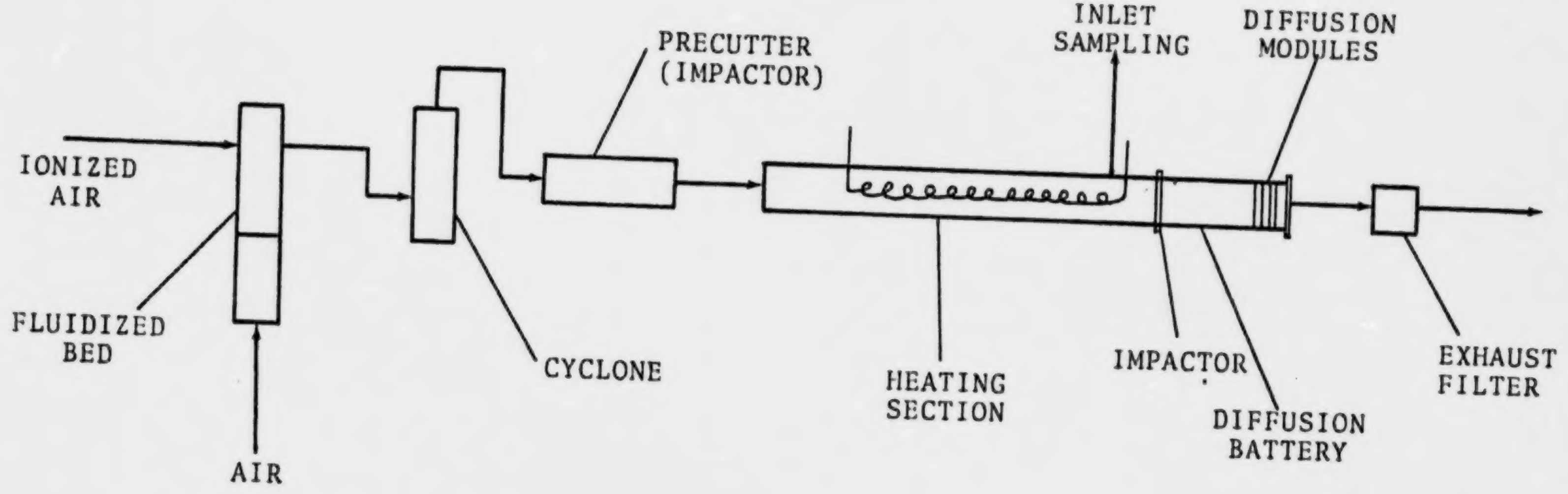
IONIZED AIR
FLUIDIZED BED
AIR
CYCLONE
PRECUTTER (IMPACTOR)
HEATING SECTION
INLET SAMPLING
IMPACTOR
DIFFUSION MODULES
DIFFUSION BATTERY
EXHAUST FILTER

Figure 43. Schematic diagram of Brownian diffusion experiment.

where N_2 = number of particles of diameter, d_p, deposited on the exhaust filter

N_1 = number of particles of diameter ,d_p, deposited in the diffusion battery

RESULTS

Diffusion experiments were run at 100°C, 300°C, 500°C, and 800°C at 1 atm pressure and at 300°C and 10 atm pressure. The superficial velocity through the screens was kept constant at 5.6 cm/s for all runs. Two screen modules were used in series. Each module contained 25 screens.

Three runs were made for each of the 100°C, 300°C and 500°C atmospheric pressure conditions. The results are presented in Tables 19, 20 and 21. Since the precutter did not have a sharp cut at 1.4 μm diameter, particles larger than 1.4 μm diameter still existed in the gas stream even though their number concentration was low.

The penetration generally increased with particle diameter up to 1.4 μm. Above 1.4 μm penetration decreased again, probably as a result of inertial deposition and interception becoming important. There does not appear to be any noticeable effect of gas temperature on penetration. This could be that any temperature effects were masked by the uncertainty in the experimental data.

Only one run was obtained for each of the 800°C, 1 atm and 300°C, 10 atm test conditions. The results from all diffusion battery runs are summarized in Table 22. There is no clear effect of temperature or pressure on penetration which is qualitatively consistent with the predictions presented in Table 18. However, the magnitude of the measured penetrations is smaller than that predicted for all temperatures and pressures tested.

Since the theoretical model does not accurately predict the penetration, an empirical approach was tried to obtain a more quantitative evaluation of the theory. It was assumed that the 100°C, 1 atm data are accurate and then these data were extrapo-

TABLE 19. DIFFUSION BATTERY DATA FOR 1 atm, 100°C.

Temperature= 100°C, Pressure= 1 atm, Velocity= 5.6 cm/s

a) 25 SCREENS

PARTICLE DIAMETER, µm	PENETRATION, Fraction			
	Run No. 38/1	38/2	38/3	$P\bar{t} \pm \sigma$
0.56	0.75	0.59	0.63	0.66 ± 0.08
0.71	0.74	0.62	0.70	0.69 ± 0.06
0.89	0.72	0.64	0.77	0.71 ± 0.07
1.12	0.70	0.65	0.81	0.72 ± 0.08
1.41	0.69	0.64	0.83	0.72 ± 0.10
1.78	0.66	0.63	0.81	0.70 ± 0.10

b) 50 SCREENS

PARTICLE DIAMETER, µm	PENETRATION, Fraction			
	Run No. 38/1	38/2	38/3	$P\bar{t} \pm \sigma$
0.56	0.62	0.37	0.45	0.48 ± 0.13
0.71	0.62	0.44	0.53	0.53 ± 0.09
0.89	0.59	0.48	0.61	0.56 ± 0.07
1.12	0.57	0.50	0.65	0.57 ± 0.08
1.41	0.54	0.51	0.65	0.57 ± 0.07
1.78	0.49	0.52	0.59	0.53 ± 0.05

TABLE 20, DIFFUSION BATTERY DATA FOR 1 atm, 300°C.

Temperature= 300°C, Pressure= 1 atm, Velocity= 5.6 cm/s

a) 25 SCREENS

PARTICLE DIAMETER, μm	PENETRATION, Fraction			
	Run No. 38/4	38/5	38/6	$P\bar{t} \pm \sigma$
0.56	0.76	0.82	0.88	0.82 ± 0.06
0.71	0.79	0.82	0.83	0.81 ± 0.02
0.89	0.82	0.81	0.78	0.80 ± 0.02
1.12	0.82	0.80	0.75	0.79 ± 0.04
1.41	0.85	0.79	0.73	0.79 ± 0.06
1.78	0.86	0.76	0.70	0.77 ± 0.08

b) 50 SCREENS

PARTICLE DIAMETER, μm	PENETRATION, Fraction			
	Run No. 38/4	38/5	38/6	$P\bar{t} \pm \sigma$
0.56	0.37	0.56	0.70	0.54 ± 0.17
0.71	0.41	0.62	0.66	0.56 ± 0.13
0.89	0.46	0.63	0.61	0.57 ± 0.09
1.12	0.51	0.65	0.58	0.58 ± 0.07
1.41	0.58	0.62	0.58	0.59 ± 0.02
1.78	0.60	0.54	0.57	0.57 ± 0.03

TABLE 21. DIFFUSION BATTERY DATA FOR 1 atm, 500°C.

Temperature= 500°C, Pressure= 1 atm, Velocity= 5.6 cm/s

a) 25 Screens

PARTICLE DIAMETER, μm	PENETRATION, FRACTION			
	Run No. 38/7	38/8	38/9	$\overline{Pt} \pm \sigma$
0.56	0.78	0.87	0.75	0.80 ± 0.06
0.71	0.84	0.92	0.70	0.82 ± 0.11
0.89	0.84	0.94	0.67	0.82 ± 0.14
1.12	0.85	0.94	0.64	0.81 ± 0.15
1.41	0.85	0.93	0.61	0.80 ± 0.17
1.78	0.85	0.96	0.57	0.79 ± 0.20

b) 50 SCREENS

PARTICLE DIAMETER, μm	PENETRATION, Fraction			
	Run No. 38/7	38/8	38/9	$\overline{Pt} \pm \sigma$
0.56	0.52	0.59	0.49	0.53 ± 0.05
0.71	0.54	0.61	0.51	0.55 ± 0.05
0.89	0.54	0.63	0.50	0.56 ± 0.07
1.12	0.57	0.65	0.48	0.57 ± 0.09
1.41	0.58	0.68	0.43	0.56 ± 0.13
1.78	0.54	0.72	0.36	0.54 ± 0.18

TABLE 22. SUMMARY OF RESULTS FOR DIFFUSION BATTERY EXPERIMENTS

a) 25 SCREENS

PARTICLE DIAMETER, µm	PENETRATION, Fraction				
	100°C 1 atm	300°C 1 atm	500°C 1 atm	800°C 1 atm	300°C 10 atm
0.56	0.66	0.82	0.80	0.61	0.66
0.71	0.69	0.81	0.82	0.64	0.67
0.89	0.71	0.80	0.82	0.68	0.67
1.12	0.72	0.79	0.81	0.71	0.69
1.41	0.72	0.79	0.80	0.73	0.65
1.78	0.70	0.77	0.79	0.72	0.65

b) 50 SCREENS

PARTICLE DIAMETER, µm	PENETRATION, Fraction				
	100°C 1 atm	300°C 1 atm	500°C 1 atm	800°C 1 atm	300°C 10 atm
0.56	0.48	0.54	0.53	0.44	-
0.71	0.53	0.56	0.55	0.48	-
0.89	0.56	0.57	0.56	0.53	-
1.12	0.57	0.58	0.57	0.58	-
1.41	0.57	0.59	0.56	0.61	-
1.78	0.53	0.57	0.54	0.59	-

lated with the following equation to estimate the penetration at higher temperatures and pressures:

$$Pt(T,P) = Pt_o^n \tag{65}$$

$$n = \frac{D_p(T,P)}{D_{po}}^{0.67} \tag{66}$$

where $Pt(T,P)$ = penetration at any temperature and pressure, fraction

Pt_o = experimental penetration at 100°C and 1 atm, fraction

$D_p(T,P)$ = particle diffusivity at any temperature and pressure, cm²/s

D_{po} = particle diffusivity at 100°C and 1 atm, cm²/s

The results are presented in Table 23. The predicted decrease in penetration with rising temperature is greater than observed experimentally. There is a slight increase in the predicted penetration for the one high pressure run. Neither of these predicted trends were observed in our experimental data.

DISCUSSION AND CONCLUSIONS

The experimental apparatus and sample acquisition procedures were not sophisticated enough to detect any effects of gas temperature and pressure on diffusional collection. Therefore, present results are not sufficient to evaluate the theoretical model in terms of its ability to predict temperature and pressure effects on particle collection by diffusion.

The major conclusion from this work is that there is no significant difference between particle collection by Brownian diffusion at room temperature and pressure and particle collection at high temperature and high pressure. For the particle size range used in the experiments (≥ 0.5 μm diameter), theory predicts that there would be no significant temperature or pres-

TABLE 23. EXTRAPOLATED PREDICTIONS FOR SCREEN DIFFUSION BATTERY TESTS.

dp, µm	EXPTL. Pt 100°C, 1atm	EXTRAPOLATED Pt, Fraction 300°C, 1atm	500°C, 1atm	800°C, 1atm	300°C, 10atm
0.56	0.48	0.40	0.34	0.25	0.51
0.71	0.52	0.45	0.39	0.31	0.54
0.89	0.55	0.49	0.44	0.39	0.56
1.12	0.57	0.52	0.47	0.40	0.57
1.41	0.56	0.51	0.47	0.41	0.56
1.78	0.53	0.48	0.44	0.39	0.52

sure effects, and present data are qualitatively consistent with this prediction. Therefore, it is likely that Brownian diffusion will play a secondary role in high temperature and pressure particulate control in a similar manner to its role in conventional control devices.

SECTION 7

ELECTRICAL MIGRATION

Electrical migration (EM) refers to the movement of a charged particle in an electric field. Generally the particles are charged to one polarity and the electric field is arranged so as to promote the migration of the particles towards a collection electrode of the opposite polarity. The main electrostatic force between the particles and collection electrode is direct Coulombic attraction and is proportional to the electric field strength and particle charge level.

Electrical migration is important as the dominant collection mechanism in electrostatic precipitators and as a secondary mechanism in electrostatically augmented granular filters and dry scrubbers. Particle charging phenomena at high temperature and pressure present severe problems in terms of suitable electrical insualtion, materials of construction, minimum particle deposition in the charger, duct corona wire design (need sharp edges yet structurally taught wire at 1,600°F). A detailed study of particle charging at high temperature was beyond the scope of this study.

THEORY

The electrical migration velocity of a charged particle is (White, 1963):

$$u_e = \frac{n_p \; e \; E_p \; C'}{3\pi \; \mu_G \; d_s} = Z_p \; E \qquad (67)$$

where u_e = migration velocity, cm/s

n_p = number of elementary charge
e = elementary charge, C
E = electric field strength, V/cm
C' = Cunningham slip correction factor, dimensionless
μ_G = gas viscosity, g/cm-s
E_p = effective precipitating electric field strength, V/cm
d_s = surface diameter of particle, cm
Z_p = electrical mobility, cm²/s-V

In the present experiments, particles were charged at ambient temperature. Therefore, "n_p" is constant and the effects of temperature and pressure on electrical migration velocity comes in through the ratio "C'/μ_G" as can be seen from equation (67).

Figure 44 shows the effect of temperature and pressure on the ratio "C'/μ_G". The ratio decreases with increasing temperature and pressure. Therefore, the electrical migration velocity will be lower at high temperature and pressure.

APPARATUS

A drawing of the experimental setup is shown in Figure 45. Since we were not looking at the effects of charging particles at high temperature, the fly ash was charged upstream from the EM test section at room temperature and the gas (air) and fly ash were then heated to the desired operating temperature.

Corona Charger

Figure 46 shows the corona particle charger. It was located upstream from the main heating sections and operated at a temperature of 100°C to 200°C.

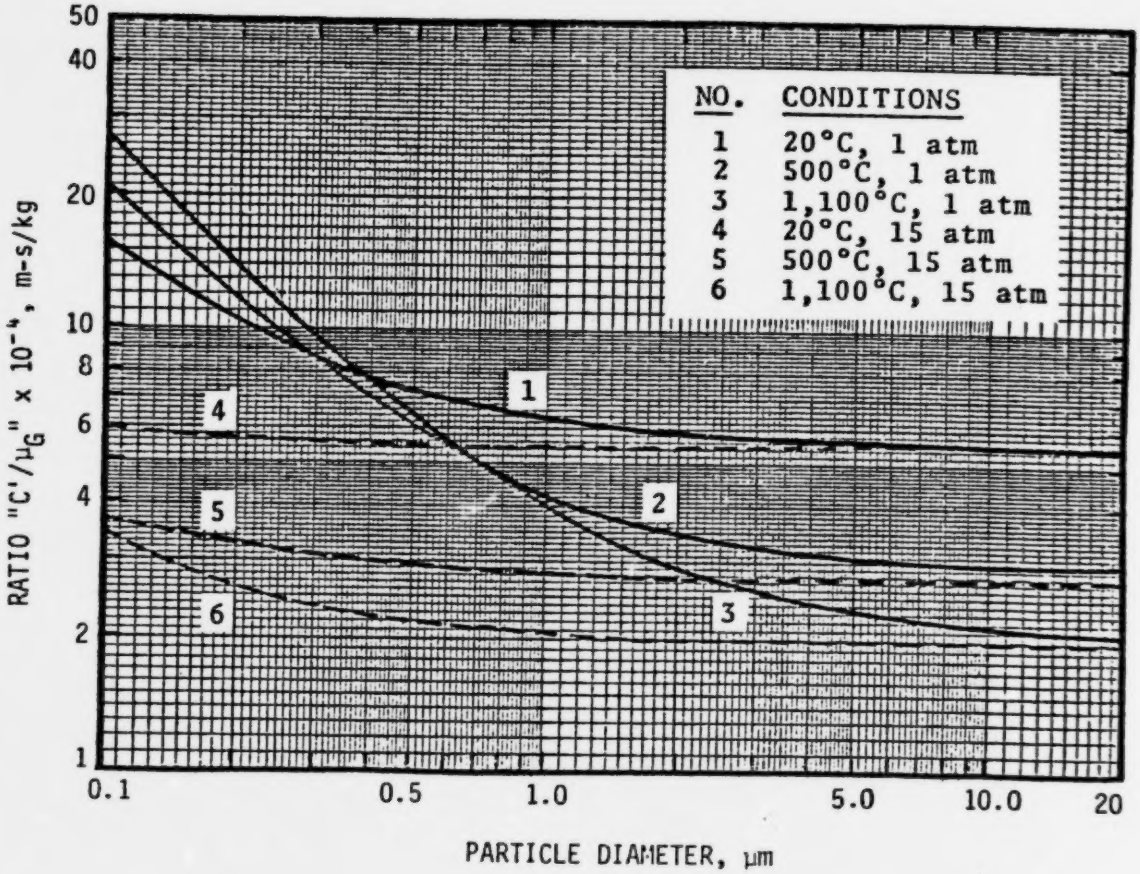

Figure 44. The effect of temperature and pressure on the ratio of the Cunningham slip correction factor to the dynamic viscosity of air.

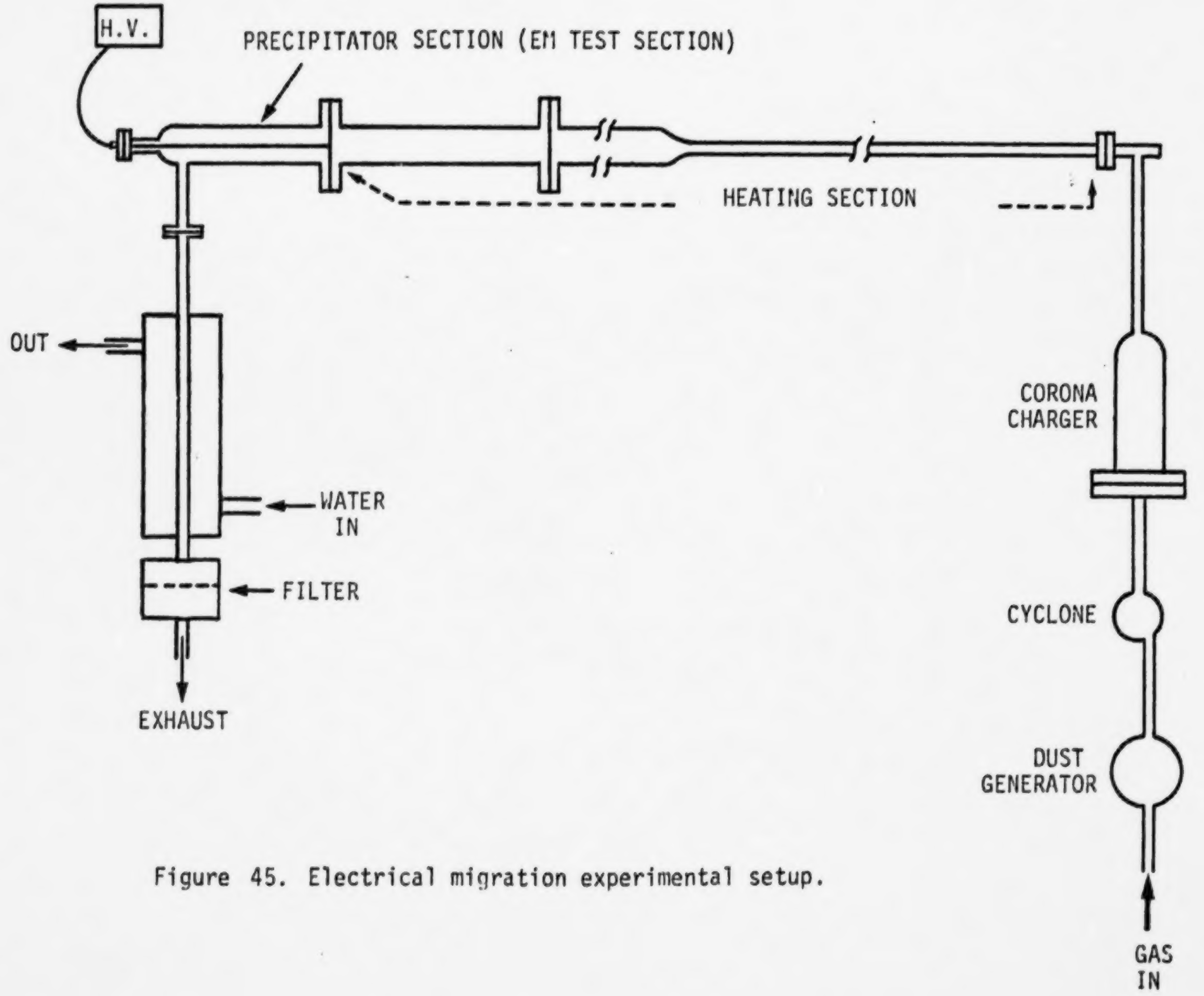
H.V.
PRECIPITATOR SECTION (EM TEST SECTION)
HEATING SECTION
OUT
WATER IN
FILTER
EXHAUST
CORONA CHARGER
CYCLONE
DUST GENERATOR
GAS IN

Figure 45. Electrical migration experimental setup.

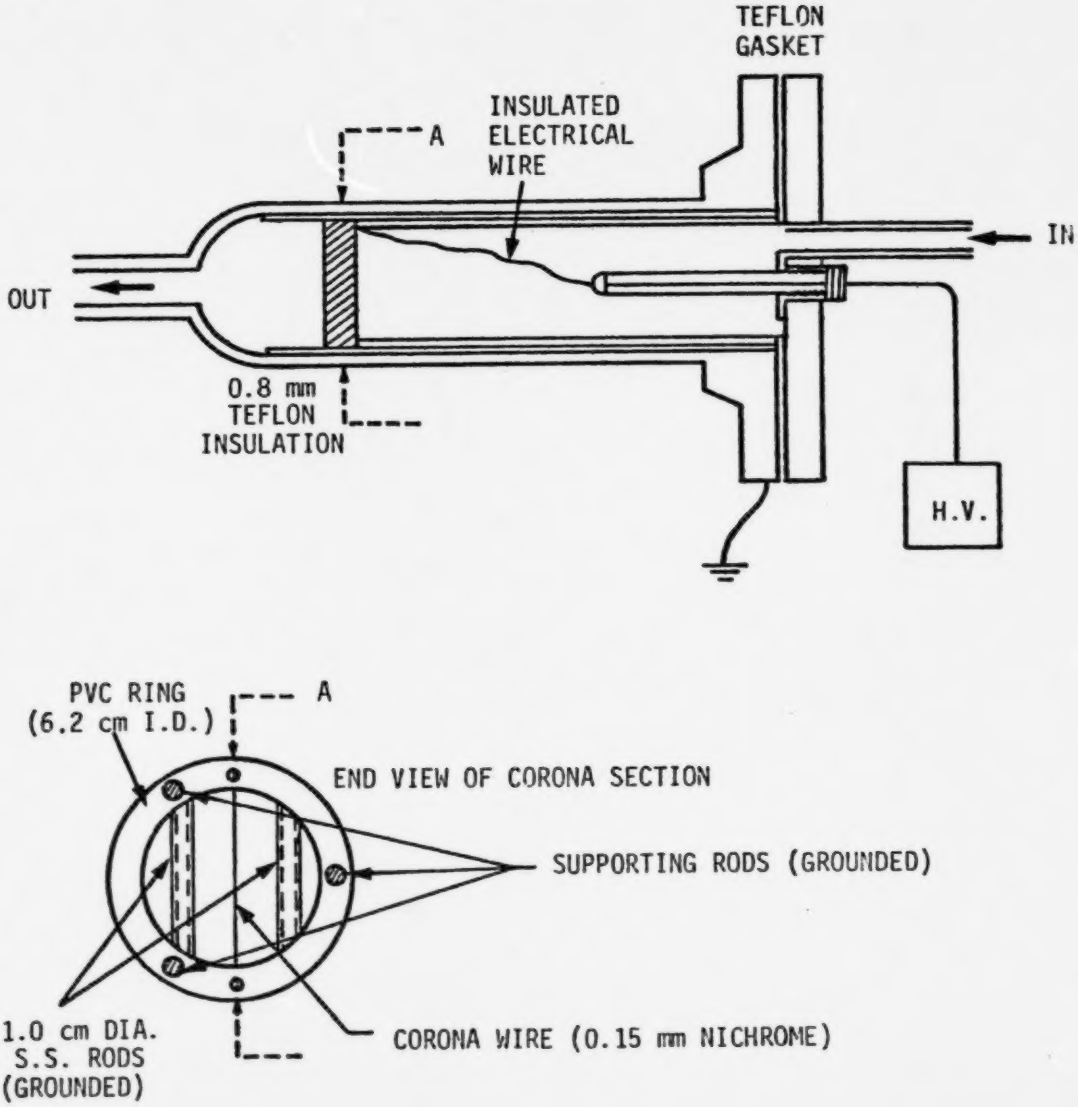
TEFLON GASKET
INSULATED ELECTRICAL WIRE
A
IN
OUT
0.8 mm TEFLON INSULATION
H.V.
PVC RING (6.2 cm I.D.)
A
END VIEW OF CORONA SECTION
SUPPORTING RODS (GROUNDED)
1.0 cm DIA. S.S. RODS (GROUNDED)
CORONA WIRE (0.15 mm NICHROME)

Figure 46. Corona charger.

A Faraday cup, which consisted of a shielded, isolated glass fiber filter grounded through an electrometer, was used to measure the charge-to-mass ratio. The filter collected the particles and their charges. The charges were leaked to the ground and measured by the electrometer. The particle charge-to-mass ratio was calculated from the measured charge and weight gain of the filter.

EM Test Section

The EM test section arrangement is shown in Figure 47. It was designed in such a way that it could be taken apart easily for particle removal and cleaning of the collection electrodes. The test section was similar to a pipe precipitator. The central electrode was made from 3 mm diameter Inconel rod and the collection tube was fabricated by rolling 0.15 mm (0.006 in) thick Inconel sheet. The central electrode was supported at one end and electrically insulated with machinable alumina ceramic tubing. Three alumina spacers were used to center the electrode. Spark plugs were used for electrical connections.

Three collection tubes in series were used. The current collected on each tube was monitored with an electrometer.

The test section was wrapped with electrical heating tape and heated to the desired test temperature to prevent heat loss during the test.

EXPERIMENTAL PROCEDURE

In starting an experiment, the system was preheated to the desired temperature. The corona charger and the fluidized bed particle generator were then turned on. A high voltage was applied to the central electrode and the current from each collection section was measured with an electrometer.

A glass fiber filter was used to remove the particles in the exhaust stream. The filter was located downstream from a water cooled quench section.

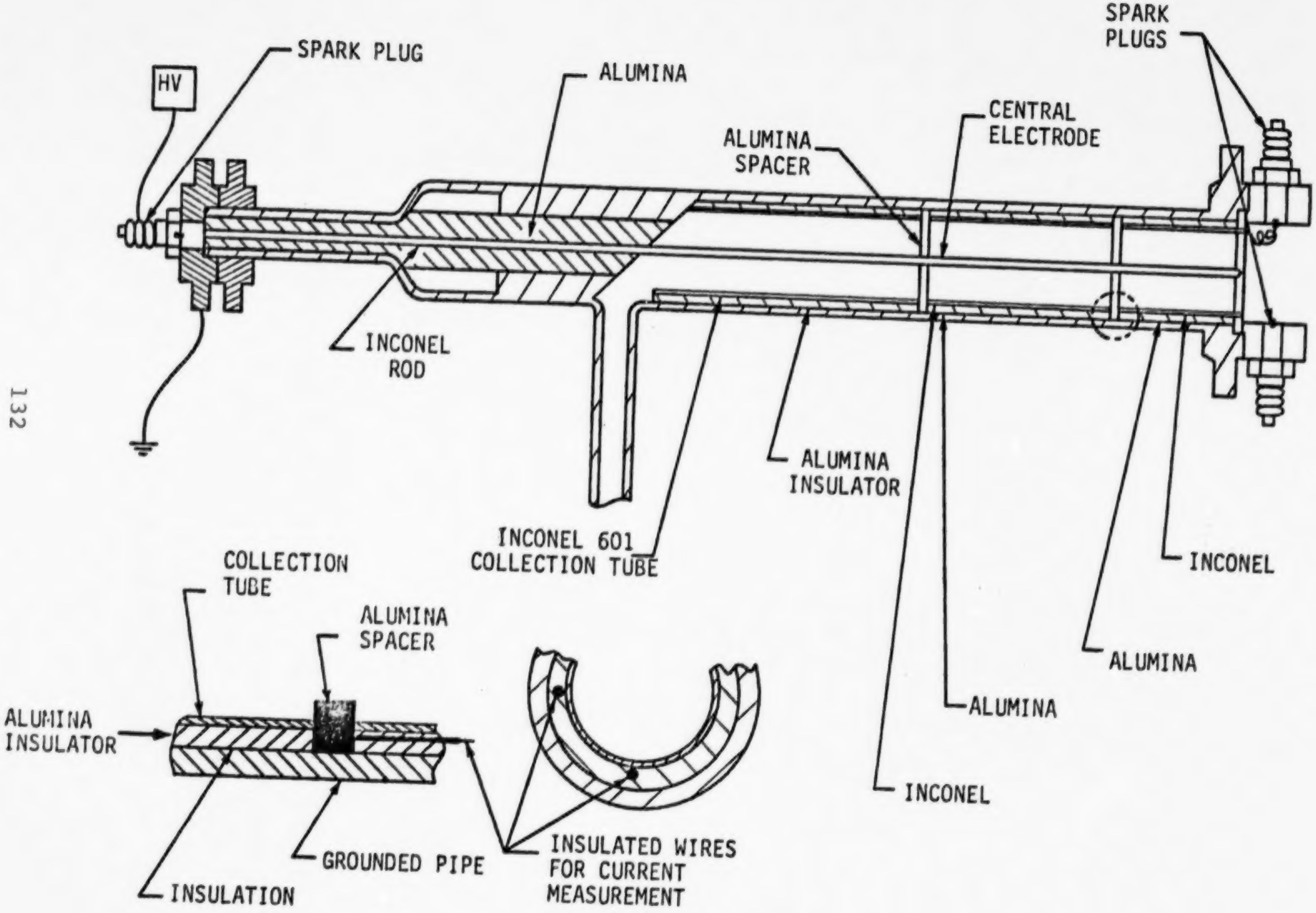
SPARK PLUG
HV
ALUMINA
ALUMINA SPACER
CENTRAL ELECTRODE
SPARK PLUGS
INCONEL ROD
ALUMINA INSULATOR
INCONEL 601 COLLECTION TUBE
INCONEL
ALUMINA
ALUMINA
INCONEL
COLLECTION TUBE
ALUMINA SPACER
ALUMINA INSULATOR
GROUNDED PIPE
INSULATION
INSULATED WIRES FOR CURRENT MEASUREMENT

Figure 47. Electrical migration test section.

After a run, each collection electrode was washed with acetone. Acetone was subsequently evaporated away. The amount of particles collected was determined by weighing and the size distribution was determined with Coulter counter.

The particles deposited in the water cooled quencher section was recovered by washing and its mass was added to the filter catch.

For each temperature, the experiment was repeated with different applied voltage to the central electrode.

Data Reduction Methods

The effects of gas temperature and pressure on electrical mobility of particle were determined from the measured current and the particle size distribution of the particles collected by the collection electrode. The theoretical backgrounds for the data reduction method are presented below:

Method 1. From Collection Electrode Collection.

The trajectory of particles in the electrical migration test section is illustrated in Figure 48. The electric field strength at any radial position, r, is given as:

$$E = \frac{V}{r} \frac{1}{\ln(r_2/r_1)} \qquad (68)$$

where:
E = electric field strength, V/cm
V = voltage on center rod, V
r_2 = radius of collecting surface, cm
r_1 = radius of center rod, cm

The radial drift velocity (migration velocity) of a charged particle which enters at location, "r" is:

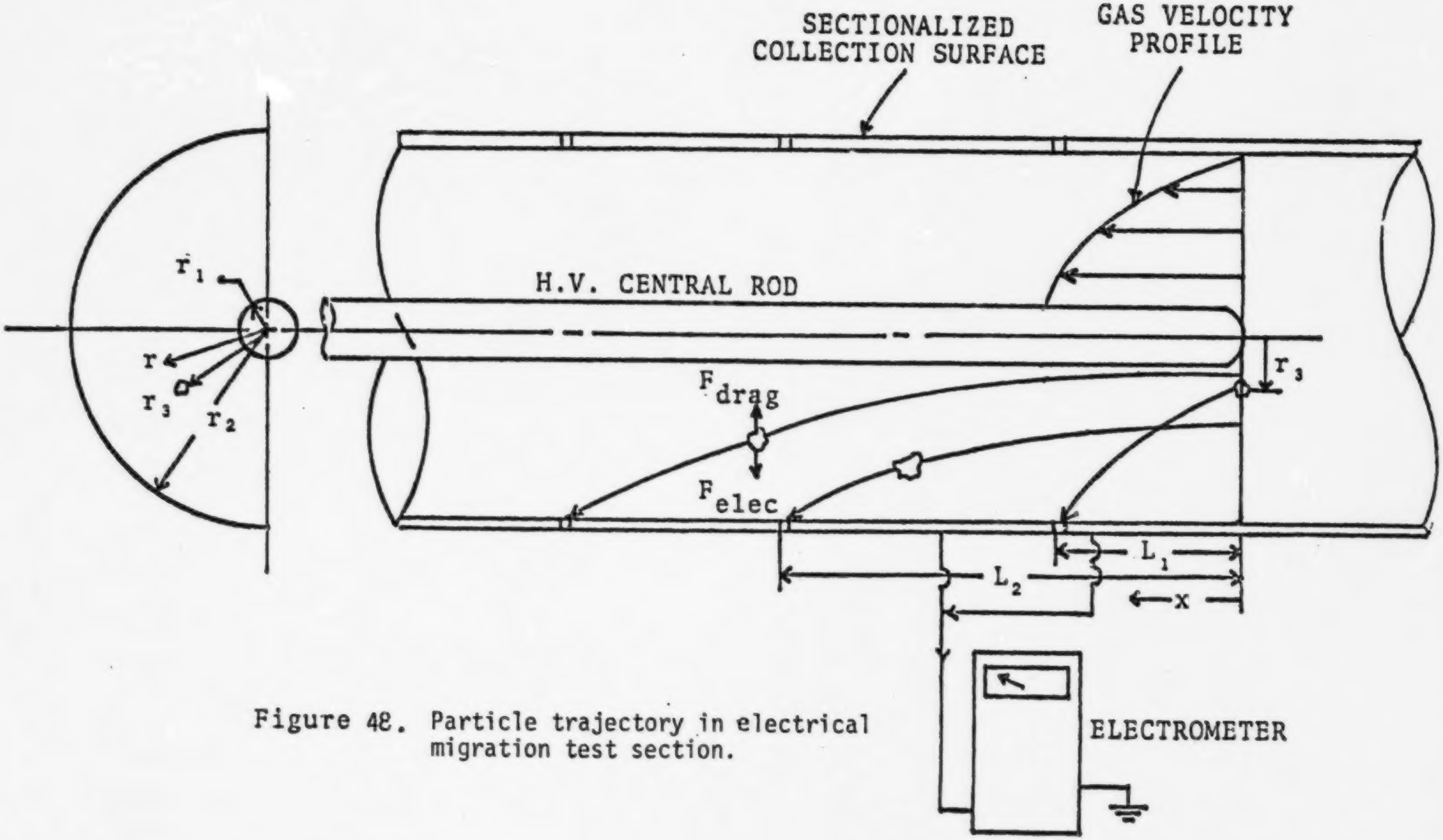
SECTIONALIZED COLLECTION SURFACE
GAS VELOCITY PROFILE
H.V. CENTRAL ROD
r_1
r
r_3
r_2
r_3
F_{drag}
F_{elec}
L_1
L_2
x
ELECTROMETER

Figure 48. Particle trajectory in electrical migration test section.

$$u_e = \frac{dr}{dt} = Z_p E \qquad (69)$$

The axial velocity field of the same particle in fully developed laminar flow is:

$$V_x(r) = 2u_G \frac{r_2^2 - r^2 - 2r_{max}^2 \ \ln(r_2/r_1)}{r_2^2 + r_1^2 - 2r_{max}^2} \qquad (70)$$

where:

$$u_G = \text{average velocity} = \frac{Q_G}{\pi(r_2^2 - r_1^2)}, \text{ cm/s} \qquad (71)$$

Q_G = gas flow rate, cm³/s

$$r_{max} = \left(\frac{r_2^2 - r_2^2}{2 \ln(r_2/r_1)}\right)^{\frac{1}{2}} \qquad (72)$$

The distance travelled by the particle is,

$$dx = u_{Gx}\, dt = \frac{u_x}{u_e}\, dr \qquad (73)$$

or,

$$L = \int_{r_3}^{r_2} dx = \int_{r_2}^{r_2} \frac{u_{Gx}}{u_e}\, dr, \text{ cm} \qquad (74)$$

By substitution of equations (79), (71) and (72) into (74), the following equation is obtained:

$$L = \int_{r_3}^{r_2} \frac{2u_G \dfrac{r_2^2 - r^2 - 2r_{max}^2 \ln(r_2/r_1)}{r_2^2 + r_1^2 - 2r_{max}^2}}{Z_p \dfrac{V}{r} \dfrac{1}{\ln (r_2/r_1)}} dr$$

$$= \frac{Q_G}{\pi V Z_p} \frac{\ln (r_2/r_1)}{(r_2^2 - r_1^2)\ (r_2^2 + r_1^2 - 2r_{max}^2)}$$

$$\Big\{(r_2^2 - r_{max}^2)(r_3^2 - r_1^2) - (r_3^4 - r_1^4)/2$$

$$+ 2\ r_{max} \Big[r_1^2 \ln(r_2/r_1) - r_4^2 \ln(r_2/r_3)\Big]\Big\} \qquad (75)$$

or the mobility of particle can be expressed as:

$$Z_p = \frac{Q_G}{V} \frac{\ln (r_2/r_1)}{\pi L\ (r_2^2 - r_1^2)(r_2^2 - r_1^2 - 2\ r_{max}^2)}$$

$$\Big\{(r_2^2 - r^2{}_{max})(r_3^2 - r_1^2) - 0.5(r_3^4 - r_1^4)\Big]\Big\}$$

$$+ 2r_{max} \Big[r_1^2 \ln(r_2/r_1) - r_3^2 \ln(r_2/r_3)$$

$$= \frac{Q_G}{V} K_1(L, r_1, r_2, r_3) \qquad (76)$$

where the factor "$K_1(L, r_1, r_2, r_3)$" contains only physical dimensions of the test section and the position of the particle where it enters the test section.

Since the test section is not designed to have clean sheath air, the radial distance of particles when they enter the test section is not a constant. The average radial distance can be determined by:

$$\bar{r}_3 = \frac{\int_{r_1}^{r_2} 2\pi r^2 \, dr}{\pi (r_2^2 - r_1^2)} = \frac{2(r_2^3 - r_2^3)}{3(r_2^2 - r_1^2)} \qquad (77)$$

Therefore the average mobility of all the particles entering the test section and being collected in the collecting surface of length, L, with applied center rod voltage of "V" is:

$$Z_p = \frac{Q_G}{V} \frac{\ln(r_2/r_1)}{\pi L(r_2^2 - r_1^2)(r_2^2 + r_1^2 - 2r_{max}^2)}$$

$$\Big\{(r_2^2 - r_{max}^2)(\bar{r}_3^2 - r_1^2) - 0.5(\bar{r}_3^4 - r_1^4)$$

$$+ 2r_{max}^2 \left[r_1^2 \ln(r_2/r_1) - \bar{r}_3^2 \ln(\bar{r}_3/r_2)\right]\Big\}$$

$$= \frac{Q_G}{V} K_1(L, r_1, r_2) \qquad (78)$$

At a moderate applied center rod voltage only the high mobility particles will be collected in collecting surface of length, L. The average particle size of the particles collected on the surface "L" must be determined by the Coulter counter. Thus, the relationship between the mobility of particle vs. particle diameter can be determined by repeating the experiment with different "Q_G" or "V" values. Since $u_e = Z_p E$, the electrical migration velocity of particle can also be determined for any applied electric field.

Method 2 - From Measured Current

For a laminar flow electrostatic precipitator, the fractional collection efficiency is (White, 1963):

$$\eta = \frac{u_e\ A}{Q_G} = \frac{n_p\ e\ E\ \pi\ d_c\ L}{3\ \pi\ d_p} \left(\frac{C'}{\mu_G}\right) \qquad (79)$$

where A = surface area of collection electrode, cm^2
Q_G = volumetric flow rate, cm^3/s
E = field strength, V/cm
L = length of collection electrode, cm
d_c = diameter of collection electrode, cm
u_e = electrical migration velocity, cm/s
d_p = particle diameter, cm
C' = Cunningham slip correction factor, dimensionless
μ_G = gas viscosity, g/cm-s
η = collection efficiency, fraction

The following assumptions were made:

1. The fly ash is monodisperse and has a diameter equivalent to the median surface diameter "d_s" of the fly ash.
2. The fly ash is well mixed at the entrance of a section.

With these assumptions, the current ratios for any two collectrion sections is equal to the "effective" collection efficiencies of these two section, i.e.

$$\frac{I_1}{I^2} = \frac{(1 - \eta_1)\ \eta_2}{\eta_1} \quad \text{and} \quad \frac{I_3}{I_1} = \frac{\{1-[(1 - \eta_1)\ \eta_2 + \eta_1]\}\ \eta_3}{\eta_1} \qquad (80)$$

RESULTS AND DISCUSSION

Figure 49 and 50 show the experimental collector current ratios as a function of the applied precipitating voltage at two different temperatures (29°C and 160°C). As the precipitating voltage was increased, more charged particles were precipitated on the first collector (the collectors were numbered in order along the flow direction) and subsequently an increase in the current "I_1" and decrease in "I_2" and "I_3".

The maximum precipitation voltage applied was limited to about 7.5 kW due to weak electrical insulation around the contral electrode. Attempts to obtain data at 500°C failed because the electrometer detected no measurable current. To pinpoint the reason for no current flow, a different experiment was done. The three collectors in the EM section were replaced with a single large 30 cm long Inconel tube. The overall collection efficiency of the tube was then determined experimentally for several gas temperatures.

At room temperature, the results were: 1.2% efficiency with no electric field or charge and 73.3% efficiency with an electric field strength of 4 kV/cm. This result indicates that at room temperature, collection was mostly by the mechanism of electrostatic precipitation.

At 500 °C gas temperature, there was essentially zero collection efficiency because there was no fly ash precipitated on the tube. Some fly ash was observed to deposit on the central electrode. This indicated that instead of carrying a negative charge, the particles carried a net positive charge.

A Faraday cup was used to measure the charge-to-mass ratio. The results are shown in Table 24. At the corona charger outlet, the charge-to mass ratio was -5×10^{-5} C/g. At the end of the EM section, the measured ratio at 25°C was -2 to -3×10^{-5} C/g, i.e. particles loss 50% of their charge during travel. The loss of charge increased with temperature. At 500 °C, the particles became positively charged because the current from the Faraday cup is positive.

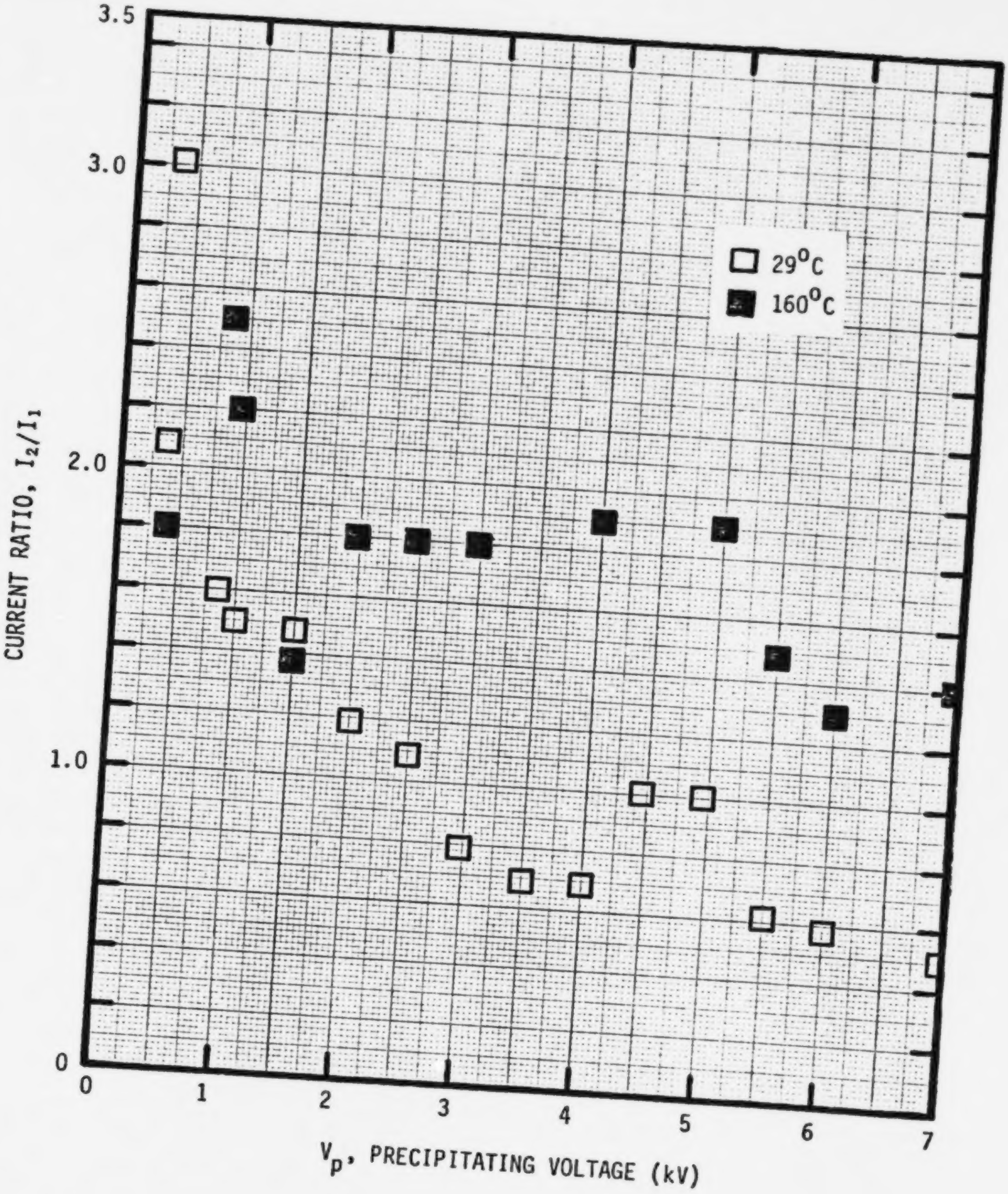

Figure 49. Experimental Current ratios for 29°C and 160°C.

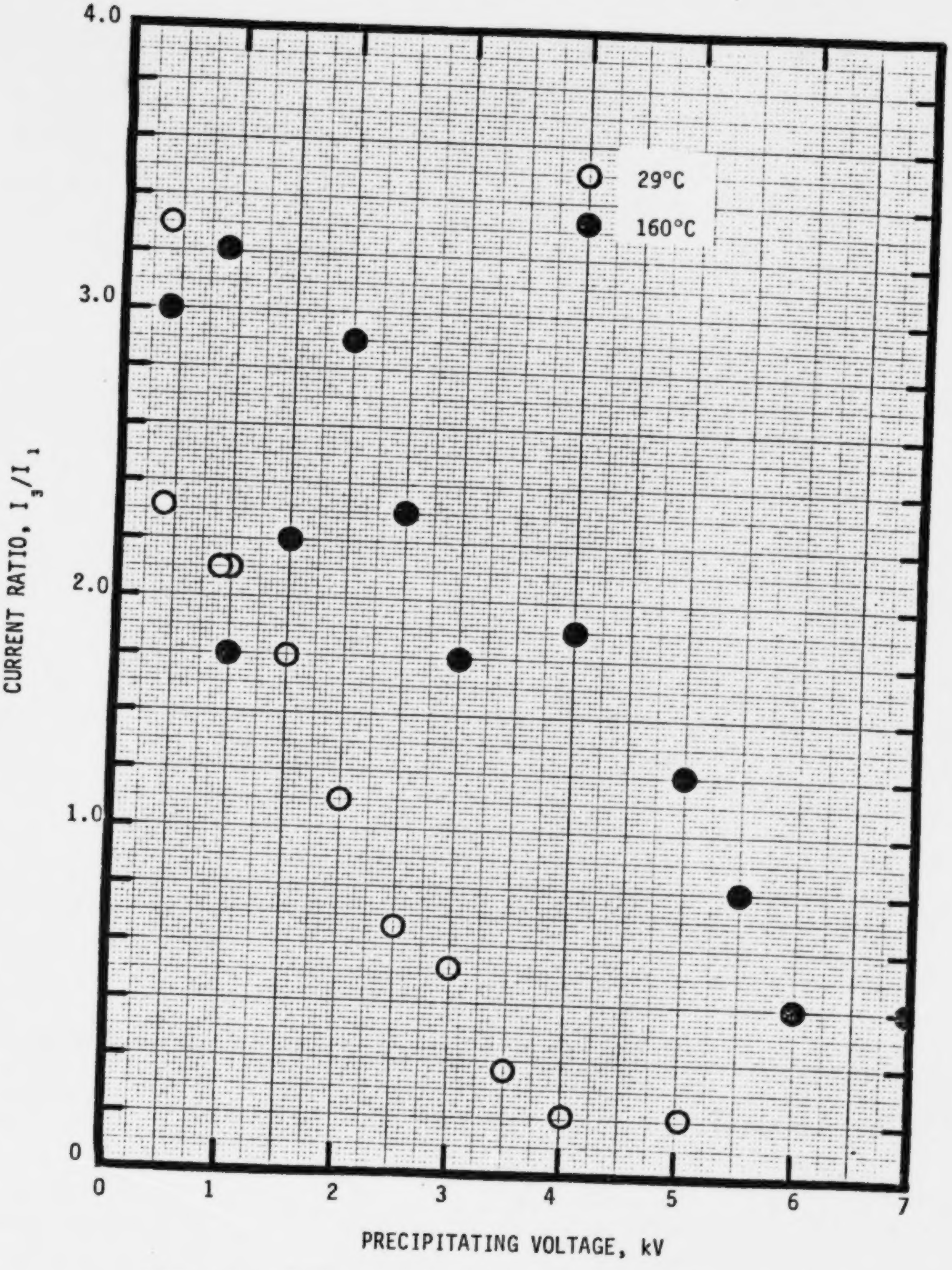

Figure 50. Experimental current ratios at 29°C and 160°C.

TABLE 24. RESULTS OF ELECTRICAL MIGRATION CHARGE MEASUREMENT

GAS TEMP (^{o}C)	CHARGE-TO-MASS RATIO (C/g)	
	Charger Output	After Heated
25°C	$-5x10^{-5}$ (Current=$-2x10^{-10}$A)	-2 to $-3x10^{-5}$ (Current=$-.8x10^{-10}$A)
300°C	(Current=$-2x10^{-10}$A)	(Current=$-0.6x10^{-10}$A)
500°C	(Current=$-2x10^{-10}$A)	(Current=$+3x10^{-11}$A)

The measured current ratio increased with increasing gas temperature as predicted from theory. However, since the particle charge also decreased with high temperature, the effect of temperature on "C'/μ_G" could not be deduced. Since negative charge loss could not be prevented, no additional experiments were done.

REFERENCES

Alexander, R. M. Fundamentals of Cyclone Design and Operation. *Proc. Australas Inst. Min. Met.* 152-3, 203-228, 1949.

Barth, W. Design and Layout of the Cyclone Separator on the Basis of New Investigations. *Brenn. Warem Kraft* 8, 1-9, 1956.

Beeckmans, J. M. Analysis of the Cyclone as Size Selective Aerosol Sampler, in *Aerosol Measurement*, ed. by Dale Lundgren, U. of Florida Press, 1979.

Byers, R. L., and S. Calvert. Particle Deposition from Turbulent Streams by Means of Thermal Force. Ind. Eng. Chem. Fundamentals, 3 (4): 646, 1969.

Calvert, S., C. Lake, and R. Parker. Cascade Impactor Calibration Guidelines. EPA-600/2-76-118 and NTIS PP-252-656, April 1976.

Calvert, S., and R. Parker. Effects of Temperature and Pressure on Particle Collection Mechanisms: Theoretical Review. EPA-600/7-77-002, NTIS PB-264-203, January 1977.

Cunningham, E. Proc. Royal Soc. (London), A83: 357, 1910.

Davies, C. N. Definitive Equations for the Fluid Resistance of Spheres, Proc. Phys. Soc. *57* (4): 18, 1945.

Davies, C. N. Proc. Instr. Mech. Engng. 1B, 185., 1952.

Davies, C. N., *Air Filtration*. Academic Press, N.Y. 1973.

Dietz, P. Collection Efficiencies of Cyclone Separators. Presented at 3rd Symposium on the Transfer and Utilization of Particulate Control Technology. Orlando, Florida, March 9-13, 1981.

D.O.E. Proceedings from the Department of Energy Contractors Meeting on Hot Gas Cleanup for PFBC processes. Morgantown, West Virginia, February 1981.

E.P.A./D.O.E. Proceedings of the EPA/DOE Symposium on High Temperature High Pressure Particulate Control. EPA-600/9-78-004, NTIS CONF-770970, March 1978.

Ernst, M., R. C. Hoke, V. J. Siminski, J. D. McCain, R. Parker, and D. C. Drehmel. Evaluation of a Cyclonic Type Dust Collector for High Temperature High Pressure Particulate Control. Presented at the 2nd Symposium on the Transfer and Utilization of Particulate Control Technology. Denver, Colorado, July 1979.

First, M. W. Fundamental Factors in the Design of Cyclone Dust Collectors. Doctoral Thesis, Harvard University, 1950.

Fuchs, N. A. The Mechanics of Aerosols. Pergamon Press, N.Y. 1964.

Goodman, F. O., and H. Y. Wachman. Formula for Thermal Accomodation Coefficients. J. Chem. Phys. 46 (6): 2376, 1967.

Goodman, F. O. Classical Theory of Small Energy Accomodation Coefficients. J. Chem. Phys. 50 (9): 3855, 1969.

Hidy, G. M., and J. R. Brock. The Dynamics of Aerocollidal Systems. Pergamon Press, N.Y., 1970.

Knowlton, T. M. and D. M. Bachovchin. Effect of Two Variables on Cyclone Performance. Coal Processing Technology, AIChE, Vol. 4, 1978.

Lapple, C. E. and C. B. Shepherd. Calculation of Particle Trajectories. Industrial and Engineering Chemistry, 32 (5): 605, 1940.

Lapple, C. E. Processes Use Many Collector Types. Chemical Engineering, 58, 144-141, 1951.

Lawless, P. A. Analysis of Cascade Impactor Data for Calculating Particle Penetration, EPA-600/7-78-189 (NTIS No. PB 288649), 1978.

Leith, D. and W. Licht. The Collection Efficiency of Cyclone Type Particle Collectors - A New Theoretical Approach. AIChE Symposium Series: Air - 1971, 1972.

Leith, D., and D. Mehta. Cyclone Performance and Design. Atmospsheric Environment. Vol. 7, pp. 527-549, 1973.

Millikan, R. A. Coefficients of Slip in Gasses and the Law of Reflection of Molecules from the Surfaces of Solids, and Liquids, Phys. Rev. 21: 3: 217, 1923a.

Millikan, R. A. The General Law of Fall of a Small Spherical Body Through a Gas, and its Bearing Upon the Nature of Molecular Reflection from Surfaces, Phys. Rev. 22: 1: 1, 1923b.

Moore, C. V. "The Design of Barricades for Hazardous Pressure Systems", in Pressure Vessels and Pipings; Design and Analysis, Volume 2; Components and Structural Dynamics, A.S.M.E., 1972.

Parent, J. D. Efficiency of Small Cyclones as a Function of Loading, Temperature, and Pressure Drop. Trans AIChE, 42: 989, 1946.

Parker, R., and S. Calvert. Alternatives for High-temperature/ High-pressure Particulate Control. EPA-600/7-79-019. NTIS PB-292-687, January 1979.

Patterson, R. and S. Calvert. Submicron Particle Size Measurement with a Screen Diffusion Battery. EPRI-FP-840, August 1978.

Pich, J. Theory of Aerosol Filtration by Fibrous and Membrane Filters, in Aerosol Science, Davies (ed), Academic Press, New York, 1966

Ramesh, V., and D. J. Marsden. Rotational and Translational Accomodation Coefficients of Nitrogen on Nickel, Silver, and Gold. Vacuum, 24 (7): 291, 1974.

Rao, A. K. and K. T. Whitby. Non-ideal Collection Characteristics of Inertial Impactors- I. Single-stage Impactors and Solid

Particles, Aerosol Science, 9:77-86, 1979.

Rosin, P. Principles and Limits of Cyclone Dust Removal. Z. Ver. Deut. Ing., 76, 443-437, 1932.

Shepherd, C. B. and C. E. Lapple. Flow Pattern and Pressure Drop in Cyclone Dust Collectors. Ind. Eng. Chem. 32, 1246-1248, 1940.

Smith, W. B., R. R. Wilson, and D. B. Harris. A Five-Stage Cyclone System for In-Situ Sampling. Environmental Science and Technology, 13(11), 1387-1392, 1979.

Sproull, W. T. Air Pollution and Its Control. Exposition Press, New York, 1970.

Stickney, R. E. Momentum Transfer Between Gas Molecules and Metallic Surfaces in Free Molecule Flow. Physics of Fluids, 5 (12): 1617, 1962.

Stairmand, C. J. Pressure Drop in Cyclone Separators. Engineering, 16B, 409-411, 1949.

Stairmand, C. J. The Design and Performance of Cyclone Separators. Trans. Inst. Chem. Engrs. 29, 356-383, 1951.

Strauss, W. Industrial Gas Cleaning. Pergamon Press, New York, 1966.

Wachman, H. Y. The Thermal Accomodation Coefficient: A Critical Survey. A.R.S. Journal, 32: 2, 1962.

Wachman, H. Y. Thermal Accommodation Coefficients of Helium on Tungsten at 325°, 403°, and 473°K. J. Chem. Phys. 45 (5): 1532, 1966.

White, H. J. Industrial Electrostatic Precipitation, Addison-Wesley Pub. Co., Reading, Mass., 1963.

Willeke, K. Temperature Dependence of Particle Slip in a Gaseous Medium. J. Aerosol Science, 7: 381, 1976.

APPENDIX A

ADDITIONAL IMPACTION DATA

TABLE A1. GRADE PENETRATION DATA FOR INERTIAL IMPACTION TESTS

	PARTICLE DIA, µm COLLECTED AT SPECIFIED % Pt								
RUN NO.	10	20	30	40	50	60	70	80	90
30-6	-	-	-	-	1.15	0.80	0.59	-	-
30-11	-	-	-	1.61	1.26	1.12	1.03	0.94	0.83
30-12	-	-	-	1.30	1.08	0.95	0.83	0.70	0.56
30-13	-	-	1.75	1.49	1.32	1.21	1.11	1.03	0.96
31-1	-	-	-	1.81	1.45	1.18	0.96	0.76	-
31-2	-	-	-	1.89	1.31	1.05	0.84	0.63	-
31-3	-	-	1.75	1.41	1.15	0.93	-	-	-
31-4	-	-	1.39	1.15	0.95	0.74	0.54	-	-
31-6	-	-	-	1.32	1.11	0.97	0.87	0.76	-
31-15	-	-	1.26	1.08	0.98	0.87	0.80	0.73	0.63
31-16	-	-	1.32	1.15	1.01	0.90	0.80	0.52	-
31-17	-	1.80	1.25	1.11	1.00	0.90	0.81	0.74	0.65
31-25	-	-	-	-	1.20	0.98	0.83	0.69	-
31-31	-	-	-	1.55	1.29	1.16	1.00	0.84	-
32-28	-	-	-	-	1.31	1.24	0.98	0.82	-
33-1	-	-	-	1.80	1.61	1.46	1.33	1.21	1.07
33-7	1.40	1.17	1.05	0.98	0.92	0.88	0.85	0.82	0.79
33-9	1.43	1.18	1.01	0.88	0.74	0.58	-	-	-
33-10	1.53	1.20	0.97	0.83	0.73	0.66	0.60	-	-
33-24	-	1.63	1.30	1.17	1.08	0.98	0.88	0.77	0.62
33-26	-	1.64	1.38	1.28	1.19	1.10	1.01	0.92	0.81
33-27	-	1.65	1.29	1.15	1.05	0.92	0.70	-	-
34-3	-	-	2.66	2.00	1.70	1.54	1.45	1.35	1.24
34-4	-	2.82	2.06	1.73	1.51	1.33	1.12	0.81	-
34-5	-	-	2.21	1.90	1.69	1.51	1.34	1.13	0.84

cont'd.

TABLE A1. CONTINUED

	PARTICLE DIA, m COLLECTED AT SPECIFIED % Pt								
RUN NO.	10	20	30	40	50	60	70	80	90
34-6	-	2.36	1.80	1.45	1.20	0.95	0.62	-	-
34-11	-	2.10	1.41	1.25	1.12	0.77	0.64	-	-
34-12	-	-	-	1.38	1.12	0.82	0.66	0.56	-
34-13	-	-	-	1.57	1.43	1.28	1.15	1.02	0.90
34-16	-	-	1.71	1.45	1.30	1.18	1.10	0.98	0.79
34-17	-	-	1.68	1.51	1.40	1.23	1.10	0.98	0.83
34-19	-	-	-	2.98	2.70	2.50	2.30	2.10	1.84
35-2	-	-	-	-	2.20	1.99	1.83	1.68	1.55
35-3	-	-	-	2.67	2.25	2.03	1.82	1.51	-
35-6	-	-	-	2.60	2.18	1.89	1.65	1.46	1.31
35-7	-	-	-	-	2.60	2.27	2.00	1.77	1.56
36-12	-	-	-	-	2.04	1.62	1.39	1.23	1.06
36-14	-	-	3.07	2.44	2.02	1.68	1.38	1.10	0.83
36-16	-	-	2.68	2.08	1.72	1.48	1.30	1.16	-

APPENDIX B

ADDITIONAL CYCLONE DATA

TABLE B1. GRADE EFFICIENCY DATA FOR CYCLONE SEPARATION TESTS (PHYSICAL DIAMETER)

Run No.	Particle Dia., μm Collected At Specified % Efficiency								
	10	20	30	40	50	60	70	80	90
48-1	-	1.85	2.1	2.3	2.5	2.8	3.1	3.5	4.6
48-2	-	2.0	2.4	2.6	2.9	3.2	3.5	4.0	4.8
48-3	-	-	-	2.7	3.8	4.5	5.2	6.0	7.3
48-4	-	-	2.9	3.9	4.5	5.2	5.8	6.4	7.4
48-5	-	5.8	7.3	8.3	9.5	11.1	13.0	-	-
48-6	-	2.5	4.7	6.0	7.3	8.5	9.7	11.3	13.4
48-7	-	10.5	12.8	13.8	14.6	15.7	17.2	-	-
49-1	-	-	3.8	5.0	5.6	6.3	7.2	8.3	10.6
49-2	-	-	-	2.1	3.1	3.7	4.3	5.1	6.3
49-3	-	-	-	-	1.4	1.8	2.0	2.3	3.1
49-4	-	-	-	-	1.3	1.6	1.8	2.2	3.2
49-5	-	-	-	-	-	-	1.2	1.6	2.3
49-6	-	-	-	-	-	1.0	1.3	1.6	2.0
49-7	-	-	-	-	1.0	1.1	1.2	1.5	2.2
49-8	-	-	-	-	-	0.9	1.1	1.2	1.7
49-9	-	-	2.8	3.9	4.5	5.1	5.7	6.6	8.5
50-1	-	3.9	4.6	5.0	5.6	6.4	7.3	8.5	13.6
50-2	-	-	3.8	4.4	4.9	5.6	6.6	8.2	12.2
50-3	6.7	8.9	10.5	11.6	12.6	15.0	-	-	-
55-2	-	-	-	-	-	-	-	1.4	1.6
55-3	-	-	-	-	-	-	-	-	1.3
55-4	-	-	-	-	-	-	0.9	1.1	1.4
55-5	-	-	-	-	-	-	0.9	1.0	1.3
55-6	-	-	-	-	-	-	-	0.9	1.2

TABLE B1. GRADE EFFICIENCY DATA FOR CYCLONE SEPARATION TEST (PHYSICAL DIAMETER) (cont.)

Run No.	Particle Dia., µm Collected At Specified % Efficiency								
	10	20	30	40	50	60	70	80	90
55-7	-	-	-	-	-	0.9	1.1	1.2	1.6
55-8	-	-	-	-	-	-	-	0.9	1.2
55-9	-	-	-	-	-	-	0.9	1.2	1.7
55-10	-	-	-	-	-	-	-	1.0	1.6
55-11	-	-	-	-	-	-	-	1.1	1.6
55-12	-	-	-	-	-	0.9	1.1	1.4	1.8
55-13	-	-	-	-	-	-	-	1.2	1.6